Adjuvant Interactions with Lipid Membranes and Their Effect on Cellular Immune Responses

By

Lorena R. Antúnez Napolitano

Submitted to the graduate degree program in Pharmaceutical Chemistry and the Graduate Faculty of the University of Kansas in partial fulfillment of the requirements for the degree of Doctor of Philosophy

_____

Chair: Dr. Cory Berkland

_____

Co-Chair: Dr. Prajnaparamita Dhar

_____

Dr. David Volkin

_____

Dr. Teruna Siahaan

_____

Dr. Arghya Paul

Date Defended: May 5, 2017

The dissertation committee for Lorena R. Antúnez Napolitano

certifies that this is the approved version of the following dissertation:

Adjuvant Interactions with Lipid Membranes and Their Effect on Cellular Immune Responses

_____

Chair: Dr. Cory Berkland

_____

Co-Chair: Dr. Prajnaparamita Dhar

Date Approved: May 5, 2017

Abstract

Adjuvants are commonly included in vaccines and have been invaluable in making them safer and more robust. Despite their prolific use, adjuvant mechanisms of action remain poorly understood. Many receptor-mediated mechanisms have been proposed for adjuvants, and many likely contribute to their mechanisms of action, but several adjuvants also interact with the plasma membrane. Although few have considered how lipid-mediated interactions contribute to adjuvanticity, previous studies suggested aluminum-based adjuvants (ABAs) have high affinity for sphingomyelin and cholesterol, which allowed them to activate dendritic cells exclusively through lipid sorting. This dissertation sought to understand how lipid interactions contribute to the immunostimulatory properties of adjuvants. The membrane interaction of Alhydrogel (AH) and Adju-Phos (AP) was initially investigated in a simple lipid monolayer representative of the outer leaflet of the plasma membrane. AH and AP interacted with the model monolayer and promoted lipid clustering, although the physiochemical properties of each adjuvant caused them to interact differently. In a more complex lipid system containing sphingomyelin and cholesterol, the lipid interaction behavior was consistent and revealed AH and AP stabilized sphingomyelin- and cholesterol-rich lipid domains even in the presence of an antigen. Lipid raft clustering observed in dendritic cells exposed to ABAs *in vitro* was reminiscent of domain clustering observed in the monolayer and corresponded to conditions which enhanced cell activation, suggesting membrane interactions and lipid sorting could indeed contribute to ABA mechanisms of action. Lipid-interactions were also considered while designing an adjuvant-based antigen-specific immunotherapy (ASIT). An MF59-analog (MF59a) made in our lab was selected to co-deliver ovalbumin and dexamethasone based on its ability to solubilize dexamethasone, extend its release, and enhance its membrane permeability and internalization. The combination of MF59a, ovalbumin, and dexamethasone inhibited several pro-inflammatory cytokines in dendritic cells and ovalbumin-educated splenocytes, and proved emulsion adjuvants could provide an ideal vehicle to create targeted, tolerizing ASITs. Therefore, lipid interactions can provide valuable insight while selecting the physiochemical properties of an adjuvant for pro- and anti-inflammatory applications. Our results provide compelling evidence that lipid interactions participate in adjuvant mechanisms of action, and should be considered when developing novel vaccines and adjuvants.

included in the KU Pharm Chem family. I am also indebted to all the administrative staff in the department, particularly Nancy Helm, Nicole Brooks, and Karen Hall. Thank you to all the labs that helped me conduct my research, especially the labs of the Macromolecule and Vaccine Stabilization Center, and Francisco Martinez Becerra and Olivia Arizmendi of the Kanas Vaccine Institute.

I had many leadership opportunities while in the department, but none was quite like my experience organizing the Globalization of Pharmaceutics Education Network (GPEN) 2016 meeting. My time organizing the GPEN2016 meeting provided an element of personal and professional development I could not have attained in the lab, and I am grateful to Dr. Borchardt for conceiving this graduate student-centered conference, and allowing me to help organize it. I am also incredibly grateful for my co-organizers, Michaela McNiff and Samantha Pace, our faculty advisor, Dr. Jeff Krise, and Nancy Helm, who through this conference proved to me that there is nothing she cannot do.

To all the past and present group members I have had the pleasure of working with: Brittany Hartwell, Laura Northrup, Chad Pickens, Melissa Pressnall, Shara Thati, Brad Sullivan, Chris Kuehl, Connor Dennis, Nashwa El-Gendy, Joshua Sestak, Jian Qian, Saba Ghazvini, Aishik Chakraborty, Matt Christopher, Martin Leon, Jimmy Song, Jeannie Salash, and Sam Peterson, thank you for all your help and support both in and out of work. It was wonderful to work alongside so many intelligent, capable, and kind people. Thank you to the undergrads that contributed to my work: Andrea Livingston, Taylor Brasted, Evan Bonner, and Kathrine Hickerson.

I cannot go without thanking my family and friends who were instrumental in me earning this degree. To my in-laws, Mike and Marla Napolitano and Katrina, Gary, Gregory, Grace, and Elijah Aumiller, thank you for your love and encouragement over the past few years. To my brothers, Emilio and Luis, and my sister-in-law Helen, thank you for always being great role models, and for all your advice, guidance, and perspective. And last, but certainly not least, I am grateful beyond words to my parents, Emilio and Imelda Antúnez. Thanks to your sacrifices, successes, and unconditional love I have had every opportunity I could have imagined. Thank you for instilling in me the value of hard work and a

good education, for being my biggest fans and greatest advocates, and for never letting me fall short of my potential.

And finally, to my husband, Chris Napolitano, I am so grateful to have had you by my side. Thank you for being there through all the long hours, late nights, frustrations, and successes, and for taking care of everything I could not in the time leading up to my defense. Thank you for never letting me sell myself short, for making me smile, for keeping me sane, and for your unconditional love and encouragement.

I thank God for the abundant blessings that have filled my life, and I hope with this degree I will be able to share those blessings and make a difference in the lives of others.

Lorena R. Antúnez Napolitano

May 5, 2017

Table of Contents

Chapter I: Introduction

Vaccines have been an essential part of reducing the severity, if not eliminating many infectious diseases. The availability, safety, and efficacy of many of these vaccines can be attributed in many ways to the use of adjuvants. Adjuvants are used to enhance and shape an antigen-specific immune response. The ability to isolate the immunogenic portion of a pathogen into a highly-purified protein antigen has made vaccines safer; however, administering this purified antigen alone typically does not create any robust immune protection without multiple immunizations. Therefore, a purified antigen may be delivered in combination with an adjuvant to elicit stronger immune protection with far less antigen [1].

Many materials have been investigated for use as adjuvants, but until recently the only FDA-approved adjuvants were aluminum-based adjuvants (ABAs). Squalene-based oil-in-water emulsions AS03 and MF59 were approved for use in flu vaccines in the US in 2013 and 2015, respectively, nearly twenty years after the approval of MF59 in Europe. Interestingly, despite their long history of use, particularly for the ABAs, the precise mechanisms of action for either of these adjuvants are poorly understood. In general, these adjuvants are observed to 1) promote antigen uptake by antigen-presenting cells (APCs), particularly dendritic cells and macrophages, 2) create damage or inflammation, and 3) recruit cells to the injection site [2].

A variety of factors undoubtedly play a role in each adjuvant's mechanisms of action; however, investigating the dynamic interactions between the plasma membrane and an adjuvant, like those summarized in **Table 1**, could provide insight. Here, we delve into how the characteristics of approved, particulate adjuvants, such as ABAs and emulsions may dictate their stabilizing or disruptive effect on the cell membrane, and how this interaction shapes the immune response.

1. The cell membrane and immunity

The plasma membrane is an astoundingly heterogeneous and complex surface which mediates cell function and communication. The mammalian plasma membrane is primarily composed of glycerophospholipids, and has the highest content of sphingolipids and sterols, namely cholesterol, compared to other cellular membranes (**Fig 1**) [3]. Glycerophospholipids are a diverse family of lipids,

and are the major component of cell membranes. Cells synthesize phospholipids with a variety of chemical moieties linked to their common phosphate base to produce anionic headgroups, such as phosphatidylinositol (PI), phosphatidylserine (PS), and phosphatidylglycerol (PG), or zwitterionic headgroups, such as phosphatidylcholine (PC) and phosphatidylethanolamine (PE). Additionally, lipids can differ in each of their acyl chains, which can also vary in length, saturation, and linkage to the glycerol backbone [3, 4]. Much like phospholipids, many sphingolipids can be produced by adding various side chains and head groups to ceramide, but the main sphingolipids are sphingomyelin and glycosphingolipid with saturated fatty acid chains [3]. Certain phospholipids are enriched in either the inner or outer leaflet of the bilayer. Anionic lipids and PE localize on the inner leaflet, while PC and sphingomyelin are mostly found in the outer leaflet [3, 5]. Furthermore, phospholipids are distributed differently within the leaflet. Differences in lipid charge and fatty acid chain structure promotes different affinities and packing between lipids, resulting in the formation of microdomains within the membrane and heterogeneity in the lateral distribution of lipids [3, 5]. For instance, as a small, rigid, and hydrophobic lipid, cholesterol preferentially interdigitates within hydrophobic, rigid unsaturated fatty acid chains and regulates membrane structure and fluidity. Although cholesterol associates with phospholipids, it has high affinity for the complementary structure of sphingomyelin. The preferential mixing of cholesterol and sphingomyelin produces tight, highly ordered domains and forms the basis for lipid rafts [3, 5, 6]. The raft-hypothesis, originally presented by Simon and co-workers, proposes that to coordinate different cellular functions, membrane lipids laterally phase separate into highly organized nanostructures or domains [7]. While the raft hypothesis is still contentious, recent technological advances uphold the hypothesis by providing compelling evidence of membrane heterogeneity and preferential self-association in living cells [3, 8].

Lipid rafts are ordered lipid domains rich in sphingolipids, cholesterol, and proteins. Rafts are 4-200 nm in diameter, typically composed of tightly packed saturated lipids, and are laterally mobile in the mostly unsaturated, fluid-disordered sea of membrane lipid [9-11]. Lipid rafts appear to be critical in

spatially organizing molecules and in the initiation and maintenance of signaling. Signaling encompasses a complex series of events and necessitates the organization of proteins, lipids, and a number of chemical processes. Evidence suggests lipid rafts can significantly reduce the mobility of associated proteins, and thus can provide a platform to sort and facilitate receptor-mediated signaling at the appropriate time and place [3, 11, 12]. In immune cells, lipid rafts maintain separation of activating signaling proteins in resting cells. While some important immune-signaling proteins reside in lipid rafts, such as CD14, CD4/CD8, Src-family kinases, and the linker for activation in T cells (LAT), they do not exert their effect until additional proteins partition into rafts upon ligand binding [3, 12, 13]. For instance, TLRs typically exist outside lipid rafts, but after activation by LPS or lipoteichoic acid, TLR4 and TLR2, respectively, translocate into lipid rafts [11, 14]. Similarly, both the T-cell receptor (TCR) and B-cell receptor (BCR) translocate into lipid rafts following conformational changes that occur after binding antigen [3, 11, 15, 16]. Additionally, MHC-II has been shown to be constitutively lipid raft-associated in many antigen presenting cells such as B cells, monocytes, and dendritic cells [9]. Upon ligand binding, raft-associated proteins with help from the actin cytoskeleton are observed to coalesce into larger domains to form immunological synapses. The aggregation of lipid rafts organizes signaling and adhesion molecules at the center and periphery of the synapse, respectively, to enable phosphorylation and signaling events resulting in robust immune activation [3, 6, 15, 17, 18]. Once signaling is complete, or in the absence of sufficient stimulation, the lipid rafts diffuse away.

In contrast to signaling activated by highly ordered lipid rafts, disrupted and damaged membranes also result in immune responses. The immune response to membrane changes following cell death can differ greatly depending on whether the cell is undergoing apoptotic or necrotic cell death. Apoptosis is a healthy, programed form of cell death involving membrane blebbing, cell shrinkage, and condensation and fragmentation of nuclear contents [19, 20]. In homeostatic cell death, apoptotic cells release chemoattractants, such as ATP, to recruit antigen presenting cells, and mark themselves for phagocytosis by exposing typically-intracellular lipids, like phosphatidylserine to the extracellular space [19, 21].

Apoptotic cells are typically cleared by phagocytes before releasing their intracellular contents and promote the secretion of immunosuppressive cytokines, and thus can be silently removed without initiating an immune response [20, 21]. Conversely, cells undergo necrosis after membrane injury or infection. Necrosis is associated with the loss of membrane integrity and the release of danger associated molecular patterns (DAMPs) from the intracellular contents. DAMPs, such as monosodium urate precipitated from uric acid and host DNA, are recognized by pattern recognition receptors on antigen presenting cells and stimulate the inflammasome and subsequently adaptive immune responses [21, 22]. Literature reveals a multitude of pathways that can initiate cell death, therefore both the trigger and the means by which cell death is communicated can have a significant impact on the resultant immune response [21]. Thus, lipid organization and disruption can play a large role in potentiating immune responses, and understanding how adjuvants may interact with membrane lipids and their associated signaling pathways may improve our understanding of their mechanisms of action.

2. Membrane interactions of adjuvants

2.1 Aluminum-based adjuvants

Despite their abundance, the mechanisms of action of aluminum-based adjuvants (ABAs) remain elusive. There are many forms of ABAs including alum, referring to hydrated potassium aluminum sulfate, aluminum oxyhydroxide (Alhydrogel), aluminum hydroxyphosphate (Adju-Phos), and the experimentally used combination of magnesium hydroxide and aluminum hydroxycarbonate (Imject) (**Fig 3**). Particularly in the case of Imject, the differences in composition could contribute to the disparities in reported mechanisms of action, and thus mechanisms reviewed here will be limited to the clinically relevant Alhydrogel and Adju-Phos [23, 24]. Particulate aluminum salts possess a high charge density and typically electrostatically adsorb antigens to their surface. However, aluminum adjuvants with surface hydroxyls are also capable of forming covalent bonds with antigens that possess phosphate groups. Aluminum has a higher affinity for phosphate groups than hydroxyl groups, therefore phosphate groups can displace surface hydroxyls to create an inner-sphere surface complex with aluminum and effectively

create a covalent bond [25, 26]. Upon injection and exposure to the interstitial fluid, antigens associated to ABAs via weaker electrostatic interactions tend to release faster, whereas antigens that are bound to the ABA may not release at all depending on their degree of phosphorylation and ligand exchange [25, 27, 28].

Early hypotheses regarding ABA mechanisms of action proposed formation of a depot at the injection site which slowly released antigen, but the necessity of depot formation has since been contradicted given the strong antigen-specific antibody response that occurs even after immediately excising the injection site [29]. ABAs have consistently been observed to promote immune cell recruitment to the injection site, antigen uptake, and migration to the draining lymph nodes [30, 31]. The particulate nature of ABAs is credited with enhancing antigen uptake, as aluminum-adsorbed antigen can be several hundred nanometers or in the micrometer range, allowing them to more efficiently be taken up by antigen presenting cells like dendritic cells (DCs) and macrophages [32]. However, the call to take up antigen is suspected to be linked to ABA-induced inflammation. In fact, inflammation may be a significant part of ABA's adjuvanticity.

ABAs can induce local irritation in muscle tissue, which produces pro-inflammatory cytokines, chemokines, and radical oxygen species resulting in cell damage and, most commonly, necrosis (**Fig 2**) [22, 33, 34]. Release of extracellular contents after necrosis produces danger-associated molecular patterns (DAMPs). After ABA administration, DAMPs such as uric acid, ATP, and host DNA are commonly observed [35] and can activate the NLRP3 inflammasome. NLRP3 activation (and its necessity for ABA adjuvanticity) has been detailed and debated extensively elsewhere [36]. Although the initiation of the inflammasome pathway and its involvement in ABA adjuvanticity remains controversial, the disruption of lipid membranes to release cytoplasmic or phagosomal contents appears to be important in its activation. Seminal papers on NLRP3's role in ABA's adjuvanticity propose the adjuvants may indirectly activate NLRP3 via release of MSU and ATP, or may directly activate it by disrupting the phagolysosome after uptake, subsequently releasing cathepsin B into the cytoplasm [22-24, 37, 38]. Although not

frequently considered, the nanoscale interaction between aluminum adjuvants and membrane lipids could provide insight to this and other membrane-associated mechanisms of action.

Inflammasome activation necessitates phagocytosis of the ABA vaccine particle, but it is possible ABAs exert their adjuvanticity without entering an antigen presenting cell (APC). Adjuvants are generally accepted to enhance particle phagocytosis by APCs, indeed ABA uptake has been observed in several macrophage and dendritic cell cultures [31, 39-41], but in a publication by Flach and Ng *et. al.*, aluminum-based adjuvants reportedly potentiated immune responses via association with the dendritic cell membrane. Experiments using pronase-treated DC2.4 cells and an aluminum adjuvant-modified AFM tip revealed ABAs did not have a receptor, but had high affinity for sphingomyelin and cholesterol, the major components of lipid rafts, which mediated its strong interaction with the membrane. Lipid engagement induced lipid sorting and signaling typically associated with phagocytosis, but contrary to previous observations, the adjuvant particle was not phagocytosed. Instead, antigen was delivered by endocytic uptake and was still processed and presented on MHC II. Lipid sorting induced phagocytic-signaling by the ITAM-Syk-PI3K pathway, and not the NLRP3 inflammasome, and activated DCs that engaged and activated CD4^{+} T cells [42, 43]. Despite their report that DCs do not phagocytose ABAs, it is worthwhile to note the authors acquiesced both the detection of intracellular aluminum, and the abortive phagocytosis observed may be unique to their experimental conditions [42]. Additionally, the lack of phagocytosis in the immortalized DC cell line was based on Imject or cesium aluminum crystals, which have drastically different composition and crystal morphology compared to clinically-relevant ABAs (**Fig 3**). Though experiments which used both Imject or cesium aluminum and an aluminum hydroxide adjuvant showed comparable results.

The ability of aluminum adjuvants to sort membrane lipids, particularly lipid-raft relevant lipids, and initiate signaling offers additional insight into mechanisms. Studies in Langmuir troughs using synthetic zwitterionic lipid monolayers, typically considered to have low ABA-affinity [42, 44], revealed surface activity of both Alhydrogel and Adju-Phos. Each adjuvant was observed to interact with the

DPPC:DOPC monolayer and promote the formation of liquid-ordered (L_o) domains, although they appeared to do so differently. Whereas the negatively-charged Adju-Phos facilitated the organization of large, condensed domains without compromising the integrity of the monolayer, positively-charged Alhydrogel promoted domain-clustering to a point, after which its proposed insertion in the monolayer interrupted lipid packing leading to the monolayer's collapse [44]. Furthermore, in lipid systems composed of an equimolar ratio of POPC:POPE:Sphingomyelin:Cholesterol, compared to the lipid alone both Alhydrogel and Adju-Phos stabilized the presence of condensed L_o domains similar in composition to lipid rafts, even in the presence of antigen (*Antúnez et. al. manuscript in preparation*). Basal phosphorylation of raft-resident proteins with immunoreceptor tyrosine-based activation motifs (ITAM) is observed in DCs [45]. Therefore ABA-induced clustering of raft-associated phosphorylated ITAMs or resident intracellular proteins could propagate signaling cascades leading to activation. Thus, lipid-sorting-induced signaling could indeed be part of the mechanism of action of aluminum adjuvants.

Aluminum adjuvants most likely interact with membrane lipids predominantly via ligand exchange and electrostatic interactions. As detailed earlier, phospholipids are the major lipid component of the plasma membrane and possess phosphate moieties in their head groups [3]. The phosphate group may undergo ligand exchange with available hydroxyl groups on the surface of aluminum adjuvants and form a covalent bond [46]. In fact, novel adjuvant formulations have capitalized on the Alhydrogel-phospholipid association to deliver poorly soluble TLR-ligands on ABAs by first encapsulating them in PC- or PG-based liposomes [47, 48]. Conceivably, the ABA-phospholipid bond is less productive in the cell membrane and could disrupt lipid packing or remove lipid from the membrane, causing the cell damage that has been observed with ABAs. Ligand exchange is possible even in the presence of repulsive charges [25]; however, complementary electrostatic interactions are the more common mode of ABA adsorption and a likely mechanism of lipid interaction. The association of charged particles with synthetic and natural lipid membranes and the ensuing changes in lipid packing have been well documented [49, 50]. For instance, in single-component PC bilayer vesicles, negatively charged nanoparticles were

observed to interact with the N^+ terminus of the headgroup and caused local gelling of otherwise fluid lipids by promoting an extended orientation of the zwitterionic head group, aligning the head group with the lipid tails and allowing them to pack more closely (**Fig 4**). Conversely, positively charged nanoparticles preferentially interacted with the phosphate group and oriented the headgroup at a greater angle from the lipid tails, providing greater space between the lipids and locally fluidizing otherwise gelled membranes [51]. Interestingly, cationic particles are frequently observed to form holes in both synthetic and cellular lipid membranes [49]. Likewise, charged ABAs have been observed to alter membrane packing, and has been offered as part of its mechanism of action.

Aluminum adjuvants are not the only particle structures capable of promoting non-receptor-meditated inflammation and activation. MSU crystals were also discovered to have strong affinity for cholesterol, allowing them to strongly interact with DC membranes resulting in their activation. MSU-cholesterol binding also induced clustering of lipid rafts and ITAM-receptors resulting in the same Syk and PI3K signaling observed in the aluminum studies. Contrary to some reports on aluminum adjuvants discussed above [42], MSU particles were successfully phagocytosed. In the same study, latex beads were also found to similarly potentiate binding and activation of DCs, but basic calcium phosphate and allopurinol did not have membrane interaction, consistent with reports that these crystals do not activate DCs [45]. These data would suggest selective, particulate-initiated interactions may be sufficient to engage innate immune pathways or transmit activating signals across the membrane. Therefore, the nature of a particle's interaction with membrane lipids and the resulting lipid sorting or damage could be a valuable consideration in selecting adjuvant surface properties and tuning immune responses.

2.2 Emulsions

Emulsions also have a long history as adjuvants, and their hydrophobic properties promote nonspecific interactions with lipid membranes. Among the earliest and most-used of these emulsions are Freund's adjuvants. Freund's adjuvants are water-in-oil adjuvants composed of non-metabolizable mineral oil and mannide monooleate surfactant. Alone these components are referred to as Incomplete

Freund's Adjuvant, and become Complete Freund's Adjuvant with the addition of mycobacteria. The viscous adjuvant is thought to create strong antibody responses by forming a depot at the injection site, protecting and slowly releasing the antigen while stimulating local innate immune responses [52]. Although later iterations of Freund's adjuvants are more tolerable, the emulsion was determined to be unacceptable for use in humans due to severe reactions at the injection site such as abscesses, granulomas, and ulcerative necrosis [52, 53]. IFA reactivity was partially attributed to the heterogeneous chain lengths of the hydrocarbons that make up mineral oil, as well as mannide monooleate. Mannide monooleate can produce toxic fatty acids, and shorter chain lengths (<C14) present in the mineral oil are associated with injection-site reactivity and have detergent-like effects which can disrupt the cell membrane, resulting in cell lysis [33, 54, 55]. Although precluded from use in humans, Freund's adjuvants continue to be used in veterinary vaccines [56].

Likewise, saponin-based adjuvants are common in veterinary vaccines and have known membrane-disrupting properties. Saponins are isolated from a variety of natural sources, and as such they are a heterogeneous family which produces a range of immunostimulatory effects, but the most common fraction is isolated from the bark of the *Quillaja saponaria* tree, QS21 [56-60]. Saponins are proposed to exert their adjuvant effect through the induction of cytokines [56], but they are also capable of forming irreparable gaps in the cell membrane via interaction with cholesterol [56, 58]. Saponins may interact with the polar heads of phospholipids or the hydroxyl groups of cholesterol to create insoluble aggregates which permeabilize the membrane and may allow endocytosis of the antigen or cell lysis [33, 56, 58]. QS-21, although less toxic than other saponins, still has hemolytic activity which is attributed to its fatty acid moiety [57]. To mitigate its reactivity but maintain its strong action as an adjuvant, QS21 and other saponin fractions have been formulated in liposomes or emulsions (i.e. AS01, AS02, ISCOMs) which typically include phospholipids or cholesterol to intercept its membrane activity [56, 60, 61]. Immune stimulating complexes (ISCOMs) have also been observed to destabilize the endosomal membrane [62]. Progress has been made in making both saponin-based and Freund's adjuvants more tolerable, allowing

their use in veterinary vaccines; however, successful emulsion adjuvants used in humans thus far have been based on metabolizable oils.

2.3 MF59

MF59 is an oil-in-water emulsion based on metabolizable squalene. The emulsion is composed of squalene droplets 150-200 nm in diameter stabilized by the non-ionic surfactants Span 85 and Polysorbate 80 suspended in citrate buffer [63]. Although approved for use in Europe since 1998, it only recently gained FDA approval in 2015 for use in the seasonal flu vaccine, Fluad. Unlike the ABAs, MF59 does not associate with the antigen, which is typically present in the aqueous phase. The mechanism of action of MF59 is also poorly understood, but it appears to begin its adjuvant effect in the local muscle tissue where the release of chemokines and cytokines is initiated. Waves of immune cells are attracted to the injection site and add to the "immunocompetent environment" which promotes antigen uptake, migration of antigen-loaded antigen presenting cells (APCs) to the draining lymph nodes, differentiation of monocytes to DCs, and strong adaptive immune responses [63].

MF59 may be able to achieve this environment by easily interacting with many cell types. The adjuvant was observed to enhance all forms of endocytosis, and it was visually confirmed to enter both APCs, like monocytes, macrophages, and DCs, and muscle tissue cells like fibroblasts and myotubes [64, 65]. In fact, MF59 interaction with ATP-rich muscle fibers appears to be an important part of its mechanism of action. The release of ATP at the injection site is critical to MF59's adjuvanticity as consumption of MF59-induced ATP using apyrase abrogated its ability to recruit cells and create robust antibody titers [65, 66]. Interestingly, despite a study showing no individual component of MF59 could produce the full adjuvant effect of the whole formulation, the surfactants present in the MF59 formulation were necessary for ATP release [66, 67].

Surfactants by nature are typically amphiphilic and many surfactants easily incorporate into membranes. Although Span 85 and Polysorbate 80 may not be solely responsible for the adjuvant effect of MF59, their ability to interact with the cell membrane can still initiate some immune response [66]. In

cases of cell death, surfactants can permeabilize the cell membrane leading to necrosis, apoptosis, or cell cycle arrest in a surfactant- and concentration-dependent manner [19]. Evidence of MF59-induced necrosis in macrophages has been observed *in vitro* [31]. *In vivo*, apoptotic macrophages were found to activate DCs in the lymph node with the help from the pro-inflammatory milieu [68]. Interestingly, although MF59 uptake leads to ATP and DAMP release, MF59 was found to exert its adjuvanticity in a NLRP3 inflammasome-independent manner [66, 69, 70]. In fact, MF59 reportedly does not disrupt the lysosome, but rather acidifies and stabilizes it [65].

Even if surfactant-interaction does not lead to cell death, uptake and metabolism of the surfactants and squalene can increase accumulation of neutral lipids and inflammation [65]. Significant MF59 uptake was observed in the aforementioned APCs and muscle cells, and high- and low-density lipid inclusions were observed, indicative of metabolized and engulfed MF59, respectively (**Fig 5**) [31, 65]. Squalene is a precursor of cholesterol, and while it did not increase total cholesterol levels in cells, it did increase the levels of cholesterol metabolites. Likewise, oleic acid metabolites from Polysorbate 80 likely contributed to the increase in triglycerides. Notably, a "massive" accumulation of diacylglycerols (DAGs) was observed in MF59-treated cells, which was also speculated to be a result of surfactant metabolites [65]. Accumulation of DAGs is particularly interesting as they are important signaling lipids in the immunological synapse [3, 65]. Overall, the buildup of neutral lipids including squalene have been shown to have pro-inflammatory and pro-apoptotic properties and may be able to activate innate signaling pathways [65].

While the exact mechanism of lipid interaction requires more investigation, the surfactant content and hydrophobic nature of MF59 facilitates its interaction with the plasma membrane. Permeabilization of the membrane by surfactants could expose phosphatidylserine in apoptotic cells or release DAMPs in necrotic cells, all of which would recruit and promote uptake by APCs. Alternatively, ATP release is also a product of phagocytosis, and emulsion metabolism within the cell has been proven to initiate a slew of

immune activating signals, which could complement any danger-associated signaling. Therefore, the role of lipids in the mechanism of MF59 could be multifaceted.

3. Concluding Remarks

The cell membrane is an exceedingly complex surface we are only beginning to appreciate as our ability to study it improves. Lipids play a major role in initiating and propagating immune responses by providing an organizing platform for signaling molecules, or by serving as signaling molecules themselves in the immunological synapse or in cell damage and death. Receptor-mediated pathways are undeniably instrumental in potentiating immunity; however, non-specific membrane interactions (i.e. charge, hydrophobic interactions, specific lipid affinity) may point to the most fundamental means by which cells can detect and react to their surroundings.

Both aluminum-based and emulsion adjuvants are capable of interacting with lipids in the cell membrane, and there is strong evidence to support this interaction could contribute to their mechanisms of action. Disparities in the observed mechanisms of action reported in the literature may even be attributed to membrane interactions. For instance, while one aluminum adjuvant may promote local lipid domain formation, organization, and activation via electrostatic interactions, a different concentration or aluminum adjuvant may lead to greater binding of phosphate groups in phospholipids leading to membrane damage and a separate immune signaling pathway. In the case of emulsions, the concentration and selection of surfactants can influence whether the droplets are endocytosed and processed or induce cell lysis. Additionally, metabolism of fatty acid chains in emulsions can lead to the formation of new lipid species which can both up- and down- regulate immune activation [3]. Interestingly, non-specific hydrophobic interactions with membrane receptors could also have some role in how emulsions work. Although MF59, IFA, and saponin emulsions have all been shown to function independent of TLR activation, all these adjuvants show overlap with TLR gene products or signaling pathways [53, 60, 62, 69, 71]. Both TLR2 and TLR4 are reportedly promiscuous receptors and can be activated by several hydrophobic structures [72], highlighting that non-specific interactions not only with the membrane, but

with membrane bound receptors may contribute to adjuvant mechanisms. Therefore, although the cell membrane is often overlooked, lipid-adjuvant interactions warrant greater attention. The lessons learned with current adjuvants can be used to our advantage to synthesize and formulate novel adjuvants which improve our ability to tune desired immune responses.

Table 1. Examples of adjuvants with known membrane activity

Adjuvant	Class	Examples	Membrane interaction	Immune-activating effects	Ref
Aluminum Salts	Particulate	Alhydrogel, Adju-Phos	Charge interactions, Phospholipid ligand exchange, Affinity for sphingomyelin & cholesterol	Membrane damage/necrosis, ROS formation by surface hydroxyls, Lipid sorting and clustering (particularly lipid rafts)	[34] [42, 73] [44]
Emulsions	Oil-in-water emulsion	MF59, AS03	Hydrophobic interactions	Necrosis following membrane permeabilization/detergent effects of surfactants/short chain fatty acids, Accumulation of neutral lipids, Uptake by non-phagocytic cells	[66] [67] [19] [31]
	Water-in-oil emulsion	Freund's Adjuvants	Hydrophobic Interactions		[33] [54] [55]
Saponins	Liposomes, Emulsions	AS01, AS02, ISCOM/ ISCOMATRIX	Affinity for cholesterol	Aggregates with cholesterol and forms holes in plasma membrane	[57] [74] [56] [61] [60]
Monosodium Urate	Particulate, Crystal		Affinity for cholesterol	Lipid raft clustering	[45]

Phospholipid	Chemical Moiety (X)	Net Charge at pH7	Shape volume
Phosphatidylcholine (PC)		0	
Phosphatidylserine (PS)		-1	
Phosphatidylglycerol (PG)		-1	Cylindrical
Phosphatidylethanolamine (PE)		0	
Phosphatidic acid (PA)		-1	Inverted Cone
Phosphatidylinositol (PI)		-1	Cone
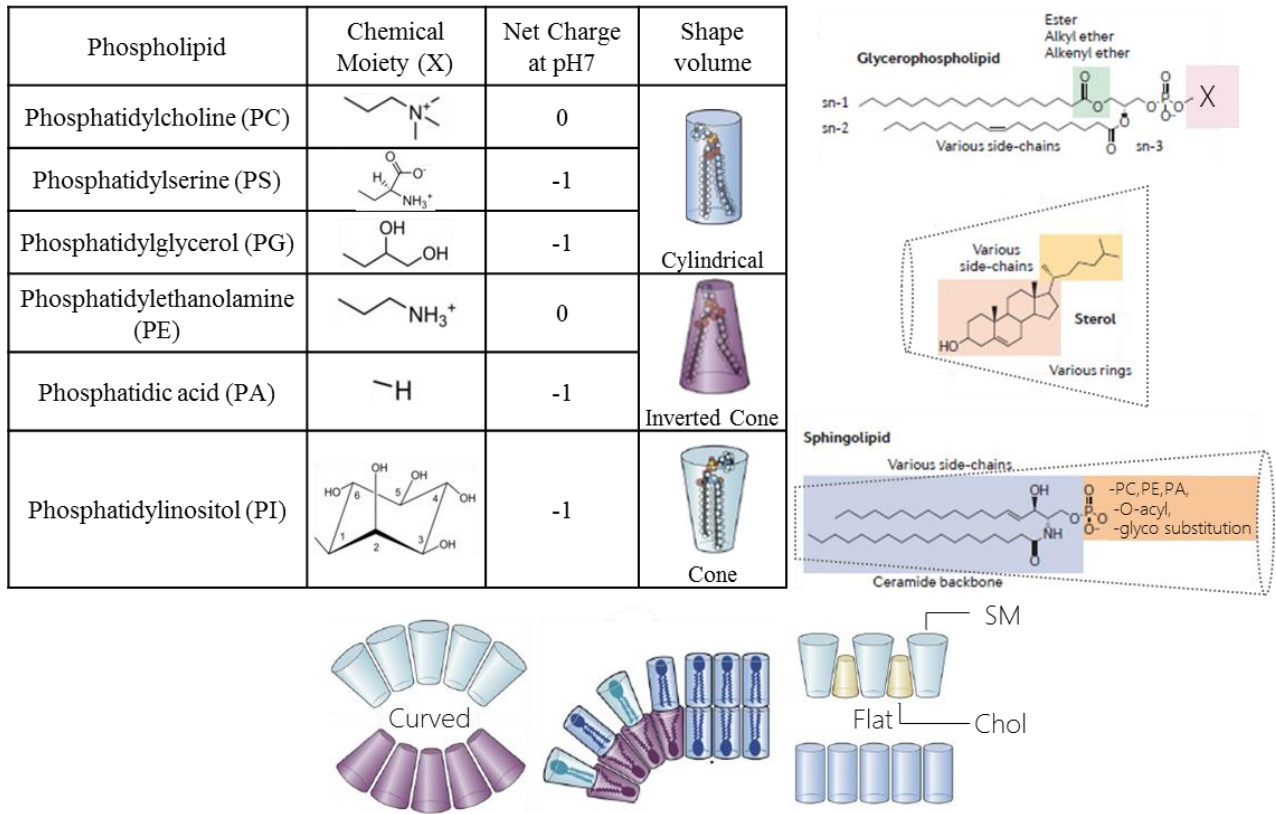
Figure 1. Diversity in lipid structures. Cells can generate a wide array of glycerophospholipid and sphingolipid species by linking different chemical moieties to their common phosphate base at the sn-3 position. Fatty acid side chains of variable length and saturation add further lipid heterogeneity. Common molecular-shape volumes occupied by each lipid are shown, as well the lipid polymorphisms produced by their assembly. The shape volumes commonly associated with sterols and sphingolipids are inverted cone and cone, respectively. SM, sphingomyelin; Chol, cholesterol. Figure adapted from [3], [5, and [75]
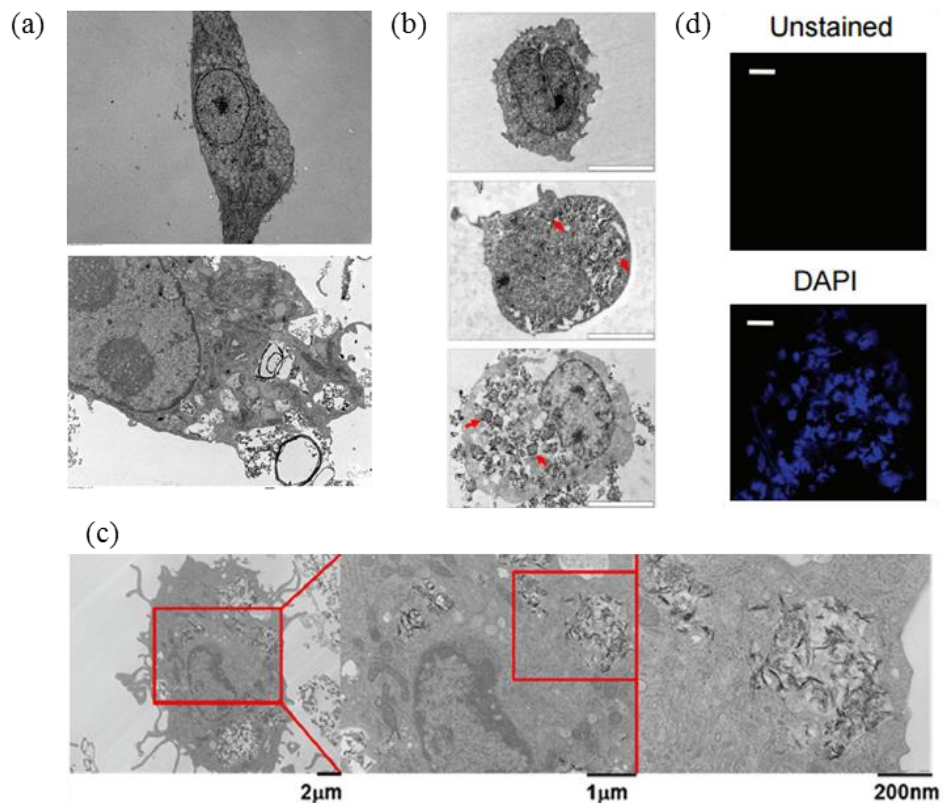
Figure 2. Evidence of membrane damage after exposure to aluminum adjuvants. Loss of membrane integrity has been observed in (a) dendritic cells [42], (b) THP-1-derived macrophages exposed to 50 µg/mL (middle) or 200 µg/mL AlO(OH) [39], and (c) bone-marrow derived macrophages cultured with aluminum adjuvants [31]. (d) Extracellular accumulation of DNA was also observed at the injection site after intramuscular injection with aluminum hydroxide adjuvant [35].
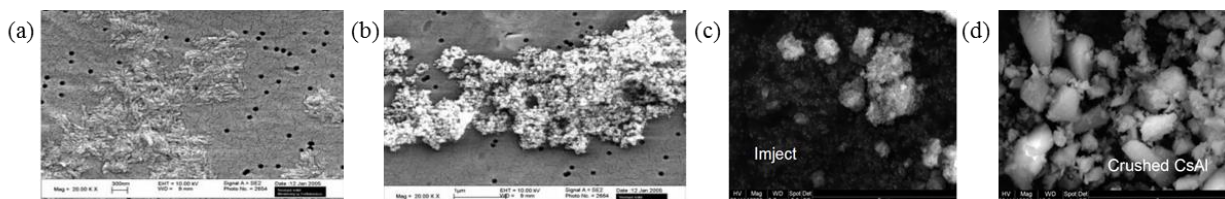
Figure 3. TEM images showing the structure of (a) Alhydrogel, (b) Adju-Phos, (c) Imject, and (d) cesium aluminum adjuvants. (a) and (b) adapted from [76], (c) and (d) from [42]
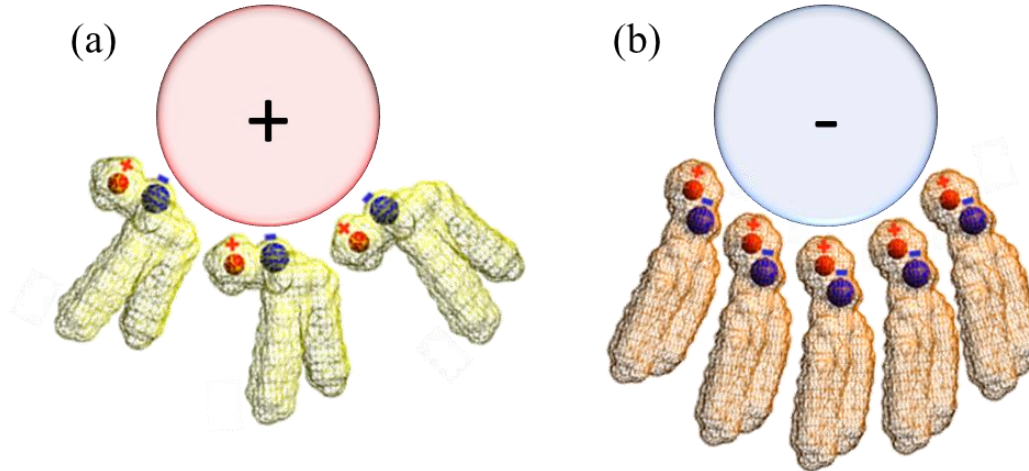
Figure 4. Charged particles reorient phospholipid heads and alter lipid packing. (a) Positively charged nanoparticles promote a more extended orientation of the PC head, preventing lipids from packing as tightly, creating a more fluid membrane. (b) Negatively charged particles prefer to interact with the positive terminus of the PC head, lengthening the phospholipid and allowing the lipids to pack more densely, creating a more solid or gelled membrane. Figure adapted from [51]
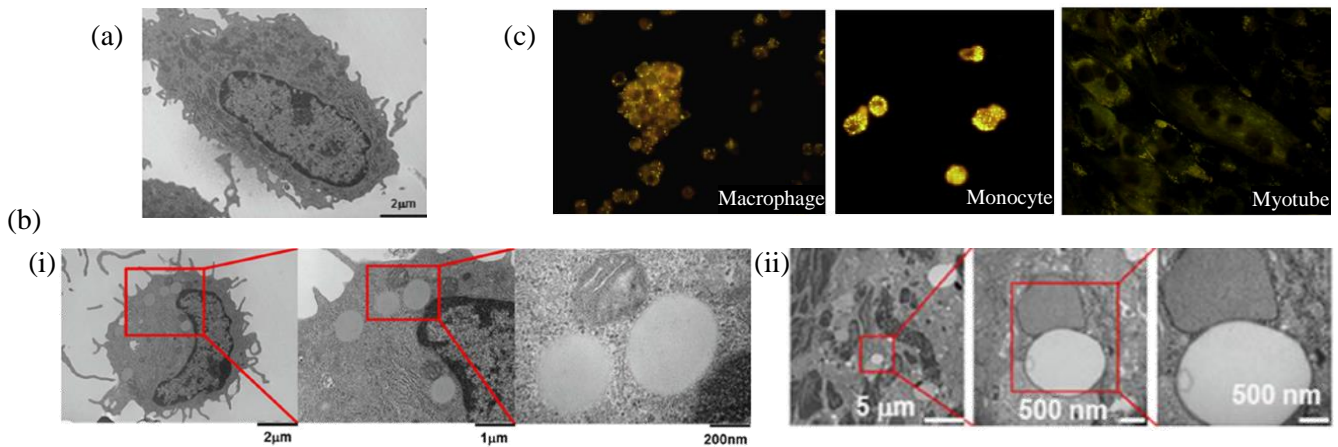
Figure 5. MF59 uptake and metabolism in various cells. (a) An untreated bone marrow-derived macrophage (BMM). (b) Dark, high-electron dense bodies indicative of lipid metabolism and brighter, low-electron dense bodies indicative of engulfed MF59 are observed (i) in single BMMs and (ii) in the lymph nodes of mice. Images adapted from [31]. (c) Neutral lipid accumulation in macrophages, monocytes, and myotubes after incubation with MF59. Images adapted from [31, 65].

References

1.   Leroux-Roels, G., *Unmet needs in modern vaccinology: adjuvants to improve the immune response.* Vaccine, 2010. **28 Suppl 3**: p. C25-36.
2.   Reed, S.G., M.T. Orr, and C.B. Fox, *Key roles of adjuvants in modern vaccines.* Nat Med, 2013. **19**(12): p. 1597-608.
3.   Wu, W., X. Shi, and C. Xu, *Regulation of T cell signalling by membrane lipids.* Nat Rev Immunol, 2016. **16**(11): p. 690-701.
4.   Koberlin, M.S., et al., *A Conserved Circular Network of Coregulated Lipids Modulates Innate Immune Responses.* Cell, 2015. **162**(1): p. 170-83.
5.   Peetla, C., S. Vijayaraghavalu, and V. Labhasetwar, *Biophysics of cell membrane lipids in cancer drug resistance: Implications for drug transport and drug delivery with nanoparticles.* Adv Drug Deliv Rev, 2013. **65**(13-14): p. 1686-98.
6.   Head, B.P., H.H. Patel, and P.A. Insel, *Interaction of membrane/lipid rafts with the cytoskeleton: impact on signaling and function: membrane/lipid rafts, mediators of cytoskeletal arrangement and cell signaling.* Biochim Biophys Acta, 2014. **1838**(2): p. 532-45.
7.   Simons, K. and D. Toomre, *Lipid rafts and signal transduction.* Nat Rev Mol Cell Biol, 2000. **1**(1): p. 31-9.
8.   Lingwood, D. and K. Simons, *Lipid rafts as a membrane-organizing principle.* Science, 2010. **327**(5961): p. 46-50.
9.   Anderson, H.A. and P.A. Roche, *MHC class II association with lipid rafts on the antigen presenting cell surface.* Biochim Biophys Acta, 2015. **1853**(4): p. 775-80.
10.   Triantafilou, M., et al., *Location, location, location: is membrane partitioning everything when it comes to innate immune activation?* Mediators Inflamm, 2011. **2011**: p. 186093.
11.   Varshney, P., V. Yadav, and N. Saini, *Lipid rafts in immune signalling: current progress and future perspective.* Immunology, 2016. **149**(1): p. 13-24.
12.   Dykstra, M., et al., *Location is everything: lipid rafts and immune cell signaling.* Annu Rev Immunol, 2003. **21**: p. 457-81.
13.   Tanimura, N., et al., *Dynamic changes in the mobility of LAT in aggregated lipid rafts upon T cell activation.* J Cell Biol, 2003. **160**(1): p. 125-35.
14.   Cuschieri, J., J. Billigren, and R.V. Maier, *Endotoxin tolerance attenuates LPS-induced TLR4 mobilization to lipid rafts: a condition reversed by PKC activation.* J Leukoc Biol, 2006. **80**(6): p. 1289-97.
15.   Gupta, N. and A.L. DeFranco, *Visualizing lipid raft dynamics and early signaling events during antigen receptor-mediated B-lymphocyte activation.* Mol Biol Cell, 2003. **14**(2): p. 432-44.
16.   Zech, T., et al., *Accumulation of raft lipids in T-cell plasma membrane domains engaged in TCR signalling.* EMBO J, 2009. **28**(5): p. 466-76.
17.   Owen, D.M., et al., *High plasma membrane lipid order imaged at the immunological synapse periphery in live T cells.* Mol Membr Biol, 2010. **27**(4-6): p. 178-89.
18.   Sohn, H.W., P. Tolar, and S.K. Pierce, *Membrane heterogeneities in the formation of B cell receptor-Lyn kinase microclusters and the immune synapse.* J Cell Biol, 2008. **182**(2): p. 367-79.
19.   Yang, Y.W., C.A. Wu, and W.J. Morrow, *Cell death induced by vaccine adjuvants containing surfactants.* Vaccine, 2004. **22**(11-12): p. 1524-36.
20.   *Vaccine Supplement Glossary.* Vaccine, 2010. **28**(S3): p. C37-C40.
21.   Yatim, N., S. Cullen, and M.L. Albert, *Dying cells actively regulate adaptive immune responses.* Nat Rev Immunol, 2017. **17**(4): p. 262-275.
22.   Oleszycka, E. and E.C. Lavelle, *Immunomodulatory properties of the vaccine adjuvant alum.* Curr Opin Immunol, 2014. **28**: p. 1-5.
23.   Marrack, P., A.S. McKee, and M.W. Munks, *Towards an understanding of the adjuvant action of aluminium.* Nat Rev Immunol, 2009. **9**(4): p. 287-93.

24. Hogenesch, H., *Mechanism of immunopotentiation and safety of aluminum adjuvants.* Front Immunol, 2012. **3**: p. 406.

25. Hem, S.L. and H. Hogenesch, *Relationship between physical and chemical properties of aluminum-containing adjuvants and immunopotentiation.* Expert Rev Vaccines, 2007. **6**(5): p. 685-98.

26. Giese, M., *Molecular Vaccines: From Prophylaxis to Therapy.* 2013: Springer International Publishing.

27. Hansen, B., et al., *Relationship between the strength of antigen adsorption to an aluminum-containing adjuvant and the immune response.* Vaccine, 2007. **25**(36): p. 6618-24.

28. Iyer, S., H. HogenEsch, and S.L. Hem, *Effect of the degree of phosphate substitution in aluminum hydroxide adjuvant on the adsorption of phosphorylated proteins.* Pharm Dev Technol, 2003. **8**(1): p. 81-6.

29. Hutchison, S., et al., *Antigen depot is not required for alum adjuvanticity.* FASEB J, 2012. **26**(3): p. 1272-9.

30. Mosca, F., et al., *Molecular and cellular signatures of human vaccine adjuvants.* Proc Natl Acad Sci U S A, 2008. **105**(30): p. 10501-6.

31. Giusti, F., et al., *Ultrastructural Visualization of Vaccine Adjuvant Uptake In Vitro and In Vivo.* Microsc Microanal, 2015. **21**(4): p. 791-5.

32. Bachmann, M.F. and G.T. Jennings, *Vaccine delivery: a matter of size, geometry, kinetics and molecular patterns.* Nat Rev Immunol, 2010. **10**(11): p. 787-96.

33. Batista-Duharte, A., E.B. Lindblad, and E. Oviedo-Orta, *Progress in understanding adjuvant immunotoxicity mechanisms.* Toxicol Lett, 2011. **203**(2): p. 97-105.

34. Kool, M., et al., *Alum adjuvant boosts adaptive immunity by inducing uric acid and activating inflammatory dendritic cells.* J Exp Med, 2008. **205**(4): p. 869-82.

35. Marichal, T., et al., *DNA released from dying host cells mediates aluminum adjuvant activity.* Nat Med, 2011. **17**(8): p. 996-1002.

36. Lebre, F., C.H. Hearnden, and E.C. Lavelle, *Modulation of Immune Responses by Particulate Materials.* Adv Mater, 2016. **28**(27): p. 5525-41.

37. Eisenbarth, S.C., et al., *Crucial role for the Nalp3 inflammasome in the immunostimulatory properties of aluminium adjuvants.* Nature, 2008. **453**(7198): p. 1122-6.

38. Hornung, V., et al., *Silica crystals and aluminum salts activate the NALP3 inflammasome through phagosomal destabilization.* Nat Immunol, 2008. **9**(8): p. 847-56.

39. Mold, M., et al., *Unequivocal identification of intracellular aluminium adjuvant in a monocytic THP-1 cell line.* Sci Rep, 2014. **4**: p. 6287.

40. Morefield, G.L., et al., *Role of aluminum-containing adjuvants in antigen internalization by dendritic cells in vitro.* Vaccine, 2005. **23**(13): p. 1588-95.

41. Mile, I., et al., *Al adjuvants can be tracked in viable cells by lumogallion staining.* J Immunol Methods, 2015. **422**: p. 87-94.

42. Flach, T.L., et al., *Alum interaction with dendritic cell membrane lipids is essential for its adjuvanticity.* Nat Med, 2011. **17**(4): p. 479-87.

43. Mbow, M.L., E. De Gregorio, and J.B. Ulmer, *Alum's adjuvant action: grease is the word.* Nat Med, 2011. **17**(4): p. 415-6.

44. Antunez, L.R., et al., *Physiochemical Properties of Aluminum Adjuvants Elicit Differing Reorganization of Phospholipid Domains in Model Membranes.* Mol Pharm, 2016. **13**(5): p. 1731-7.

45. Ng, G., et al., *Receptor-independent, direct membrane binding leads to cell-surface lipid sorting and Syk kinase activation in dendritic cells.* Immunity, 2008. **29**(5): p. 807-18.

46. Zhao, Q. and R. Sitrin, *Surface phosphophilicity of aluminum-containing adjuvants probed by their efficiency for catalyzing the P--O bond cleavage with chromogenic and fluorogenic substrates.* Anal Biochem, 2001. **295**(1): p. 76-81.

47.   Fox, C.B., et al., *Adsorption of a synthetic TLR7/8 ligand to aluminum oxyhydroxide for enhanced vaccine adjuvant activity: A formulation approach.* J Control Release, 2016. **244**(Pt A): p. 98-107.

48.   Fox, C.B., *Characterization of TLR4 agonist effects on alhydrogel(R) sedimentation: a novel application of laser scattering optical profiling.* J Pharm Sci, 2012. **101**(11): p. 4357-64.

49.   Verma, A. and F. Stellacci, *Effect of surface properties on nanoparticle-cell interactions.* Small, 2010. **6**(1): p. 12-21.

50.   Nel, A.E., et al., *Understanding biophysicochemical interactions at the nano-bio interface.* Nat Mater, 2009. **8**(7): p. 543-57.

51.   Wang, B., et al., *Nanoparticle-induced surface reconstruction of phospholipid membranes.* Proc Natl Acad Sci U S A, 2008. **105**(47): p. 18171-5.

52.   Apostolico Jde, S., et al., *Adjuvants: Classification, Modus Operandi, and Licensing.* J Immunol Res, 2016. **2016**: p. 1459394.

53.   O'Hagan, D.T. and E. De Gregorio, *The path to a successful vaccine adjuvant--'the long and winding road'.* Drug Discov Today, 2009. **14**(11-12): p. 541-51.

54.   Aucouturier, J., et al., *Montanide ISA 720 and 51: a new generation of water in oil emulsions as adjuvants for human vaccines.* Expert Rev Vaccines, 2002. **1**(1): p. 111-8.

55.   Gupta, R.K., et al., *Adjuvants--a balance between toxicity and adjuvanticity.* Vaccine, 1993. **11**(3): p. 293-306.

56.   Singh, M. and D.T. O'Hagan, *Recent advances in veterinary vaccine adjuvants.* Int J Parasitol, 2003. **33**(5-6): p. 469-78.

57.   Sun, H.X., Y. Xie, and Y.P. Ye, *Advances in saponin-based adjuvants.* Vaccine, 2009. **27**(12): p. 1787-96.

58.   Francis, G., et al., *The biological action of saponins in animal systems: a review.* Br J Nutr, 2002. **88**(6): p. 587-605.

59.   Song, X. and S. Hu, *Adjuvant activities of saponins from traditional Chinese medicinal herbs.* Vaccine, 2009. **27**(36): p. 4883-90.

60.   Drane, D., et al., *ISCOMATRIX adjuvant for prophylactic and therapeutic vaccines.* Expert Rev Vaccines, 2007. **6**(5): p. 761-72.

61.   Dowling, D.J. and O. Levy, *Pediatric Vaccine Adjuvants: Components of the Modern Vaccinologist's Toolbox.* Pediatr Infect Dis J, 2015. **34**(12): p. 1395-8.

62.   Coffman, R.L., A. Sher, and R.A. Seder, *Vaccine adjuvants: putting innate immunity to work.* Immunity, 2010. **33**(4): p. 492-503.

63.   O'Hagan, D.T., et al., *The mechanism of action of MF59 - an innately attractive adjuvant formulation.* Vaccine, 2012. **30**(29): p. 4341-8.

64.   Seubert, A., et al., *The adjuvants aluminum hydroxide and MF59 induce monocyte and granulocyte chemoattractants and enhance monocyte differentiation toward dendritic cells.* J Immunol, 2008. **180**(8): p. 5402-12.

65.   Kalvodova, L., *Squalene-based oil-in-water emulsion adjuvants perturb metabolism of neutral lipids and enhance lipid droplet formation.* Biochem Biophys Res Commun, 2010. **393**(3): p. 350-5.

66.   Vono, M., et al., *The adjuvant MF59 induces ATP release from muscle that potentiates response to vaccination.* Proc Natl Acad Sci U S A, 2013. **110**(52): p. 21095-100.

67.   Calabro, S., et al., *The adjuvant effect of MF59 is due to the oil-in-water emulsion formulation, none of the individual components induce a comparable adjuvant effect.* Vaccine, 2013. **31**(33): p. 3363-9.

68.   Dupuis, M., et al., *Immunization with the adjuvant MF59 induces macrophage trafficking and apoptosis.* Eur J Immunol, 2001. **31**(10): p. 2910-8.

69.   Seubert, A., et al., *Adjuvanticity of the oil-in-water emulsion MF59 is independent of Nlrp3 inflammasome but requires the adaptor protein MyD88.* Proc Natl Acad Sci U S A, 2011. **108**(27): p. 11169-74.

70. Ellebedy, A.H., et al., *Inflammasome-independent role of the apoptosis-associated speck-like protein containing CARD (ASC) in the adjuvant effect of MF59.* Proc Natl Acad Sci U S A, 2011. **108**(7): p. 2927-32.
71. Lim, S.K., *Freund adjuvant induces TLR2 but not TLR4 expression in the liver of mice.* Int Immunopharmacol, 2003. **3**(1): p. 115-8.
72. Seong, S.Y. and P. Matzinger, *Hydrophobicity: an ancient damage-associated molecular pattern that initiates innate immune responses.* Nat Rev Immunol, 2004. **4**(6): p. 469-78.
73. Maughan, C.N., S.G. Preston, and G.R. Williams, *Particulate inorganic adjuvants: recent developments and future outlook.* J Pharm Pharmacol, 2015. **67**(3): p. 426-49.
74. Alving, C.R., et al., *Adjuvants for human vaccines.* Curr Opin Immunol, 2012. **24**(3): p. 310-5.
75. Li, J., et al., *A review on phospholipids and their main applications in drug delivery systems.* Asian Journal of Pharmaceutical Sciences, 2015. **10**(2): p. 81-98.
76. Lindblad, E.B., *13 - Mineral adjuvants A2 - Schijns, Virgil E.J.C*, in *Immunopotentiators in Modern Vaccines*, D.T. O'Hagan, Editor. 2006, Academic Press: London. p. 217-233.

Chapter II: Physiochemical Properties of Aluminum Adjuvants Elicit Differing Reorganization of Phospholipid Domains in Model Membranes

1. Introduction

Vaccines are a staple of modern, preventative medicine, and have become increasingly safer and more potent due in large part to the use of highly purified antigens and adjuvants. Adjuvants are regularly added to vaccine formulations to bolster the immune response to what are typically insufficiently reactive isolated antigens [1, 2]. The most common adjuvants, aluminum salts, have been in vaccines since 1926; yet, fairly little is known about their precise mechanism of action [3, 4]. The prevailing mechanism of action suggests aluminum-based adjuvant particles initiate "danger signals" or enhance receptor-mediated antigen uptake by antigen presenting cells, particularly dendritic cells (DCs), but Shi and co-workers recently offered a paradigm shift in aluminum interaction mechanisms [2-5]. Using DCs, Flach and Ng et al. showed the adjuvanticity of aluminum relied neither on inflammasome activation, receptors for the antigen, nor any receptor for aluminum [5, 6]. Instead, the authors proposed a novel mechanism after observing aluminum adjuvants can directly engage and reorganize lipids that form the major components of lipid rafts in membranes [1, 5, 7, 8]. However, details of colloidal, aluminum adjuvant-induced lipid organization remain unexplored and provide the main motivation for this study.

Elucidating the mechanisms of adjuvant-induced lipid reorganization in cellular membranes requires understanding the interactions between the adjuvant and individual phospholipids. In this study, we wished to elucidate if all major components of lipid rafts (namely sphingomyelin and cholesterol) were also essential for adjuvant-lipid interactions in model membranes. Therefore, in this study, we focused on adjuvant induced lipid clustering in zwitterionic phospholipid monolayers composed of saturated dipalmitoyl-phosphatidylcholine (DPPC) and unsaturated dioleoyl-phosphatidylcholine (DOPC). The choice of saturated and unsaturated PC lipids mimic the biphasic nature, as well as the major phospholipid headgroup of the outer leaflet of cell membranes. We compared the lipid domain clustering and reorganization induced by two common aluminum adjuvants, Alhydrogel and Adju-Phos. Alhydrogel (AH) contains crystalline, needle-like nanoparticles that form loose aggregates of approximately 15 μm, while Adju-Phos (AP) has an amorphous, plate-like structure with particles approximately 50 nm in diameter that form roughly 5 μm aggregates [3]. Furthermore, AH and AP are

24

positively and negatively charged, respectively, at physiological pH [2, 9-11]. Using both surface pressure-area isotherms and fluorescence imaging techniques, our results establish, for the first time, that colloidal, aluminum-based adjuvants are capable of reorganizing lipid ordered domains even in simple two-component zwitterionic phospholipid mixtures. However, each adjuvant organizes and condenses the lipid domains differently, likely due to differences in charge and morphology.

2. Materials and Methods

2.1 Materials

Lipid solutions contained a 1:1 ratio by weight of 1,2-dipalmitoyl-*sn*-glycero-3-phosphatidylcholine (DPPC) and 1,2-dioleoyl-*sn*-glycero-3-phosphatidylcholine (DOPC) (Avanti Polar Lipids, Alabaster, AL) suspended in high performance liquid chromatography grade chloroform (Fisher Scientific) to a total lipid concentration of 1 mg/mL. For imaging studies, the lipids were mixed with 1 wt% Texas Red -DHPE (Life Technologies, Carlsbad, CA). Alhydrogel 2% (AH) and Adju-Phos 2% (AP) were purchased from Sergeant Adjuvants (Clifton, NJ).

2.2 Surface Pressure-Area Isotherms

A Langmuir trough (KSV-NIMA-Biolin Scientific, Linthicum Heights, MD) was used to measure the interaction of the adjuvants with the lipid monolayers. DPPC:DOPC in chloroform was spread dropwise with a Hamilton microsyringe (Hamilton, Reno, NV) to form a monolayer on the surface of an ultrapure-distilled water subphase (18.2 MΩ/cm; Millipore, Billerica, MA) to a mean molecular area of approximately 90 Å^2/molecule. Water was used in these experiments to avoid any effects of free ions in a buffer solution interacting with the monolayer or the adjuvants. The monolayer at the air-water interface was compressed symmetrically at 25 mm/min using two Teflon barriers, decreasing the trough surface area from 87 cm^2 to 20 cm^2. The resulting changes in the pressure of the phospholipid film were recorded by a Wilhelmy plate pressure sensor. A wet filter paper was used as the pressure sensor probe and was calibrated using a bare air-water interface.

In adjuvant experiments, each adjuvant stock was mixed into the subphase prior to spreading the monolayer. A range of concentrations of adjuvants were initially tested, but surface pressure vs area isotherms of DPPC:DOPC films showed that changing the adjuvant concentration over several orders of magnitude minimally changed the compression isotherm (**Figure S3**). The working concentration for all studies was selected to be 0.03 mg Al/mL and remained well-suspended throughout the subphase during each experiment; no precipitated adjuvant particles were observed within the trough (**Figure S4**). The methods used to isolate and test the adjuvant suspension buffer and to create the aluminum ion solution are detailed in the supplementary information (Figure S1 and S2, respectively). Surface pressure vs. area isotherms were repeated at least three times for each experimental condition and the replicates of the surface pressure at each mean molecular area were averaged. GraphPad Prism was used to calculate and plot the averages and standard error of the mean (GraphPad, San Diego, CA).

2.3 Monolayer Compressibility Modulus

Monolayer compressibility modulus defines a Langmuir monolayer's ability to store the energy provided by an applied force, or the monolayer's ability to resist strain. Mathematically, the bulk compressibility modulus, β, is defined as

$$\beta = -A \frac{\partial \Pi}{\partial A}$$

High compressibility modulus indicates rigid monolayers due to limited motion of the highly ordered lipid molecules. Similarly lower values of the compressibility modulus are associated with fluid films. Because β is a derivative of the Gibbs free energy, G, a discontinuity in the slope of the compressibility modulus indicates a first order phase transition and appears as a dip in the profile. To more accurately identify aluminum adjuvant-induced changes in the mechanical properties of the monolayer, including phase transitions, the compressibility modulus was calculated from the surface pressure vs mean molecular area isotherms with the built-in differentiation tool available in Origin 8.6 (OriginLab, Northampton, MA). The raw data was smoothened by applying a five-point Fourier filter, also available in Origin.

2.4 Fluorescence Microscopy

Fluorescence microscopy was used to monitor changes in the morphology of the lipid domains in the presence of the aluminum adjuvants. The Langmuir trough was placed under a custom-modified Nikon Eclipse LV100 fluorescence microscope with an extra-long working distance lens and tube collimators that allow simultaneous imaging of the phospholipid film during monolayer compression. Images of the lipid monolayers were captured throughout the compression cycle using an Andor Luca S camera and Solis software (Belfast, Ireland). The morphology of the lipid films is visible in fluorescence imaging due to selective segregation of the bulky Texas Red-DHPE dye molecules into fluid lipid phases.

2.5 Image Analysis

The area of each condensed lipid domain was analyzed using the "Analyze Particles" tool in ImageJ (National Institutes of Health, Bethesda, MD). Only particles with circularities between 0.1 and 1 were analyzed to exclude any background noise, and edges were excluded from analysis. The detected particle areas were organized and plotted as a normalized histogram in Origin 8.6. The number of bins, calculated as the square root of the number of measured domains, was used to assign bin widths. Adjuvant-induced condensation of lipid domains was based on the percent area of the image composed of dark domains and was calculated as the total area of condensed domains divided by the total area of the image.

3. Results and Discussion

Figure 1 presents representative surface pressure vs area compression isotherms of a DPPC:DOPC monolayer in the absence (solid line) and presence of AH and AP in the subphase. DPPC:DOPC smoothly increased in surface pressure from zero (referred to as the "lift-off" area) to 50 mN m^{-1} as the trough barriers were compressed, decreasing the mean molecular area (MMA). Beyond the maximum surface pressure phospholipid molecules collapse into the bulk subphase, referred to as the collapse surface pressure. Corresponding to the changes in the surface pressure, the bulk modulus, β, steadily increased with decreasing MMA (Figure 1 b). The compressibility modulus reveals a phase transition observed as a dip to 35 mN m^{-1} near 60 Å^2 molecule^{-1}, indicating a reorganization of the

phospholipid film. This change could be attributed to DOPC collapsing near 35 mN m^{-1}, resulting in a DPPC-rich phospholipid film. The maximum compressibility reached by the film also corresponds to a rigid film.

Addition of each of the adjuvants to the bulk subphase altered the characteristic DPPC:DOPC compression isotherm. Addition of AH (Figure 1 a) and AP (Figure 1 c) to the bulk subphase shifted the "lift off" area to higher MMAs compared to the DPPC:DOPC control, indicating an interaction with the phospholipids. The interaction of AH decreased the collapse surface pressure and lowered the maximum compressibility modulus. Since the compressibility modulus measures the rigidity of monomolecular films, the decrease suggests a disruption in the molecular packing and a reduction in the strength of the film. Conversely, the compressibility modulus of the monolayer was unaltered in the presence of AP, indicating the shift to higher MMAs resulted from enhanced packing density of the phospholipid molecules.

The aluminum adjuvant-monolayer interactions were further explored with fluorescence microscopy. Representative images of the monolayer at physiologically relevant surface pressures are shown in **Figure 2**. The well-packed liquid condensed domains exclude the bulky fluorescent dye and appear dark against the bright liquid expanded regions. As has been previously reported in equivalent bilayer systems, DPPC:DOPC monolayers (Figure 2 a) contained small, fairly round, evenly-distributed domains which grew with increasing surface pressure [12-14]. Most of the domains ranged in size between 1.0–2.0 μm^2 at 20 mN m^{-1} and between 2.25–4.25 μm^2 at 30 mN m^{-1} (**Figure 3 a**). The domains were drastically condensed upon exposure to AH and AP (Figure 2 b,c), creating large, irregular-shaped domains. The adjuvants did not only increase the total image area composed of liquid condensed domains (Figure 3d), but also increased the median domain area and range of domain areas by more than an order of magnitude (Figure 3 b, c). Further, liquid condensed domains began appearing at approximately 12 mN m^{-1} for the DPPC:DOPC monolayer alone, 10 mN m^{-1} in the presence of AH, and 6 mN m^{-1} in the presence of AP. The early appearance and shape of the AP-induced domains and lack of change in the

compressibility modulus could indicate the AP particles provide nucleation points to promote lipid clustering and domain growth without disrupting the monolayer.

McConnell and co-workers have shown that the size and morphology of liquid ordered domains is determined by the electrostatic repulsion between the molecular dipoles formed between the lipid headgroups at the air/water interface and the line tension between the ordered and disordered domains [15]. Further, some of us have shown that the entropy of mixing requires that the lipid domains demonstrate a domain size distribution [16, 17]. The increase in width and the loss of the Gaussian domain distribution in the presence of AH and AP are possibly due to changes in the electrostatic interactions of the lipid headgroups around the aluminum adjuvants. Further, the incorporation of adjuvants into the lipid membrane could change the line tension between the lipid domain boundaries and cause the transition from circular to irregular shapes.

Although aluminum-based adjuvants are particulate matter, similar counterion mediated clustering in lipid membranes is well established for lipid molecules involved in signaling. For example, divalent cations such as Ca^{2+} enhance condensation and organization of important anionic signaling lipids such as phosphatidylserine, phosphatidic acid, and PIP2 [18-21]. Electrostatic and phosphate-driven interactions between cell membranes and aluminum ions have also been proposed to explain well-known toxic effects of aluminum ions [22-25]. To prove that the observed lipid reorganization was induced by adjuvants and not free ions in solution, we exposed the DPPC:DOPC films to the adjuvant suspension buffer containing sodium (and other ions in trace amounts) and to a solution of free aluminum ions. The domains created in the presence of the suspension buffer and the DPPC:DOPC alone showed no morphological or quantitative difference (**Figure S1**). To obtain a solution containing free aluminum ions, aluminum chloride was suspended in 100 mM MES buffer at pH 4.2. The DPPC:DOPC film was monitored at these acidic conditions both with the buffer alone and with the buffer containing aluminum chloride (**Figure S2**). Although the presence of the aluminum ions increased the relative count of domains at higher surface pressures, the size distribution of the lipid domains remained in the same range, unlike in the case of the adjuvants, where the domain sizes increased by at least an order of magnitude,

compared to the control (pure DPPC:DOPC). The morphology of the lipid domains and the compression isotherms in both conditions were also not significantly different. Therefore, the observed changes can be conclusively attributed to the particulate aluminum adjuvant and not free ions in solution.

We speculate the altered lipid domain organization is influenced by the physicochemical properties of the adjuvants. While both adjuvants induced reorganization of the lipid domains, AP significantly increased the percentage of liquid condensed domains. These differences may be explained by two different effects. Much as the electrostatic characteristics of ions dictate how they interact with lipids, the opposite charges of the two aluminum-based adjuvants may explain their different modes of interaction and organization. While our results suggest the zwitterionic phosphatidylcholine can associate with both the positively charged AH and negatively charged AP; it is possible that the orientation of the dipole moment P^--N^+ for a PC headgroup may differ in the presence of the two different particulate systems. Previous nuclear magnetic resonance studies in PC systems have shown that ions which penetrate further into lipid layers more greatly deflect the P^--N^+ dipole and make the headgroup more perpendicular to the plane of the monolayer.[26] Likewise in DOPC membranes, small cations in ion pairs could not only strongly interact with negative phosphate and carbonyl groups, but also oriented the interaction of its anion with the positive region of the head [26].

Therefore, we hypothesize that the differences in the compressibility modulus and the percent of condensed domains may be attributed to differences in the orientation of the PC headgroups, and therefore packing around the oppositely charged adjuvant particles. Favorable binding or electrostatic interactions between the positive AH and internal phosphate groups could help the particles penetrate and organize the phospholipids. In contrast, the phosphate-covered AP particles would attract the positively charged nitrogen moieties and would enhance domain growth at the air-water interface. Evidence of highly incorporated, disruptive AH particles in the monolayer is provided by the reduced compressibility modulus in our AH systems as well as **Supplementary Figure S5**, which shows fluorescently tagged AH molecules associating with the lipid membranes. Interestingly, even though significant quantities of tagged AP particles were found in the bulk solution, unlike the AH, most of these particulate matter was

not found to associate with the lipid domains, when viewed together. These hypotheses are also corroborated by Figure 3 where by serving as nucleation points at the interface, AP particles allow the lipids to pack into larger clusters until collapse, unlike the AH particles, whose insertion eventually stunts domain growth beyond a certain size.

The physical qualities of the adjuvants also provides support for the theory of monolayer organization by insertion vs nucleation for the AH and AP, respectively. Cho et. al. found the surface charge of gold nanoparticles played a large role in uptake by SK-BR-3 breast cancer cells [27]. Gold nanoparticles modified to have a negative charge interacted moderately well with positive patches of the cell surface, but positively charged nanoparticles associated significantly more with the cell membrane and were endocytosed. Because endocytosis occurs to maintain the charge distribution of the membrane, they propose the presence of the positive particles initiates changes in the rigidity and permeability of the membrane and promotes their internalization [27].

Aside from charge, nanoparticle characteristics such as particle size, shape (i.e. aspect ratio), surface roughness and functionalization, and hydrophobicity have been shown to influence membrane interaction [28]. Simulations performed by Hoek et. al. suggest that surface roughness on the nanoparticle can enhance membrane interaction, even in some instances when the interaction would otherwise be unfavorable, as in the case of repulsive electrostatic or hydrophobic interactions [29]. Therefore, in physiological conditions where the net negative charge of the membrane may repulse the AP, the amorphous, rough quality of the nanoparticle could allow it to interact with phospholipids and provide a nucleation point for domain condensation. Additionally, experiments that studied rod- and disc-shaped nanoparticles demonstrated that particle aspect ratio and size are important factors in cellular uptake [30-32]. While shorter, thin rods can still effectively cross membranes, as the aspect ratio grows the rate at which the particle is engulfed is reduced [31, 32]. Especially as the particle becomes wider, it becomes increasingly less energetically favorable for the membrane to wrap around the particle and thus may remain on the outer cell membrane [28, 33]. Ergo, the differences in monolayer organization could also be explained in light of the morphological differences between the adjuvants. Regardless of the nature of

either particle's affinity for lipids, previous studies would suggest that the ability of the adjuvants to generate organized domains may be sufficient to organize key signaling proteins necessary to initiate an immune response [5, 6, 34]. Studies correlating the adjuvant-induced changes in cell signaling with the adjuvant-induced changes in lipid domain morphology and clustering are currently underway in our laboratories and will form the subject of a future work.

4. Conclusions

In conclusion, our results present conclusive evidence that common aluminum-based adjuvants Alhydrogel and Adju-Phos are both capable of reorganizing phospholipid domains in model zwitterionic membranes. We argue that the aluminum adjuvant-induced lipid reorganization presented here supports a lipid-mediated mechanism of action and thus an alternative method for enhancing immune responses. The pronounced effect of each adjuvant on the phospholipid domain organization was not equal, likely due to differences in the physicochemical properties of the adjuvant particles. The wider, negatively charged AP particles appeared to remain at the air-water interface, predominantly serving as nucleation points that allowed condensation or complexation of the zwitterionic phospholipid domains. Conversely, the positively charged, elongated AH particles may have helped it penetrate into the membrane, affecting the packing of the phospholipids and reducing the compressibility and integrity of the monolayers. The weakening of the monolayer in the presence of AH could explain the membrane damage and inflammation typically associated with the adjuvant, but it also raises further questions regarding the mechanism of action across different aluminum adjuvants, particularly because different forms of the adjuvant appear to produce disparate results in the literature.

However, it should be noted that, while the outer leaflet of the cell membrane has been shown to be PC-rich, our DPPC:DOPC monolayer certainly is not fully representative of the complexity, charge, or compressibility of the bilayer cell membrane [23]. Our model lacks key proteins as well as signaling and organizational lipids found in immune cell membranes including sphingomyelin and cholesterol. As such, the properties of organized domains and the adjuvant-membrane interaction are expected to be markedly

different in a cell. Nonetheless, the persisting interaction of the adjuvants with these typically low-affinity phospholipids, even in the absence of cholesterol and sphingomyelin, provides an interesting starting point for the proposed mechanism of adjuvant-membrane interaction. The ability of adjuvants to organize and condense lipid domains supports the "membrane affinity triggered signaling" theory suggested for aluminum and monosodium urate (MSU), a product of uric acid occasionally released after cell damage by aluminum adjuvants [5, 34]. Although neither aluminum nor MSU crystals have receptors on DCs, previous studies have shown the force of the interaction can rearrange lipid domains and initiate signaling [5, 34]. Signaling may occur through 'danger' signals after membrane damage, or through proteins, such as TLRs and MHC II, which tend to localize in highly organized lipid domains, particularly lipid rafts [1, 8, 35, 36]. More complex models including organizational lipids, such as cholesterol and sphingolipids to simulate lipid rafts, or signal-initiating lipids, such as anionic lipids, will be necessary to help us explain how these adjuvants may interact with membranes and activate immune cells. Future experiments in our lab will focus on the effect of antigen-loaded adjuvants on phospholipid organization in model membranes, as well as methods to study the orientation and interaction of the adjuvants with the lipid molecules, which was not directly investigated in this communication. We also hope that the results presented here will motivate in-depth structural analyses of the theorized adjuvant-induced reorganization of lipid membranes that will further establish the role of lipid sorting in antigen uptake and presentation. Ultimately, understanding how adjuvants interact with the cell membrane could influence how we use and design novel adjuvants in the future.
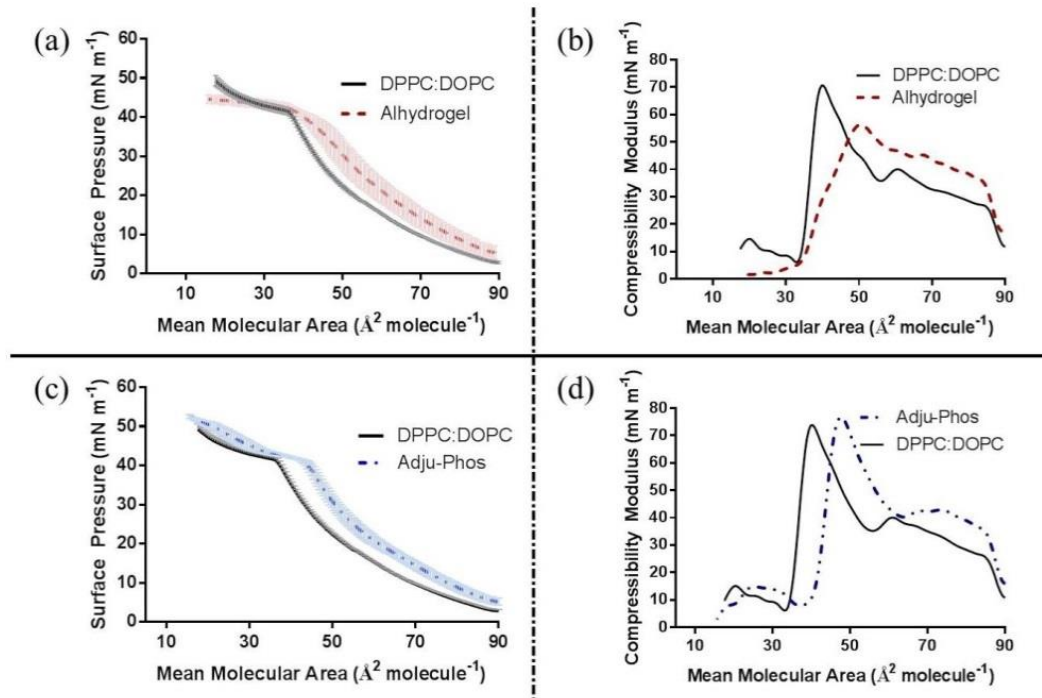
Figure 1. Surface pressure (left) and compressibility modulus (right) of the DPPC:DOPC monolayer change as a function of mean molecular area in the presence of each adjuvant. Alhydrogel (a,b) appears to insert into and weaken the monolayer at higher surface pressures, while the interaction of Adju-Phos (c,d) does not change the mechanical properties of the monolayer. Graphs represent the average of a minimum of three experimental replicates. Data presented as average ± SEM.
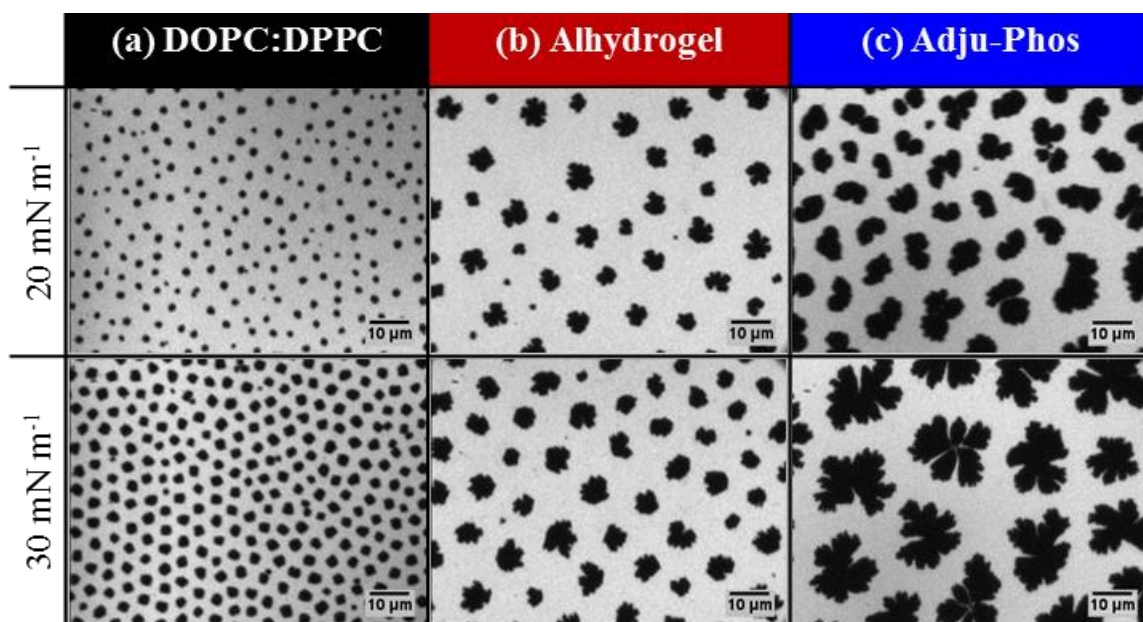
Figure 2. Fluorescent images of the DOPC:DPPC model monolayer (a) alone, (b) in the presence of Alhydrogel, and (c) in the presence of Adju-Phos. Both aluminum adjuvants cause condensation of the lipid domains and drastic lipid reorganization. Images are representative of at least two individual experiments.
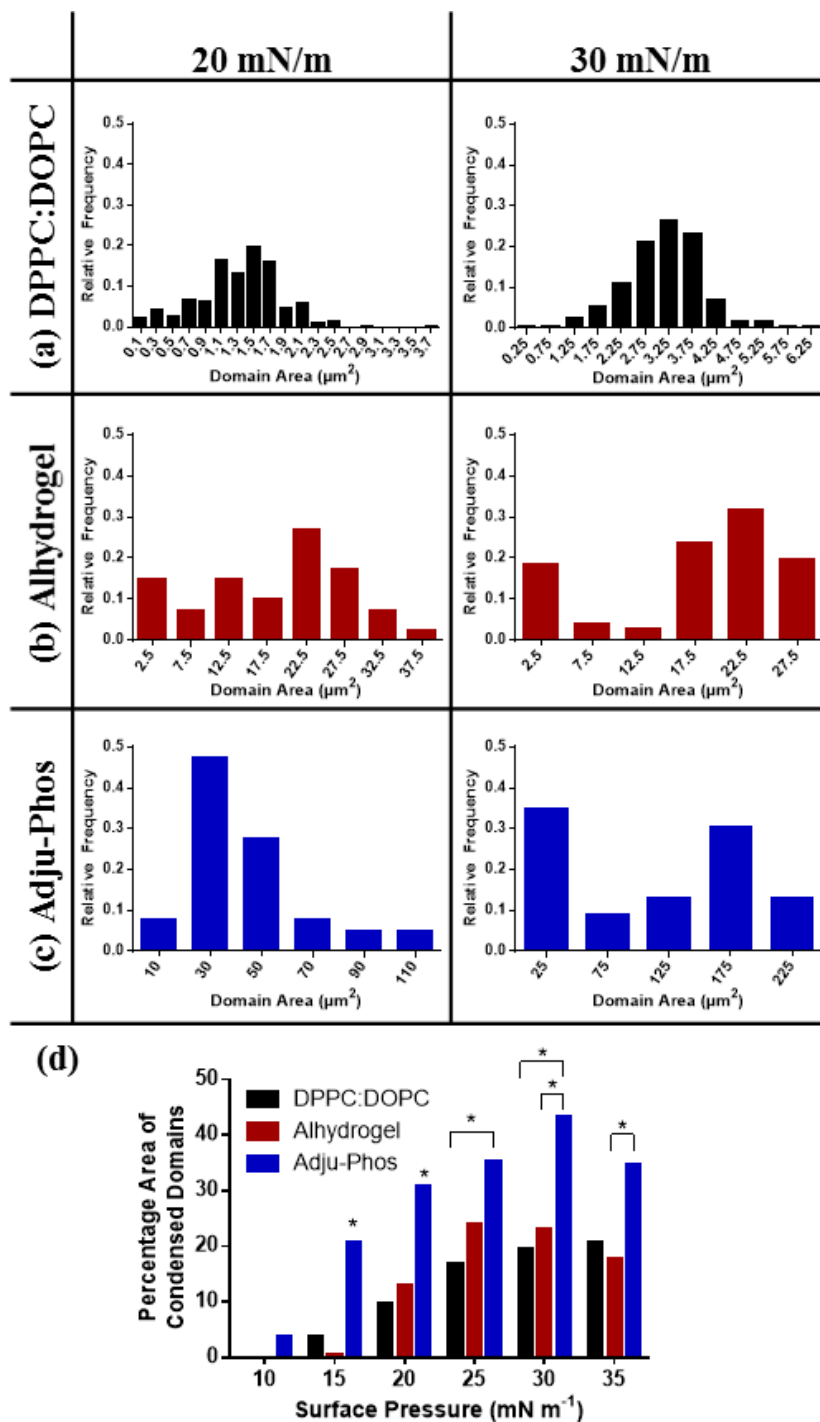
Figure 3. Distribution of the condensed domain areas in the (a) DPPC:DOPC monolayer alone and the monolayer in the presence of (b) Alhydrogel and (c) Adju-Phos. Addition of either adjuvant, but particularly Adju-Phos, increases the average area of a condensed domain by at least an order of magnitude compared do the DPPC:DOPC monolayer alone. (d) The percent of the image area composed of condensed domains is presented as a function of the surface pressure of the monolayer. Histograms were created only from the representative images shown in Figure 2. * $p<0.05$; ** $p<0.01$.
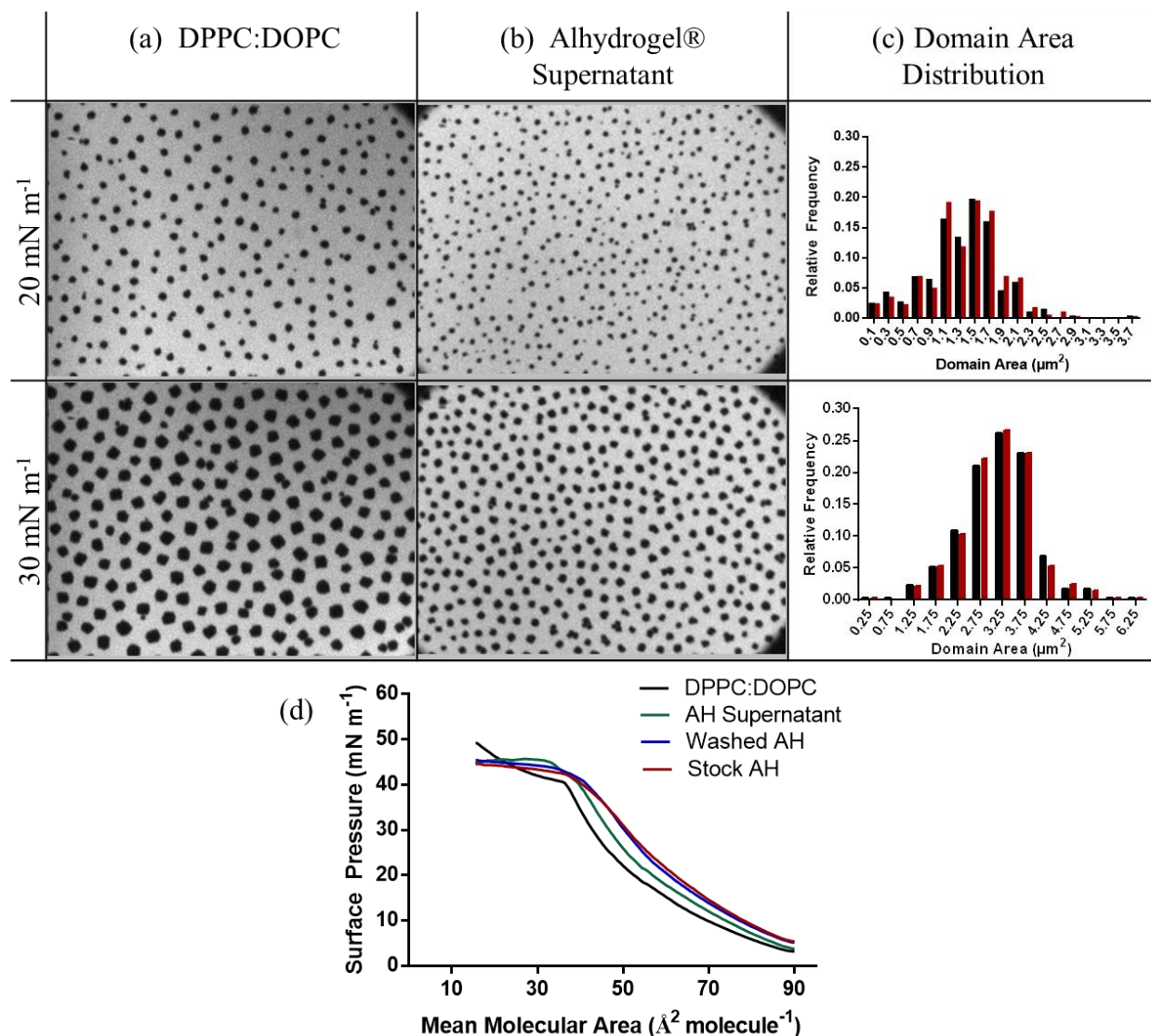
Figure S1. (a,b) Free ions present in the Alhydrogel suspension buffer are not responsible for major lipid sorting. Supernatant was separated from the Alhydrogel adjuvant via centrifugation as described in the materials and methods. The same volume of supernatant was added to the sub-phase as was used for the complete adjuvant formulation. (c) Relative frequency histograms show the distribution of domain areas produced by the DPPC:DOPC alone (black) and in the presence of the supernatant (red). (d) Surface pressure vs area isotherms show some interaction of the suspension buffer (green) with the DPPC:DOPC monolayer (blue), but Alhydrogel (in suspension buffer, black; washed, red) remains the dominant interaction.

Method: To confirm that the significant lipid reorganization reported here was not due to the presence of free ions within the adjuvant formulation, AH particles from 1 mL of AH stock solution were separated from the suspension buffer via centrifugation at 10,000xg for 3 minutes. The supernatant was removed and reserved for further analysis. In experiments conducted with the adjuvant supernatant, a volume of supernatant equivalent to the volume used with the full AH stock was mixed into the ultra-pure distilled water sub-phase, and possible alterations in the surface morphology were monitored using fluorescence microscopy.
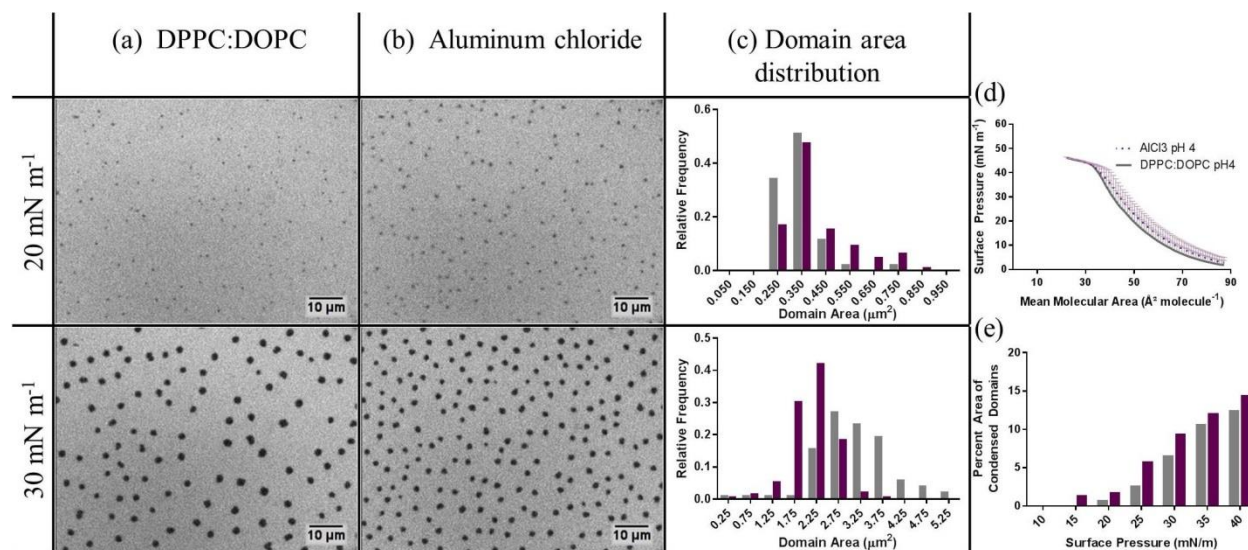
Figure S2. The DPPC:DOPC monolayer was spread over a subphase composed of 100 mM MES buffer pH 4.2. The monolayer was compressed over the subphase alone (a), and over the subphase containing 385 μM AlCl$_3$. The area of each domain in the representative images was calculated to create histograms of the domain area distributions (c) of both the monolayer alone (gray) and in the presence of AlCl$_3$ (purple). The compression isotherm (d) and the percent of the total image area composed of condensed domains (e) are derived from at least two individual experiments.

Method: Aluminum chloride was purchased from Alfa Aesar. A MES buffered saline pack (Thermo Fisher) was reconstituted in distilled water to make the 100 mM MES buffer, was adjusted to pH 4.2, and was passed through a 0.2 μm filter. To create the aluminum ion solution, the aluminum chloride was first dissolved in the correct volume of subphase outside the trough to ensure thorough mixing. The molar concentration of aluminum present was equivalent to the concentration used in the adjuvant conditions. All data shown in Figure S2 is collected at pH 4.2.
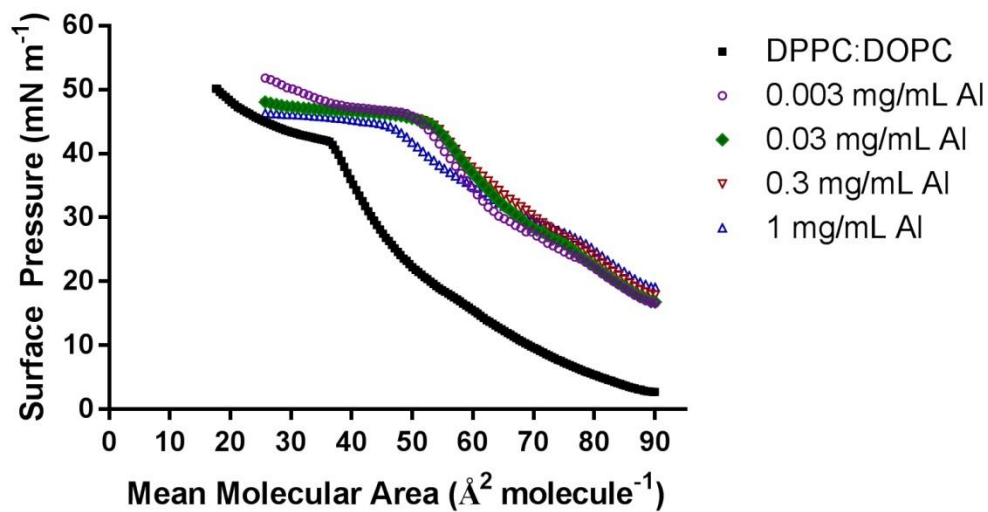
Figure S3. The DPPC:DOPC monolayer was compressed in the presence of several concentrations of Alhydrogel to identify an appropriate concentration for experimentation. Compressions were generally insensitive to concentration, therefore the lowest concentration that had consistent interaction, 0.03 mg/mL (diamonds), was selected.
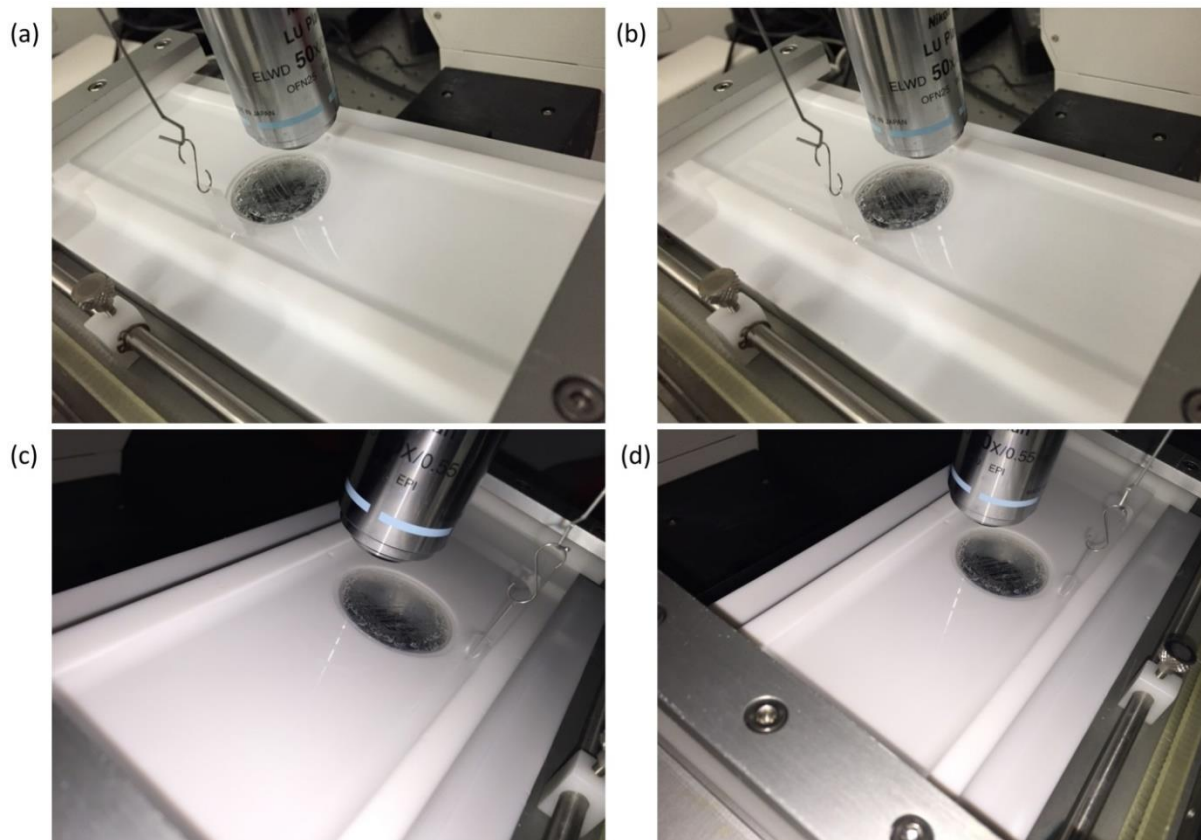
Figure S4. Representative images of the trough before (a,b) and after (c,-e) imaging show no visible evidence of adjuvant particles settling to the bottom of the trough. Alhydrogel (a,c) and Adju-Phos (b,d) remain well suspended throughout the duration of an imaging experiment (approximately 45 minutes).
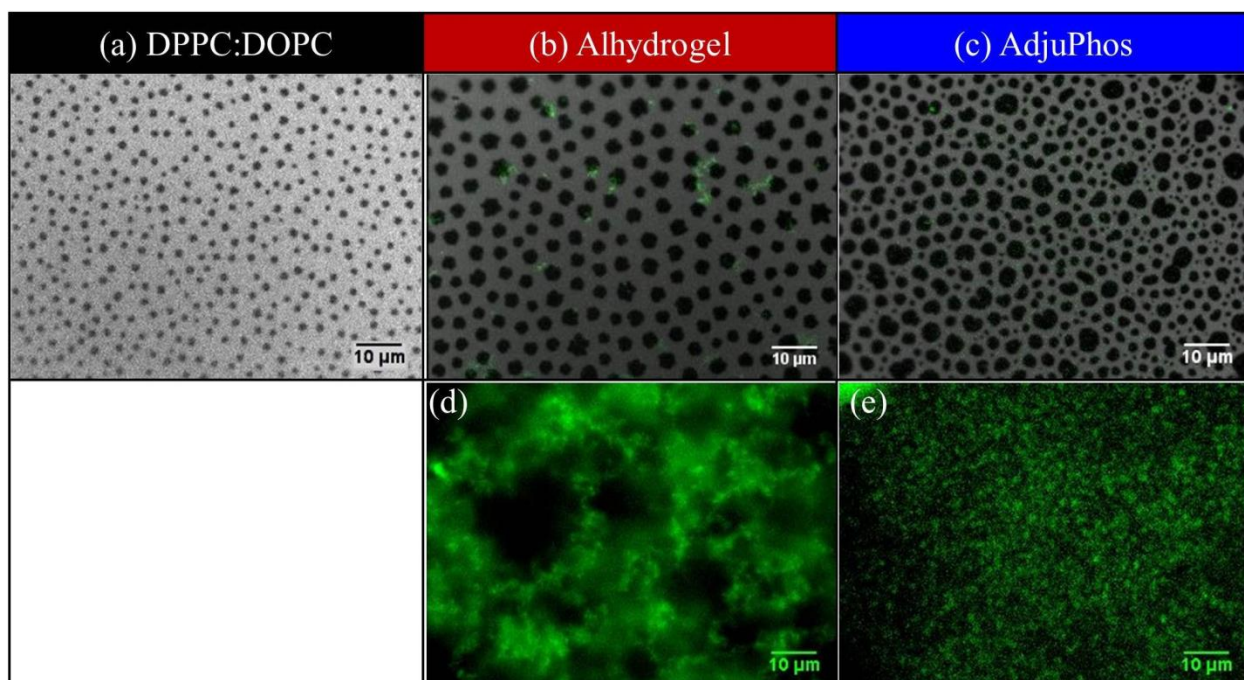
Figure S5. DPPC:DOPC spread over morin-stained adjuvants. DPPC:DOPC was spread over a 100 μL drop of distilled water (a) alone, (b) 0.03 mg/mL AH-morin, or (c) 0.03 mg/mL AP-morin. The morin-stained adjuvants are observed in green. The AH particles appeared to localize in the fluid regions along the edges of the condensed domains, while the AP particles remained under the condensed domains. Images (d) and (e) show pictures of AH and AP, respectively, at 0.5 mg/mL without any DPPC:DOPC.

Method

Morin was purchased from Sigma. A saturated 800 μM stock of morin was made in MOPS buffer. The morin stock was used to make a 1 mL solution composed of 0.5 mg Al/mL adjuvant and 250 μM morin in MOPS buffer and was allowed to rotate end-over-end at room temperature overnight. The stocks were washed by centrifuging at 3500xg for 10 minutes, removing the supernatant, and resuspending in 1 mL of fresh MOPS buffer. Each morin-stained adjuvant was diluted in distilled water to a working solution of 0.03 mg Al/mL. To obtain each image, 0.5 μL of the DPPC:DOPC lipid mixture was spread over the surface of a 100 μL droplet of either distilled water, or the working solutions of Alhydrogel or Adju-Phos on a glass slide.

References

1.	Marrack, P.; McKee, A. S.; Munks, M. W. Towards an understanding of the adjuvant action of aluminium. *Nature reviews. Immunology* **2009,** *9*, (4), 287-93.
2.	Hogenesch, H. Mechanism of immunopotentiation and safety of aluminum adjuvants. *Frontiers in immunology* **2012,** *3*, 406.
3.	Lindblad, E. B., 13 - Mineral adjuvants. In *Immunopotentiators in Modern Vaccines*, O'Hagan, V. E. J. C. S. T., Ed. Academic Press: London, 2006; pp 217-233.
4.	Oleszycka, E.; Lavelle, E. C. Immunomodulatory properties of the vaccine adjuvant alum. *Current opinion in immunology* **2014,** *28*, 1-5.
5.	Shi, Y. To forge a solid immune recognition. *Protein & cell* **2012,** *3*, (8), 564-70.
6.	Flach, T. L.; Ng, G.; Hari, A.; Desrosiers, M. D.; Zhang, P.; Ward, S. M.; Seamone, M. E.; Vilaysane, A.; Mucsi, A. D.; Fong, Y.; Prenner, E.; Ling, C. C.; Tschopp, J.; Muruve, D. A.; Amrein, M. W.; Shi, Y. Alum interaction with dendritic cell membrane lipids is essential for its adjuvanticity. *Nature medicine* **2011,** *17*, (4), 479-87.
7.	Mbow, M. L.; De Gregorio, E.; Ulmer, J. B. Alum's adjuvant action: grease is the word. *Nature medicine* **2011,** *17*, (4), 415-6.
8.	Triantafilou, M.; Lepper, P. M.; Olden, R.; Dias, I. S.; Triantafilou, K. Location, location, location: is membrane partitioning everything when it comes to innate immune activation? *Mediators Inflamm* **2011,** *2011*, 186093.
9.	Mohwald, H. Phospholipid monolayers. *Structure and dynamics of membranes* **1995,** *1*, 161-211.
10.	Peetla, C.; Stine, A.; Labhasetwar, V. Biophysical interactions with model lipid membranes: applications in drug discovery and drug delivery. *Molecular pharmaceutics* **2009,** *6*, (5), 1264-76.
11.	van Meer, G.; Voelker, D. R.; Feigenson, G. W. Membrane lipids: where they are and how they behave. *Nature reviews. Molecular cell biology* **2008,** *9*, (2), 112-24.
12.	Choucair, A.; Chakrapani, M.; Chakravarthy, B.; Katsaras, J.; Johnston, L. J. Preferential accumulation of Abeta(1-42) on gel phase domains of lipid bilayers: an AFM and fluorescence study. *Biochimica et biophysica acta* **2007,** *1768*, (1), 146-54.
13.	Vié, V.; Van Mau, N.; Lesniewska, E.; Goudonnet, J. P.; Heitz, F.; Le Grimellec, C. Distribution of Ganglioside GM1 between Two-Component, Two-Phase Phosphatidylcholine Monolayers. *Langmuir* **1998,** *14*, (16), 4574-4583.
14.	Ohta, Y.; Yokoyama, S.; Sakai, H.; Abe, M. Membrane properties of binary and ternary systems of ganglioside GM1/dipalmitoylphosphatidylcholine/dioleoylphosphatidylcholine. *Colloids Surf B Biointerfaces* **2004,** *34*, (3), 147-53.
15.	Mcconnell, H. M. Structures and Transitions in Lipid Monolayers at the Air-Water-Interface. *Annu Rev Phys Chem* **1991,** *42*, 171-195.
16.	Dhar, P.; Eck, E.; Israelachvili, J. N.; Lee, D. W.; Min, Y.; Ramachandran, A.; Waring, A. J.; Zasadzinski, J. A. Lipid-protein interactions alter line tensions and domain size distributions in lung surfactant monolayers. *Biophys J* **2012,** *102*, (1), 56-65.
17.	Lee, D. W.; Min, Y.; Dhar, P.; Ramachandran, A.; Israelachvili, J. N.; Zasadzinski, J. A. Relating domain size distribution to line tension and molecular dipole density in model cytoplasmic myelin lipid monolayers. *Proc Natl Acad Sci U S A* **2011,** *108*, (23), 9425-30.
18.	Ross, M.; Steinem, C.; Galla, H. J.; Janshoff, A. Visualization of chemical and physical properties of calcium-induced domains in DPPC/DPPS Langmuir-Blodgett layers. *Langmuir* **2001,** *17*, (8), 2437-2445.
19.	Lamberson, E. R.; Cambrea, L. R.; Hovis, J. S. Controlling the charge and organization of anionic lipid bilayers: effect of monovalent and divalent ions. *The journal of physical chemistry. B* **2007,** *111*, (49), 13664-7.
20.	Sovago, M.; Wurpel, G. W.; Smits, M.; Muller, M.; Bonn, M. Calcium-induced phospholipid ordering depends on surface pressure. *Journal of the American Chemical Society* **2007,** *129*, (36), 11079-84.

21.   Levental, I.; Christian, D. A.; Wang, Y. H.; Madara, J. J.; Discher, D. E.; Janmey, P. A. Calcium-dependent lateral organization in phosphatidylinositol 4,5-bisphosphate (PIP2)- and cholesterol-containing monolayers. *Biochemistry* **2009,** *48*, (34), 8241-8.

22.   MacKinnon, N.; Crowell, K. J.; Udit, A. K.; Macdonald, P. M. Aluminum binding to phosphatidylcholine lipid bilayer membranes: 27Al and 31P NMR spectroscopic studies. *Chemistry and physics of lipids* **2004,** *132*, (1), 23-36.

23.   Caël, V.; Van der Heyden, A.; Champmartin, D.; Barzyk, W.; Rubini, P.; Rogalska, E. Interfacial approach to aluminum toxicity: interactions of Al (III) and Pr (III) with model phospholipid bilayer and monolayer membranes. *Langmuir* **2003,** *19*, (21), 8697-8708.

24.   Koenig, M. L.; Jope, R. S. Aluminum inhibits the fast phase of voltage-dependent calcium influx into synaptosomes. *J Neurochem* **1987,** *49*, (1), 316-20.

25.   Mundy, W. R.; Kodavanti, P. R.; Dulchinos, V. F.; Tilson, H. A. Aluminum alters calcium transport in plasma membrane and endoplasmic reticulum from rat brain. *J Biochem Toxicol* **1994,** *9*, (1), 17-23.

26.   Vacha, R.; Siu, S. W.; Petrov, M.; Bockmann, R. A.; Barucha-Kraszewska, J.; Jurkiewicz, P.; Hof, M.; Berkowitz, M. L.; Jungwirth, P. Effects of alkali cations and halide anions on the DOPC lipid membrane. *The journal of physical chemistry. A* **2009,** *113*, (26), 7235-43.

27.   Cho, E. C.; Xie, J.; Wurm, P. A.; Xia, Y. Understanding the role of surface charges in cellular adsorption versus internalization by selectively removing gold nanoparticles on the cell surface with a I2/KI etchant. *Nano Lett* **2009,** *9*, (3), 1080-4.

28.   Nel, A. E.; Madler, L.; Velegol, D.; Xia, T.; Hoek, E. M.; Somasundaran, P.; Klaessig, F.; Castranova, V.; Thompson, M. Understanding biophysicochemical interactions at the nano-bio interface. *Nat Mater* **2009,** *8*, (7), 543-57.

29.   Hoek, E. M.; Agarwal, G. K. Extended DLVO interactions between spherical particles and rough surfaces. *Journal of colloid and interface science* **2006,** *298*, (1), 50-8.

30.   Champion, J. A.; Mitragotri, S. Role of target geometry in phagocytosis. *Proceedings of the National Academy of Sciences of the United States of America* **2006,** *103*, (13), 4930-4.

31.   Chithrani, B. D.; Chan, W. C. Elucidating the mechanism of cellular uptake and removal of protein-coated gold nanoparticles of different sizes and shapes. *Nano letters* **2007,** *7*, (6), 1542-50.

32.   Chithrani, B. D.; Ghazani, A. A.; Chan, W. C. Determining the size and shape dependence of gold nanoparticle uptake into mammalian cells. *Nano letters* **2006,** *6*, (4), 662-8.

33.   Hofinger, S.; Melle-Franco, M.; Gallo, T.; Cantelli, A.; Calvaresi, M.; Gomes, J. A.; Zerbetto, F. A computational analysis of the insertion of carbon nanotubes into cellular membranes. *Biomaterials* **2011,** *32*, (29), 7079-85.

34.   Ng, G.; Sharma, K.; Ward, S. M.; Desrosiers, M. D.; Stephens, L. A.; Schoel, W. M.; Li, T.; Lowell, C. A.; Ling, C. C.; Amrein, M. W.; Shi, Y. Receptor-independent, direct membrane binding leads to cell-surface lipid sorting and Syk kinase activation in dendritic cells. *Immunity* **2008,** *29*, (5), 807-18.

35.   Lambrecht, B. N.; Kool, M.; Willart, M. A.; Hammad, H. Mechanism of action of clinically approved adjuvants. *Current opinion in immunology* **2009,** *21*, (1), 23-9.

36.   Anderson, H. A.; Roche, P. A. MHC class II association with lipid rafts on the antigen presenting cell surface. *Biochimica et biophysica acta* **2015,** *1853*, (4), 775-780.

Chapter III: Aluminum Adjuvants Stabilize Lipid Raft-like Domains in Model Phospholipid Membranes and in Dendritic Cells *In Vitro*

1. Introduction

Aluminum based adjuvants (ABAs) are the oldest and most prolific adjuvants, but their mechanism of action remains largely unknown. ABAs have been observed to promote local inflammation and damage at the injection site, enhanced antigen uptake, and cell migration to the site of injection and lymph nodes, but the molecular mechanism by which they do so is still unclear [1]. Several molecular mechanisms for ABAs have been proposed and contested. However, most of these theories regarding ABA mechanisms of action revolve around receptor-mediated mechanisms, but few have considered how lipid organization and non-specific membrane interactions may contribute to their adjuvanticity.

For instance, aluminum adjuvants are suggested to activate the NLRP3 inflammasome [2, 3]. Danger-associated molecular patterns (DAMPs), such as monosodium urate (MSU) crystals and endogenous DNA, are commonly observed at the site of injection following ABA administration [4, 5]. The pattern recognition receptor NLRP3 is known to recognize such DAMPs, but is also proposed to recognize solid structures [3, 4]. After antigen presenting cells take up ABA particles or DAMPs, they may destabilize and rupture lysosomes, thereby freeing cathepsin-B and further activating the NLRP3 inflammasome [3, 4]. The involvement of the inflammasome in ABA mechanism of action was thought to be responsible for their Th2 bias; however, several papers have also reported ABA-adjuvanticity remains intact even in the absence of the NLRP3 inflammasome [5]. Several other groups attribute ABA's Th2 bias to its initiation of the Syk-PI3 kinase pathway [6]. Interestingly, this pathway was found to be activated solely by interactions between ABAs or MSU and the plasma membrane of dendritic cells (DCs). ABAs strongly bound sphingomyelin and cholesterol, and it was hypothesized that this interaction initiated lipid sorting and signaling via the Syk-PI3K pathway which activated the DC and allowed it to endocytose antigen without the aluminum particle [7]. Although ABA phagocytosis has been confirmed in other cell types [8-10], the theory of initiating immune signaling by lipid sorting, particularly sorting of the major constituents of lipid rafts, is intriguing.

45

Lipid rafts are small, highly-ordered domains composed of sphingomyelin, cholesterol, and proteins [11]. Although debate surrounding the existence of lipid rafts continues, there is evidence of highly organized domains which greatly reduce the lateral diffusion of associated proteins, but remain mobile within the plane of the membrane and can cluster together to facilitate and amplify signaling between trapped proteins [11, 12]. Lipid rafts have been shown to provide a critical platform for organizing signaling proteins which participate in the immunological synapse [12-14]. The proximity of signaling proteins organized in the lipid rafts facilitates and propagates phosphorylation events, which in turn activate the cell. While there is some baseline level of phosphorylation that occurs in raft-resident proteins, without sufficient impetus lipid rafts do not cluster and cells are not activated [15].

If ABAs can promote clustering of lipid rafts and subsequently activate antigen presenting cells, this membrane interaction could shed light on a piece of the adjuvant's mechanism of action. Previous studies reported in chapter 2 of this thesis showed both Alhydrogel (AH) and Adju-Phos (AP) could promote lipid clustering in a monolayer membrane composed of saturated and unsaturated phosphatidylcholine, a lipid for which ABAs were reported to have low affinity [7]. Here, we explore the interaction of these two clinically-relevant adjuvants in a more complex system composed of phospholipids, sphingomyelin, and cholesterol. Lipid interaction was monitored via surface pressure measurements and sphingomyelin and cholesterol-rich domain sorting via fluorescent imaging. Particular attention was given to the surface pressure of the miscibility transition, which marks the point where the segregated, condensed domains transition to a single homogeneous phase where all lipid components are mixed [16]. Consistent with our previous report, both adjuvants interacted with the lipid monolayer. Each adjuvant increased the miscibility transition surface pressure and stabilized lipid domains in this model system, but each adjuvant behaved very differently. Moreover, *in vitro* experiments with DCs revealed AH and AP could promote clustering of lipid rafts compared to control cells. Conditions which led to more punctate cell staining also tended to have greater secretion of TNFα. Therefore, this research provides support for the hypothesis that ABAs may activate antigen presenting cells by promoting lipid

raft clustering, and that non-receptor mediated interactions may be a part of aluminum-based adjuvants' mechanism of action.

2. Materials and Methods

2.1. Materials

1-palmitoyl-2-oleoyl-sn-glycero-3-phosphocholine (POPC), 1-palmitoyl-2-oleoyl-sn-glycero-3-phosphoethanolamine (POPE), porcine brain sphingomyelin (SM), and ovine wool cholesterol (Ch) were obtained from Avanti Polar Lipids, Inc. (Alabaster, AL). HPLC grade chloroform, acetonitrile and trifluoroacetic acid, Texas-Red DHPE, Cholera Toxin Subunit B-Alexa Fluor 555, DAPI, and ovalbumin (OVA) from egg white were purchased from Fisher Scientific. Alhydrogel 2% and Adju-Phos 2% were purchased from Sergeant Adjuvants (Clifton, NJ).

2.2. OVA and lipid detection via HPLC-UV

Reversed-phase chromatographic analysis was used to measure the concentration of ovalbumin. A Waters HPLC system was used consisting of an e2695 separation module, a 2489 UV/Vis absorbance detector, and a 2414 refractive index indicator with a Waters C4 XBridge protein column (300 Å, 3.5 μm, 4.6 x 150 mm, 10-500 K).

Ovalbumin was detected at 220 nm. OVA elution was achieved using a gradient method where mobile phase A contained water + 0.05% trifluoroacetic acid and mobile phase B contained acetonitrile + 0.05% trifluoroacetic acid. Gradient elution was performed at 1 mL/min beginning with 5% mobile phase B until 2.5 min, followed by 50% B at 10 min, 80% B from 18 – 20 min, and 5% B from 22 – 25 min.

Lipids were also detected at 220 nm. Lipids were eluted from the column using a shallow gradient method where mobile phase A contained 5 mM phosphate buffer at pH 7.4 and mobile phase B was pure methanol. The gradient elution was performed at 1 mL/min beginning with 90% mobile phase B until 2 min, followed by 97% mobile phase B from 2-12 min, then a decrease to 90% B from 17-11 min. All chromatograms were acquired and analyzed with Empower version 3 software.

2.3. Ovalbumin-adjuvant adsorption and characterization

OVA and ABA solutions were prepared at a 1:1 ratio in 10 mM MOPS buffer (pH 7.4) and were mixed end-over-end at 4°C for one hour to allow OVA adsorption. Solutions were diluted so that the final concentration of both adjuvant and OVA were 50 μg/mL in all experiments.

The mean particle size was measured by dynamic light scattering using a ZetaPALS (Brookhaven, Holtsville, NY). The amount of OVA associated with the adjuvant particle was determined immediately after each sample was made. 2 mL of each adjuvant-OVA solution were centrifuged at 13,000 rpm for 5 minutes to pellet the adjuvant, and a sample was drawn from the supernatant. Free OVA was detected via HPLC, and the amount associated with the adjuvant was assumed to be the initial concentration added less the free concentration detected. Data is the average of at least 3 replicates.

2.4. Lipid-adjuvant binding isotherms

Stocks of each lipid were suspended in equal parts ethanol and chloroform, and were further diluted in ethanol to make working solutions at 2x concentration. Lipids were individually distributed to an equal volume of a 2x solution of either AH or AP diluted in ultrapure distilled water. Samples were vortexed after mixing, and again 15 minutes in to incubation at room temperature. Samples were incubated for a total of 30 minutes. Samples were centrifuged at 13,000 rpm for 5 minutes to pellet the adjuvant, and supernatants were collected and analyzed via HPLC as described.

2.5. OVA release into water and cell culture medium

Ovalbumin conjugated with Rhodamine B was synthesized by our lab, and used to evaluate the release of OVA from each adjuvant. OVA-rhodamine and AH or AP solutions were prepared as described. Solutions were diluted into either ultrapure distilled water (18.2 MΩ/cm; Millipore, Billerica, MA) or cell culture medium, and 500 μL aliquots were distributed into microcentrifuge tubes. Samples were protected from light and incubated at room temperature on a rocking plate. At the specified time points, a tube from each sample was spun down at 13,000 rpm for 5 minutes to pellet the adjuvant. 200 μL of the supernatant

was withdrawn and transferred to a black, clear-bottomed 96 well plate. Fluorescence of the released

OVA-rhodamine was measured on a BioTek Synergy H4 plate reader (Winooski, VT) at ex/em 555/580

nm.

2.6. Langmuir studies

A Langmuir trough (KSV-NIMA-Biolin Scientific, Linthicum Heights, MD) was used to measure the

interaction of the adjuvant formulations with lipid monolayers. An equimolar 1mg/mL lipid mixture

containing POPC:POPE:SM:Ch was suspended in chloroform. The lipid mixture was spread drop-wise

with a Hamilton microsyringe (Hamilton, Reno, NV) to form a monolayer on the surface of an ultrapure-

distilled water sub-phase to reach a mean molecular area of 90 Å^2/molecule. The monolayer at the air-

water interface was compressed symmetrically at 25 mm/minute, and the changes in the pressure of the

monolayer were recorded using wet filter paper as a Wilhelmy plate pressure sensor. The pressure sensor

probe was calibrated using a bare air-water interface. 1 mg/mL adjuvant solutions were diluted and

thoroughly mixed into the sub-phase prior to spreading the POPC:POPE:SM:Ch monolayer.

Average compression isotherms for each sample were created using GraphPad Prism 7 (GraphPad

Software, Inc., La Jolla, CA). The compressibility modulus was calculated from the average surface

pressure vs mean molecular area compression isotherm. The first derivative of the isotherm was obtained

using the built-in differentiation and smoothing (second order, 5 point) tool available in Prism 7. The

compressibility modulus is defined by $\beta = -A\frac{d\Pi}{dA}$, where A is the mean molecular area obtained after

smoothing.

2.7. Fluorescence microscopy of lipid monolayers and image analysis

To visualize the effect of the adjuvants on lipid domain formation in our model membrane system, 1 wt%

Texas Red -DHPE (Life Technologies) was added to the POPC:POPE:SM:Ch solution. The Langmuir

trough was placed under a custom-modified Nikon Eclipse LV100 fluorescence microscope with an

extra-long working distance lens and tube collimators that allowed imaging of the phospholipid film

during monolayer compression**.** Images of the lipid monolayer throughout the compression were obtained with an Andor Luca S camera and Solis software (Belfast, Ireland).

The area of each condensed lipid domain was analyzed using the "Analyze Particles" tool in ImageJ (National Institutes of Health, Bethesda, MD). Only particles larger than 1 μm^2 were analyzed, and edges were excluded from analysis. The detected particle areas were organized and relative frequency histograms were created using Prism 7 software. The number of bins was calculated as the square root of the number of measured domains and was used to assign bin widths.

2.8. In vitro testing of adjuvant formulations

All formulations were tested *in vitro* using JAWS II cells (ATCC Manassas, VA) as a model dendritic cell (DC) population. DCs were cultured according to ATCC guidelines in culture medium containing MEM alpha (Gibco), 20% FBS (Atlanta Biologicals), 1% penecillin-streptomycin (MP Biomedicals), and 5 ng/mL GM-CSF (PeproTech, Rocky Hill, NJ). DCs were seeded at 2.5 x 10^5 cells/well in 96 well plates in media, or media containing 1 mg/mL OVA for priming, and were allowed to adhere overnight. The following morning, designated cells were activated with 100 ng/mL LPS (Sigma Aldrich) for two hours. All cells were washed with warmed MEM alpha, and fresh media was added to the wells. An equivalent volume of each formulation at 2x concentration was added to the wells to a total volume of 300 μL. Cells were incubated at 37°C and 5% CO_2. Each sample was run in duplicate, and data is the average of three independent experiments.

2.9. Measurement of TNFα

Media from each sample was collected over several time points for cytokine analysis, and was stored at -80°C until the time of analysis. TNFα secretion by the DCs was measured by ELISA (R&D systems, Minneapolis, MN) as per the manufacturer instructions. Data within each stimulation group was normalized to the untreated media control at 24 hours.

2.10. Imaging of lipid rafts in dendritic cells

7.5×10^5 cells/well were seeded on sterilized 12 mm glass coverslips in 24 well plates and were allowed to adhere overnight. Cells were stimulated as described previously. Following LPS stimulation, all cells were carefully washed twice in room temperature complete medium. Equal volumes of unmodified αMEM and 2x concentration treatment were added to each well to a total of 300 μL and were incubated for 20 minutes at room temperature. In the final 5 minutes of incubation, the plate was spun down at 350xg and 4°C for 5 minutes. The treatments were carefully removed and cells were washed twice with cold complete medium, and kept on ice for the remainder of the staining procedure. Cells were stained in a cold 1 μg/mL solution of CT-B-Alexa Fluor 555/PBS and incubated on ice, protected from light for 10 minutes. Cells were gently washed twice with cold PBS and then fixed in 2% paraformaldehyde/PBS for 20 minutes, quenched in 25 mM glycine/PBS for 10 minutes, and washed again in PBS. Finally, cell nuclei were stained with 1 mM DAPI for 20 minutes and washed twice with PBS. Coverslips were removed from the wells and mounted on glass slides with Slowfade Gold (Life Technologies). Cells were examined using an inverted fluorescence confocal microscope (Olympus IX-83 motorized microscope) with TRITC (tetramethyl rhodamine isothiocynate) and DAPI (4',6-diamidino-2-phenylindole) filters. Z-stacks were collected and processed with Olympus's cellSens software**.**

3. Results

3.1. Adjuvant-ovalbumin particle characterization

An equal concentration of OVA and either AH or AP (50 μg/mL) were mixed and the quantity of OVA adsorbed to the adjuvant was measured via HPLC. The OVA was completely adsorbed to positively charged AH due to favorable electrostatic interactions (pI OVA = 4.6 [17]), but associated much less (18.7 μg/mL) with the negatively charged AP. Consequently, the average particle size of AH+OVA was 1335.6±39.5 nm, about twice that of AH alone, which was 600.1±1.5 nm. The particle size of AP increased only slightly; AP alone was 985.4±9.9 nm and AP+OVA was 1051.4±49.5 nm.

OVA retention was also evaluated using fluorophore labeled OVA-rhodamine. OVA-rhodamine-loaded adjuvants were diluted in conditions that replicated the conditions in the Langmuir trough (ultrapure distilled water) and in cell culture (20% FBS in αMEM) (**Fig 1**). Nearly all the OVA was free in the AP samples both in water and media, as was expected since AP minimally associated with OVA. However, AH+OVA behaved differently in the Langmuir and cell culture conditions. Almost no OVA was released from AH in water over a time span much greater than a typical Langmuir experiment, but the majority of the OVA eluted from the AH within an hour of being introduced to cell culture medium.

3.2. Lipid affinity differs between ABAs

Lipid-adjuvant affinity was assessed by combining each lipid individually with AH or AP. The amount of lipid associated with the adjuvants was calculated as the initial amount of lipid added less the free lipid detected by HPLC. The maximum association, reported in mg of lipid or cholesterol per mg of adjuvant, is shown in **Table 1**. Overall, AP associated with less lipid compared to AH. AP minimally associated with any of the phospholipids or sphingomyelin, but associated most with cholesterol. AH did not retain any POPC, moderately associated with POPE, and had strong, nearly equivalent association with sphingomyelin and cholesterol.

3.3. Aluminum adjuvants interact with POPC:POPE:SM:Ch monolayers

Bare and OVA-loaded AH and AP were well mixed into the ultrapure distilled water sub-phase of the Langmuir trough and exposed to a monolayer containing lipids relevant to lipid rafts in a DC cell membrane, namely POPE:POPC:SM:Ch [7, 18]. The compression isotherms plot surface pressure against the mean molecular area (MMA), or the available surface area for the lipids to spread, and reveal bare AH and AP behave differently with the lipid monolayer (**Fig 2a**). AH increases the surface pressure compared to the lipid alone throughout much of the compression until the monolayer undergoes a phase transition, marked by the maximum in the compressibility modulus. The compressibility modulus is indicative of the monolayer's ability to resist strain; therefore, a higher compressibility modulus is

representative of lipids which are more closely packed and resist being further compressed, while a lower compressibility modulus indicates the opposite. Additionally, since the compressibility modulus is the first derivative of the compression isotherm, discontinuities in its slope are obvious as minima and maxima, and correspond to phase transitions in the monolayer. The compressibility modulus shows the membrane underwent its final phase transition into a solid state at approximately 44 Å^2/molecule for AH and 40 Å^2/molecule for lipid alone. Conversely, bare AP did not cause major deviations in compression isotherm compared to the lipid alone (Fig 2b). The compressibility moduli for the lipid and AP were also very similar. Absent the reduced maximum modulus and subtle differences at the end of the compression, it would appear AP did not insert into the monolayer and alter the lipid organization. This measurement of course, does not rule out possible association of the AP with the lipid monolayer.

We were also interested in how the adjuvant behavior would change in the presence of a model antigen, OVA. OVA on its own was very surface active, significantly increasing the surface pressure of the monolayer and decreasing its compressibility modulus throughout the compression. OVA has been previously observed to incorporate into DPPC monolayers, and was proposed to unfold such that its hydrophobic regions interacted with the aliphatic lipid tails, and formed aggregates which protruded from the monolayer with increasing surface pressure [19]. The dramatic increase in surface pressure observed here suggests OVA behaved similarly in this more complex lipid system, and may have displaced lipid from the surface. However, when OVA was adsorbed onto AH, the compression isotherm behavior much more closely followed that of the bare AH. On the other hand, when the monolayer was exposed to AP and mostly unbound OVA the monolayer's mechanical properties more closely aligned with the free protein, though the AP may have inhibited some of OVA's interaction at the interface.

3.4. Aluminum adjuvants stabilize liquid-ordered domains in sphingomyelin and cholesterol containing monolayers

To further investigate the effect of AH and AP on lipid organization, the monolayers were stained with Texas Red-DHPE to observe phase separation in the monolayer. In the images presented in **Fig 3**,

lipids which clustered in to a more tightly packed, liquid-ordered (L_o) phase excluded the large dye and appeared dark against the bright lipids in a more fluid, liquid-disordered (L_d) phase where the dye resided. The images presented are at the physiologically relevant surface pressure of 30 mN/m [20, 21], and at several points before and after the miscibility transition in this lipid mixture. The miscibility transition represents the critical surface pressure at which the line tension between the L_d and L_o phases becomes zero, and the lipids mix to form a single phase. The surface pressures surrounding critical transitions are noted at the top right corner of each image. Observations of miscibility phase transitions have been well characterized in model membranes, including lipid bilayers, giant unilammelar vescicles (GUVs) and more recently in cell membrane blebs; however, it appears live cells may regulate their physical properties to avoid such transitions [16, 22, 23].

At 30 mN/m the lipid monolayer possessed smaller, round L_o domains (Fig 3a). Domain areas were up to 20 μm^2, but most domains were less than 5 μm^2 (**Fig 4a**). As the monolayer was further compressed the domains began to grow and coalesce. At 36 mN/m, just before the lipids underwent their miscibility transition, the distribution of domain areas extended to 70 μm^2, but most domains were less than 30 μm^2. By 37 mN/m, the monolayer began its miscibility transition, marked by the blurring boundaries between the phases and completed within the next 1 mN/m to form a homogeneous monolayer like the image shown at 40 mN/m. When the bare adjuvants were added to the monolayer, the L_o domains were larger and persisted through higher surface pressures (Fig 3b-c). At 30 mN/m the distribution of domain areas exposed to either adjuvant was still centered around 5 μm^2 (Fig 4b-c), but extended to domain areas greater than observed with the lipid alone. In addition to the larger domain areas, both AH and AP stabilized the L_o domains and delayed the miscibility transition. The domains in the monolayer exposed to AP underwent similar critical fluctuations as the lipid alone, but the transition surface pressure was delayed to 39 mN/m (Fig 3c). Interestingly, the lipid exposed to AH did not appear to have a miscibility transition (Fig 3b). At 38 mN/m the condensed domains exposed to AH continued to display a sharp boundary, and at 39 mN/m a homogenous, dark liquid phase formed.

The surface activity of OVA observed in the compression isotherms was also readily visualized in the monolayer (Fig 3d). At 30 mN/m the mostly black frame indicated phase reversal due to the presence of OVA in the monolayer. Additionally, the domains had already begun the transition process, which completed at 32 mN/m. Although the interactions of OVA with the monolayer were observed to overpower those of AP in the compressibility modulus, imaging of the surface displayed AP promoted domain organization even in the presence of OVA (Fig 3f). While the miscibility transition of AP+OVA happens well before that of the AP alone (34 mN/m), it can still stabilize the Lo domains over greater surface pressures compared to the OVA alone. The organizational force of AH allowed it to maintain round, albeit much larger domains at 30 mN/m while loaded with OVA, but the presence of OVA still lowered the transition surface pressure compared to the bare AH (Fig 3e).

3.5. ABAs enhance lipid raft clustering in dendritic cells in vitro

Having studied the lipid-ABA interactions in a model lipid system, we wanted to determine whether the interactions were relevant in dendritic cells (DCs). DCs were either naïve (-LPS/-OVA), loaded and primed with OVA (-LPS/+OVA), or primed with OVA and activated with LPS (+LPS/+OVA) and were incubated with each sample. To observe how each treatment effected the presence and clustering of lipid rafts, raft-resident ganglioside 1 (GM1) was labeled using fluorescently labeled cholera toxin-B. Several small lipid raft patches were observed in unstimulated and untreated DCs (**Fig 5**a, i), but for the most part raft staining was minimal. In the presence of OVA (Fig 5a, ii), DCs were stained with slightly greater intensity and displayed greater localization of domains. Increasing levels of priming (Fig 5b, i-ii) and activation (Fig 5c, i-ii) with and without OVA showed greater staining and domain clustering, with the exception of the OVA-loaded DCs where lipid raft distribution and size did not change with the addition of more OVA. However, addition of ABAs with and without OVA substantially altered the staining and clustering of lipid rafts.

Adjuvant-treated DCs generally displayed greater lipid raft staining and clustering. Enhanced staining intensity was especially observed in AH-treated cells. Although there was higher signal dispersed

throughout the cell, -LPS/-OVA DCs treated with AH had distinct, larger patches of lipid rafts on their surface and around their perimeter (Fig 5a, iii). Raft polarization to the edge of the cell became more dramatic in AH+OVA treated cells, with lipid raft staining extending into the characteristic dendritic projections of the cell (Fig 5a, iv). Similar raft behavior was also observed in DCs first loaded with OVA and then treated with bare AH (Fig 5b, iii). OVA-loaded cells treated with AH+OVA had less dispersed raft staining and instead formed larger clusters of lipid rafts (Fig 5b, iv).

Unlike the AH-treated cells, AP-treatments consistently promoted more localized clustering of lipid rafts, and displayed less disperse lipid raft-staining. Smaller punctate rafts in unstimulated DCs treated with bare AP (Fig 5a, v) grew to form larger clusters of rafts with exposure to OVA. Again, the behavior of lipid rafts in unstimulated DCs cultured with AP+OVA (Fig 5a, vi) and OVA-loaded DCs cultured with bare AP (Fig 5b, v) was similar. OVA-loaded DCs treated with AP+OVA (Fig 5b, iv) had the most localized lipid raft staining, showing multiple large aggregates of lipid rafts.

Interestingly, the lipid raft distribution in the presence of the ABAs in fully LPS-activated and OVA-primed DCs did not necessarily match the observations in non-activated DCs. While lipid rafts in AH+OVA-treated cells (Fig 5c, iv) were still distributed across the surface of the DC with some punctate staining, DCs treated with bare AH displayed more localized small, punctate lipid raft staining (Fig 5c, iii). Conversely, DCs cultured with AP and AP+OVA (Fig 5c, v-vi) had larger lipid raft clusters compared to either of the control or AH conditions.

3.6. Bare ABAs promote additional TNFα secretion in fully activated dendritic cells in vitro

Media from DCs treated with each sample were collected to measure concentrations of the pro-inflammatory cytokine TNFα over five days. In non-LPS activated DCs, all adjuvant formulations significantly increased the concentration of TNFα in the medium compared to untreated and OVA-treated DCs after 5 days (**Fig 6**). -LPS/-OVA cells treated with AP or AP+OVA produced similar concentrations of TNFα, but the bare AH produced significantly more TNFα compared to AH+OVA. Contrarily,

differences in the concentration of TNFα in -LPS/+OVA DCs cultured with AH vs. AH+OVA were statistically insignificant, whereas the concentration released after exposure to AP+OVA was statistically higher than all other treatments in the group. Unexpectedly, adding OVA to either adjuvant in +LPS/+OVA DCs did not result in significantly different concentrations of TNFα compared to untreated cells, but both bare adjuvants significantly increased TNFα compared to the untreated cells and free- and adjuvanted-OVA.

4. Discussion

In this study, we investigated how aluminum-based adjuvants Alhydrogel and Adju-Phos organize lipid raft-like domains in a model lipid system representative of dendritic cell membranes, and in dendritic cells *in vitro*. We discovered both AH and AP could promote the formation and persistence of liquid-ordered domains in lipid monolayers composed of an equimolar ratio of POPC:POPE:SM:Ch. The organizational force was strong, and could continue to enhance domain organization even in the presence of free or adsorbed ovalbumin, which was also highly surface active. Although both AH and AP had affinity for SM and Ch and stabilized condensed domains, imaging experiments and measurements of their interaction with the monolayer revealed dramatic differences. The increased surface pressure and reduced compressibility moduli of the monolayer in the presence of AH would suggest it associated with the lipids. Furthermore, AH-stabilized domains did not appear to undergo any critical fluctuations, nor did it pass through a miscibility transition. Conversely, the negligible changes induced by AP would imply it is excluded from the monolayer, but still stabilized condensed domains at the air-water interface and increased the miscibility transition surface pressure.

Similar aluminum-based adjuvants have also been shown to have higher affinity for sphingomyelin and cholesterol compared to phosphatidylcholine (PC) and phosphatidylethanolamine (PE), which may unify some of each adjuvant's lipid interaction [7], but the charge, surface chemistry, and morphology of AH and AP yield distinct behaviors. AH is a crystalline, needle-like particle with surface hydroxyls that provide its positive charge, whereas AP is an amorphous, disc-like particle with

57

negatively charged phosphate groups. In an experiment conducted using only zwitterionic PC lipids, particles of opposite charge were observed to change the orientation of the $P^- - N^+$ head group with respect to the fatty acid tails and therefore locally alter lipid packing [24]. Positively charged nanoparticles preferentially interacted with the internal phosphate moiety, causing the head to become more perpendicular to the lipid tails and preventing adjacent lipids from packing as closely, making the membrane more fluid. Meanwhile, negatively charged particles interacted with the choline group and extended the lipid head, allowing lipids to pack more densely and gelling the membrane [24].

Electrostatic interactions can explain AP's ability to organize condensed domains, but its apparent exclusion from the membrane may be attributed to its unfavorable morphology compared to AH. Particles with high contact area but smaller diameters and subtle local curvature more easily associate with, and traverse lipid membranes because they require less curving of the membrane to be enveloped, and thus less disruption of lipid packing [25-27]. Simulations and model membrane systems alike have consistently reported thin rod or ellipsoid particles can associate with and cross membranes with greater ease than most particles, including spheres and discs [25-27]. Shape effects are also significant even within different shaped AH particles. AH particles were crystalized under different pH to produce rods, platelets, and polyhedra, and large, skinny rods continued to induce more robust immune responses compared to the other shapes [28, 29]. Therefore, the enhanced membrane perturbation observed in the compression isotherm of AH, but not AP is consistent with these shape-interaction trends.

Moreover, the images of the monolayer with AH are more reminiscent of domains exposed to a line active impurity as oppose to domains combining at a miscibility transition. When two phases coexist, there is a balance between the repulsive electrostatic forces in the dipole of the condensed lipid heads, and the attractive forces between aliphatic chains that work to reduce the line tension at the domain boundary [16]. The chains of L_o phase lipids are fully extended, and extend slightly above the surrounding L_d phase. The hydrophobic mismatch of the chain lengths results in line tension. To reduce the thermodynamically unfavorable mismatch at the boundary, similar chains cluster together to form smooth, round domains,

limited in size by the electrostatic repulsion at the head groups [16, 30]. However, compounds may insert at this interface and greatly reduce the line tension, resulting in larger domains [31]. The breaking up of the smooth, round domains into elongated, twisting domains by AH is comparable to the reduced line tension caused by line active impurities in lipid membranes, and therefore further supports the presence of AH in the monolayer. It is also important to note that unlike the control system, which underwent a miscibility phase transition, the lipid domains maintained their circular structure in the presence of AH, suggesting a lack of transition to a single homogeneous phase. The stabilization provided by AH adsorbed with OVA was less dramatic, but a darker phase was still evident at 40 mN/m.

We previously tested the interaction of AH and AP with more generic models of the outer lipid membrane (DPPC:DOPC) and also found AH was more associated with the membrane, while AP remained at the air-water interface; however, the size and shape of adjuvant-stabilized condensed domains were significantly different between AH and AP. The inherent organizational structure of cholesterol and sphingomyelin domains may explain why the condensed domains appear very similar for both adjuvants. Additionally, although it still appeared to be excluded from the monolayer, AP had a discernable interaction with the DPPC:DOPC membrane which was not observed here [32]. In addition to its generally low affinity for the lipids of the monolayer, the lack of AP association with the POPC:POPE:SM:Ch monolayer could be attributed to the enhanced rigidity typically associated with cholesterol and sphingomyelin-containing domains, which would more greatly resist deformation upon contact with an AP particle [11].

Adjuvant-induced lipid raft clustering was also apparent in dendritic cell membranes *in vitro*. Staining for lipid rafts using cholera toxin-B showed some background lipid raft clustering of untreated cells, particularly in those cells which had been LPS-activated or OVA-primed, but lipid raft staining intensified in adjuvant-treated DCs in all activation groups. The distribution and clustering patterns of the rafts changed slightly depending on the activation of the cell, but AP consistently promoted large lipid raft clusters. Conversely, lipid raft staining was more abundant in AH-treated DCs, but rafts tended to be

59

more disperse with smaller but distinct punctate clusters of rafts. Given the behavior observed in the model monolayer, these images would appear to affirm ABAs preferentially interact with sphingomyelin and cholesterol in the DC membrane. AH, which has higher sphingomyelin and cholesterol affinity and a more favorable, thin-rod morphology, quickly incorporated into the membrane and enhanced more widespread distribution of raft staining, analogous to what was observed in the monolayer. Meanwhile AP facilitated more concentrated clustering of rafts from the membrane surface. If ABA's can enhance similar lipid raft clustering *in vivo,* it is plausible that they may exert at least a portion of their adjuvant effect by initiating or amplifying activation-inducing or stress-mediated signaling [7, 15, 33].

The TNFα data produced by dendritic cells in different activation states also suggested a role for lipid interactions in aluminum adjuvanticity. As expected, all cells treated with the adjuvants had higher levels of the pro-inflammatory cytokine. However, in many cases the bare adjuvant particle produced an equivalent if not higher TNFα response compared to the adjuvant with OVA. The similar response could be due, in part, to OVA almost entirely eluting from the adjuvants after about an hour in cell culture conditions, even with AH which could fully adsorb OVA in mediums without additional protein. Although rapid antigen elution from the adjuvant is consistent with *in vivo* observations [17], it is worthwhile to emphasize the adjuvant surface exposed to the model membranes is not necessarily identical to the adjuvant surface exposed to DC membranes. Nevertheless, the most compelling result was the +LPS/+OVA DC response to either bare adjuvant. When a DC takes up and processes an antigen or pathogen and makes its way to the lymph nodes to activate T cells, it begins a maturation process marked by significantly down regulated endocytosis, upregulated sphingolipid synthesis, and enhanced levels and lifetimes of raft-associated MHC-peptide complexes at the cell surface [34-36]. Therefore, fully primed and activated DCs would not be expected to phagocytose additional particles, but may provide more lipids with which the adjuvants could interact. TNFα concentrations produced by +LPS/+OVA DCs were not significantly different between the controls and either adjuvant with OVA, but the bare adjuvants did promote significantly greater levels of TNFα compared to all other treatments. Ergo, even though ABAs

likely did not enhance pro-inflammatory signaling via particle uptake, they may still have significantly increased TNFα concentrations by clustering the lipid rafts which were more abundant in the activated cells. While the greatest lipid raft clustering appeared to occur with AP in +LPS/+OVA cells, further studies will be required to see if such an interaction is relevant *in vivo*, since AP has been observed to dissolve readily following injection [1].

5. Conclusion

We have shown that the aluminum-based adjuvants Alhydrogel and Adju-Phos can interact with monolayers containing the major lipid components of lipid rafts, namely sphingomyelin and cholesterol. Although the physicochemical properties of each adjuvant differentiated how they interacted with the membrane, both adjuvants could form larger condensed domains compared to the lipid on its own, and stabilized these condensed domains, even at higher levels of membrane compression. There was also evidence of enhanced lipid raft clustering in dendritic cells treated with adjuvants, particularly in activated cells which have higher levels of sphingolipids and cholesterol. Our studies support the hypothesis that ABAs have a high affinity for sphingomyelin and cholesterol, and that membrane interaction may contribute to their mechanism of action by aggregating or stabilizing lipid rafts which can result in enhanced, non-receptor mediated immune activation. Our studies also reaffirm all ABAs are not necessarily equal, and their unique physiochemical properties may trigger different signaling pathways, resulting in different mechanisms of action.

Data reported here also highlight the importance of considering the lipid environment when considering adjuvant effects and mechanisms of action. Our studies showed adjuvants could promote different levels of membrane organization depending on the activation state and lipid content of a single cell. Reports investigating greater membrane damage or inflammasome activation must not only be aware of the chemical composition of the adjuvant, but must also consider whether the studied cell population inherently has higher levels of lipids with which the adjuvant has higher affinity, or whether experimental methods which activate cells (i.e TLR activation via LPS) artificially upregulate these lipids such that

disruptive effects are more obvious. Therefore, these physiochemical and membrane considerations will

be helpful in understanding and designing adjuvants to target or bolster a desired immune response.
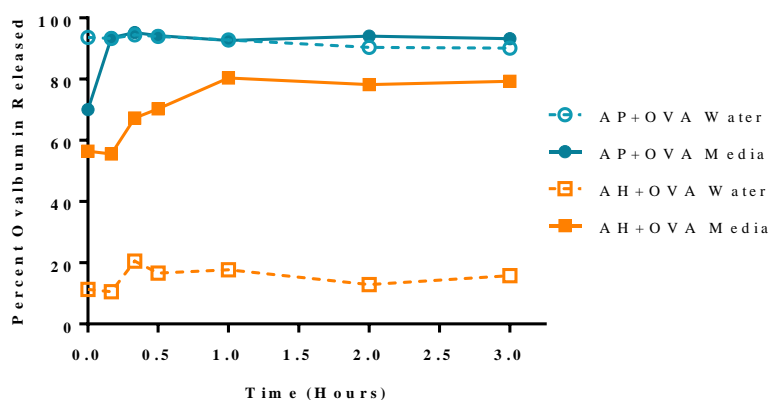
Figure 1. Ovalbumin release from AH and AP in different experimental conditions. The release rate of OVA from each adjuvant was evaluated in cell culture medium and water. OVA did not adsorb to AP and was found in the supernatant nearly immediately in both medium and water. However, OVA fully adsorbed to AH and remained adsorbed in distilled water over the test period, while most of the OVA eluted off AH in cell culture medium after an hour.

Table 1. Maximum affinity of adjuvant for each lipid reported in mg lipid/mg adjuvant

Lipid	Alhydrogel	Adju-Phos
POPC	--	0.92
POPE	1.31	0.43
Sphingomyelin	2.59	0.74
Cholesterol	2.47	1.16
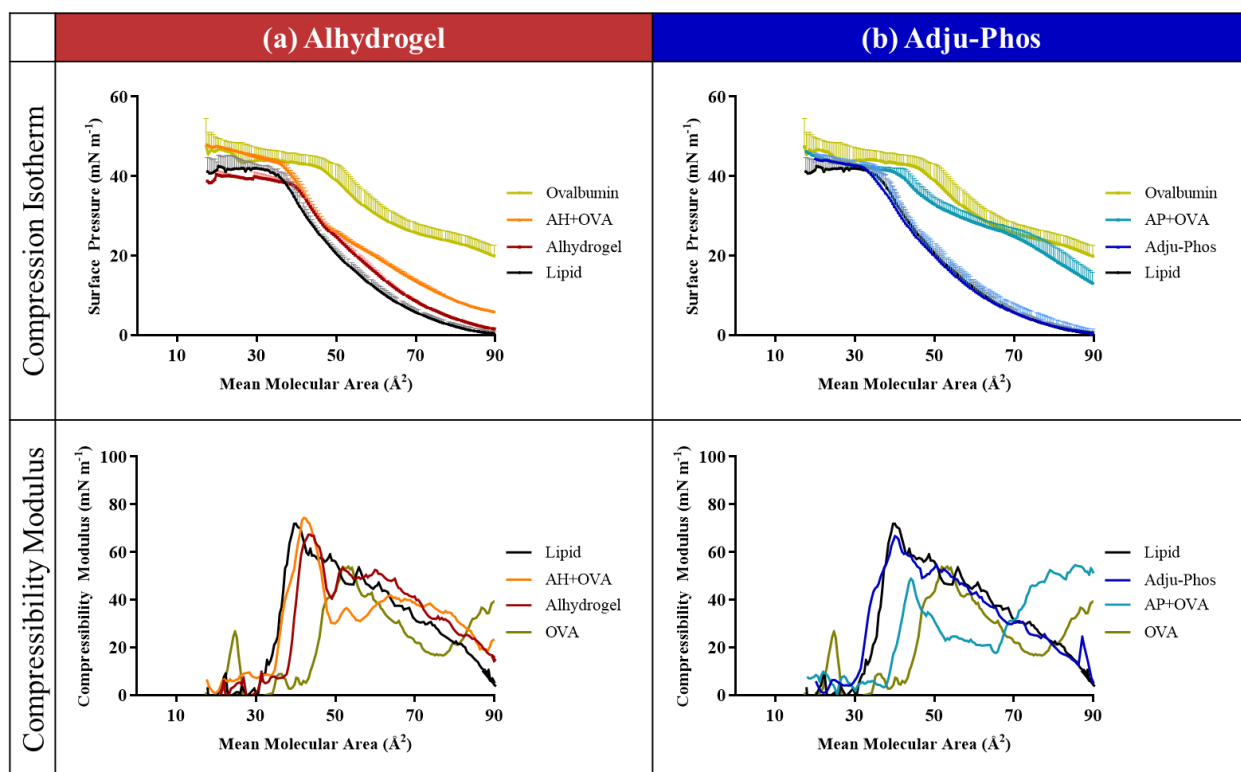
Figure 2. Compression isotherm and compressibility modulus of POPC:POPE:SM:Ch monolayers exposed to bare and OVA-loaded ABAs. (a) AH appears to associate with the lipid monolayer and disrupt lipid packing while (b) AP is excluded from the monolayer, but remains at the air-water interface. When adjuvants are loaded with OVA, AH remained the dominant force in lipid-interactions, but unbound OVA dominated the surface activity when delivered with AP.
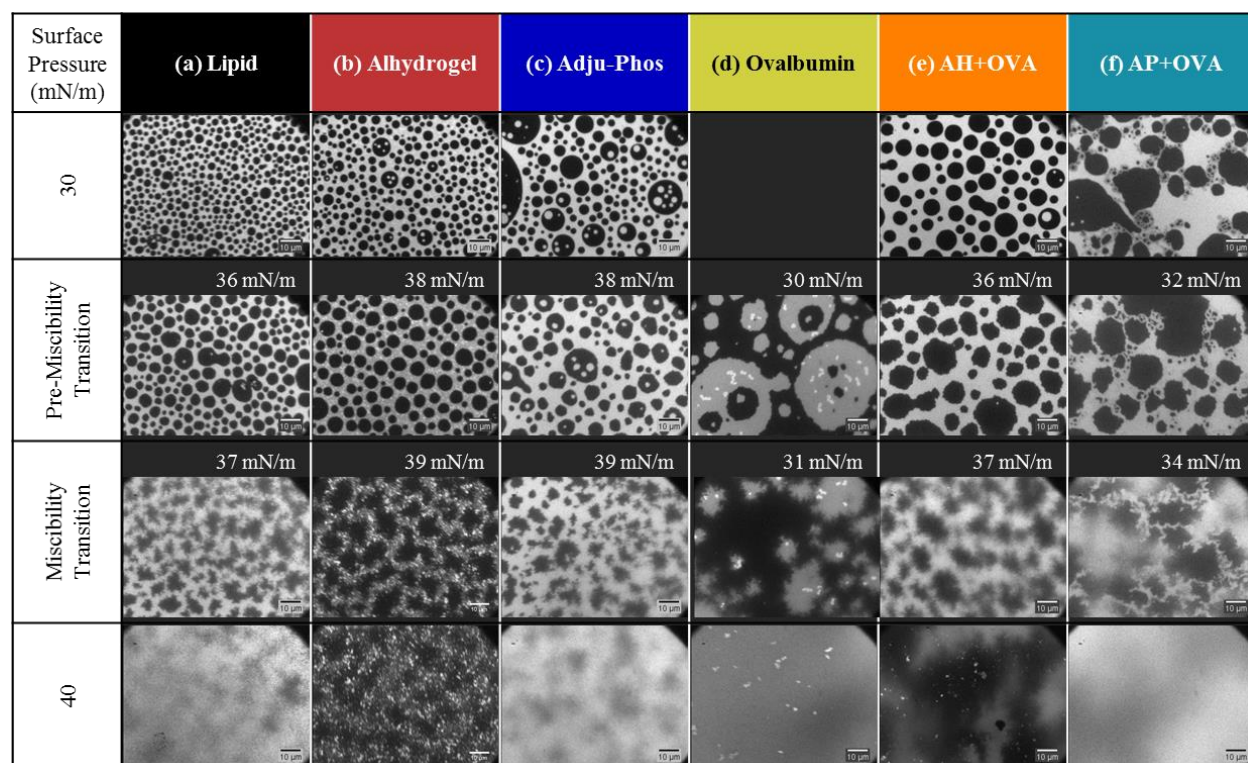
Figure 3. Fluorescent imaging of the POPC:POPE:SM:Ch monolayer alone and in the presence of adjuvant formulations. Bare adjuvants not only promoted the formation of larger liquid-ordered domains, but also stabilized the presence of the domains through higher surface pressures. Although transition surface pressures decreased when adjuvants were mixed with OVA, both adjuvants could still cluster distinct condensed domains to surface pressures beyond the transition of OVA alone. The surface pressures of critical fluctuations and the miscibility transition are reported above each image. Tightly packed liquid-ordered lipids exclude the fluorescent dye and appear dark against a bright liquid-disordered phase.
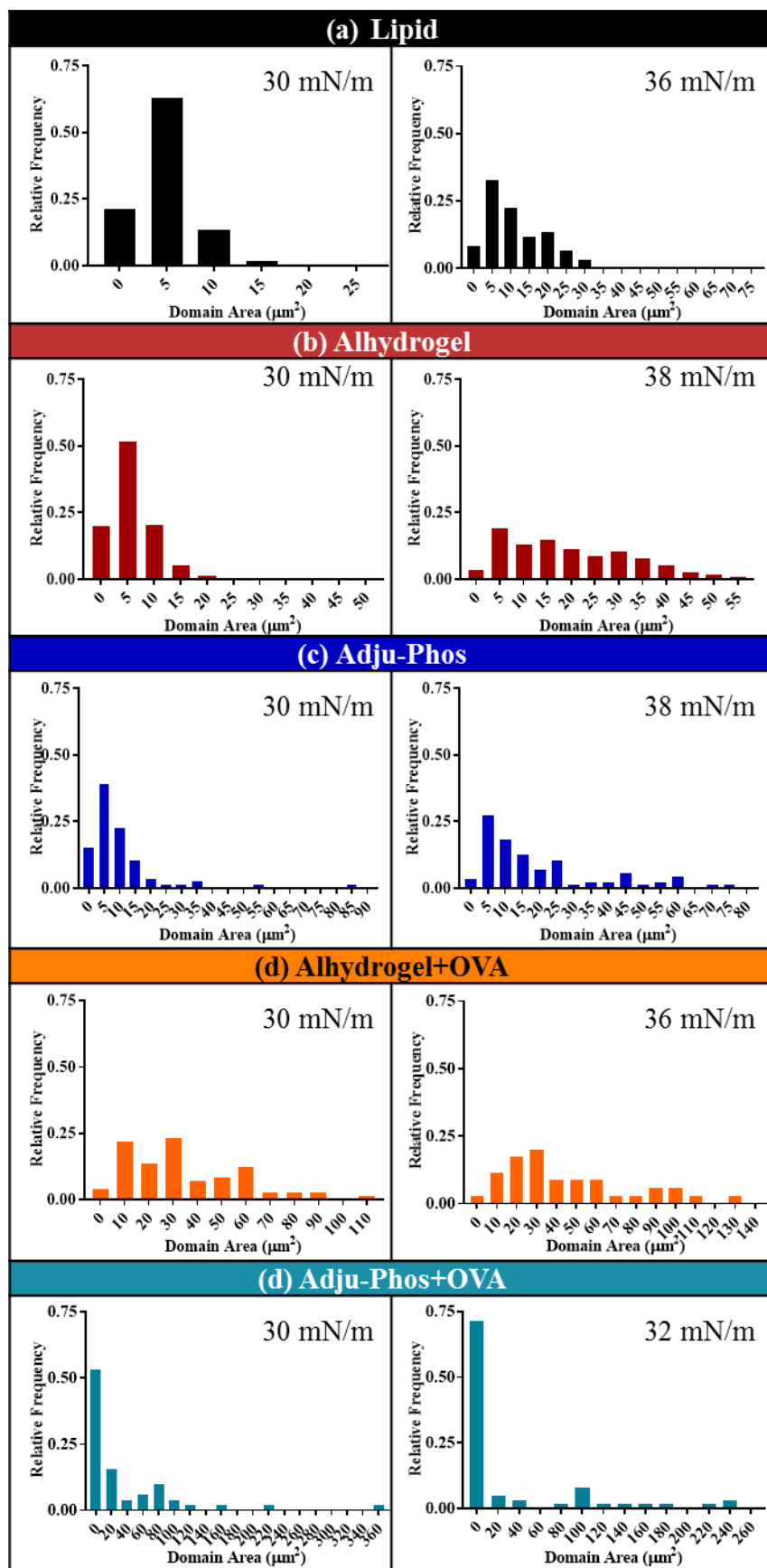
Figure 4. Liquid -ordered domain area distributions. The domain area distributions are shown for the bare and treated POPC:POPE:SM:Ch monolayer at 30 mN/m, and at the indicated surface pressures just prior to the miscibility transition. Domain areas grew as the compression and surface pressure increased, but became substantially larger in the presence of the ABAs, particularly AP.
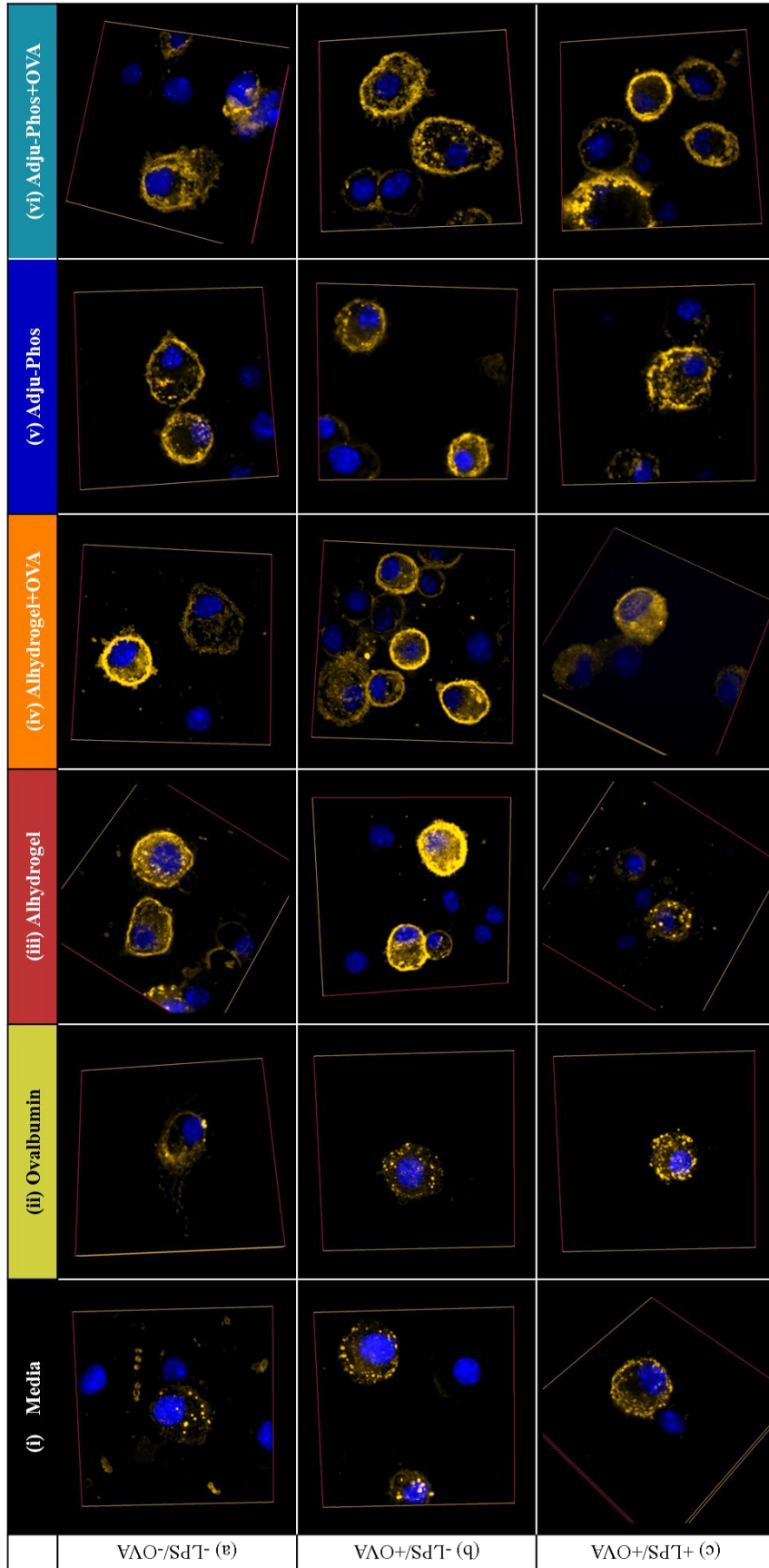
Figure 5. Lipid raft staining of treated dendritic cells *in vitro*. DCs were (b) primed with OVA, (c) primed and activated with LPS, or (a) left unstimulated and were cultured with treatments for 20 minutes. Lipid rafts were labeled using cholera toxin B-Alexa Fluor 555 and fixed. More punctate lipid raft staining was observed in adjuvant-treated DCs, with the greatest clustering of lipid rafts observed in cells cultured with AP.

67
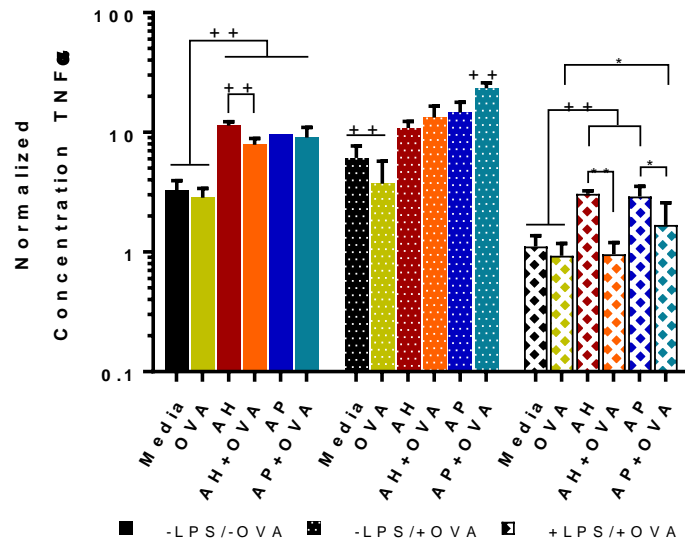
Figure 6. Normalized concentration of TNFα in the medium of treated dendritic cells at 120 hours. DCs were left unstimulated (-LPS/-OVA), loaded and primed with OVA (-LPS/+OVA), or primed and activated with LPS (+LPS/+OVA) and cultured with each treatment for 120 hours. In cells not stimulated with LPS, all adjuvant treatments increased the concentration of TNFα compared to cells cultured with unmodified medium or free OVA. However, in LPS-activated DCs the bare adjuvants produced more TNFα compared to any other treatment in the group. All measurements within each stimulation group were normalized to the untreated media control at 24 hours. *, p<0.05; **, p<0.01; ++, p<0.0001

References

1. He, P., Y. Zou, and Z. Hu, *Advances in aluminum hydroxide-based adjuvant research and its mechanism.* Hum Vaccin Immunother, 2015. **11**(2): p. 477-88.
2. Eisenbarth, S.C., et al., *Crucial role for the Nalp3 inflammasome in the immunostimulatory properties of aluminium adjuvants.* Nature, 2008. **453**(7198): p. 1122-6.
3. Hornung, V., et al., *Silica crystals and aluminum salts activate the NALP3 inflammasome through phagosomal destabilization.* Nat Immunol, 2008. **9**(8): p. 847-56.
4. Marrack, P., A.S. McKee, and M.W. Munks, *Towards an understanding of the adjuvant action of aluminium.* Nat Rev Immunol, 2009. **9**(4): p. 287-93.
5. Oleszycka, E. and E.C. Lavelle, *Immunomodulatory properties of the vaccine adjuvant alum.* Curr Opin Immunol, 2014. **28**: p. 1-5.
6. Mori, A., et al., *The vaccine adjuvant alum inhibits IL-12 by promoting PI3 kinase signaling while chitosan does not inhibit IL-12 and enhances Th1 and Th17 responses.* Eur J Immunol, 2012. **42**(10): p. 2709-19.
7. Flach, T.L., et al., *Alum interaction with dendritic cell membrane lipids is essential for its adjuvanticity.* Nat Med, 2011. **17**(4): p. 479-87.
8. Mile, I., et al., *Al adjuvants can be tracked in viable cells by lumogallion staining.* J Immunol Methods, 2015. **422**: p. 87-94.
9. Giusti, F., et al., *Ultrastructural Visualization of Vaccine Adjuvant Uptake In Vitro and In Vivo.* Microsc Microanal, 2015. **21**(4): p. 791-5.
10. Mold, M., et al., *Unequivocal identification of intracellular aluminium adjuvant in a monocytic THP-1 cell line.* Sci Rep, 2014. **4**: p. 6287.
11. Lingwood, D. and K. Simons, *Lipid rafts as a membrane-organizing principle.* Science, 2010. **327**(5961): p. 46-50.
12. Wu, W., X. Shi, and C. Xu, *Regulation of T cell signalling by membrane lipids.* Nat Rev Immunol, 2016. **16**(11): p. 690-701.
13. Tanimura, N., et al., *Dynamic changes in the mobility of LAT in aggregated lipid rafts upon T cell activation.* J Cell Biol, 2003. **160**(1): p. 125-35.
14. Dykstra, M., et al., *Location is everything: lipid rafts and immune cell signaling.* Annu Rev Immunol, 2003. **21**: p. 457-81.
15. Ng, G., et al., *Receptor-independent, direct membrane binding leads to cell-surface lipid sorting and Syk kinase activation in dendritic cells.* Immunity, 2008. **29**(5): p. 807-18.
16. Simons, K. and W.L. Vaz, *Model systems, lipid rafts, and cell membranes.* Annu Rev Biophys Biomol Struct, 2004. **33**: p. 269-95.
17. Hogenesch, H., *Mechanism of immunopotentiation and safety of aluminum adjuvants.* Front Immunol, 2012. **3**: p. 406.
18. Santinha, D.R., et al., *Profiling changes triggered during maturation of dendritic cells: a lipidomic approach.* Anal Bioanal Chem, 2012. **403**(2): p. 457-71.
19. Kamilya, T., P. Pal, and G.B. Talapatra, *Interaction of ovalbumin with phospholipids Langmuir-Blodgett film.* J Phys Chem B, 2007. **111**(5): p. 1199-205.
20. Marsh, D., *Lateral pressure in membranes.* Biochim Biophys Acta, 1996. **1286**(3): p. 183-223.
21. Ji, S.R., et al., *Monomeric C-reactive protein activates endothelial cells via interaction with lipid raft microdomains.* FASEB J, 2009. **23**(6): p. 1806-16.
22. Johnson, S.A., et al., *Temperature-dependent phase behavior and protein partitioning in giant plasma membrane vesicles.* Biochim Biophys Acta, 2010. **1798**(7): p. 1427-35.
23. Lee, I.H., et al., *Live cell plasma membranes do not exhibit a miscibility phase transition over a wide range of temperatures.* J Phys Chem B, 2015. **119**(12): p. 4450-9.
24. Wang, B., et al., *Nanoparticle-induced surface reconstruction of phospholipid membranes.* Proc Natl Acad Sci U S A, 2008. **105**(47): p. 18171-5.

25.   Tree-Udom, T., et al., *Shape Effect on Particle-Lipid Bilayer Membrane Association, Cellular Uptake, and Cytotoxicity.* ACS Appl Mater Interfaces, 2015. **7**(43): p. 23993-4000.
26.   Yang, K. and Y.Q. Ma, *Computer simulation of the translocation of nanoparticles with different shapes across a lipid bilayer.* Nat Nanotechnol, 2010. **5**(8): p. 579-83.
27.   Nangia, S. and R. Sureshkumar, *Effects of nanoparticle charge and shape anisotropy on translocation through cell membranes.* Langmuir, 2012. **28**(51): p. 17666-71.
28.   Sun, B., et al., *Engineering an effective immune adjuvant by designed control of shape and crystallinity of aluminum oxyhydroxide nanoparticles.* ACS Nano, 2013. **7**(12): p. 10834-49.
29.   Maughan, C.N., S.G. Preston, and G.R. Williams, *Particulate inorganic adjuvants: recent developments and future outlook.* J Pharm Pharmacol, 2015. **67**(3): p. 426-49.
30.   Min, Y., et al., *Critical and off-critical miscibility transitions in model extracellular and cytoplasmic myelin lipid monolayers.* Biophys J, 2011. **100**(6): p. 1490-8.
31.   Trabelsi, S., et al., *Linactants: surfactant analogues in two dimensions.* Phys Rev Lett, 2008. **100**(3): p. 037802.
32.   Antunez, L.R., et al., *Physiochemical Properties of Aluminum Adjuvants Elicit Differing Reorganization of Phospholipid Domains in Model Membranes.* Mol Pharm, 2016. **13**(5): p. 1731-7.
33.   Zhang, Y., et al., *Ceramide-enriched membrane domains--structure and function.* Biochim Biophys Acta, 2009. **1788**(1): p. 178-83.
34.   Anderson, H.A. and P.A. Roche, *MHC class II association with lipid rafts on the antigen presenting cell surface.* Biochim Biophys Acta, 2015. **1853**(4): p. 775-80.
35.   Koberlin, M.S., et al., *A Conserved Circular Network of Coregulated Lipids Modulates Innate Immune Responses.* Cell, 2015. **162**(1): p. 170-83.
36.   Bhardwaj, N., *Processing and presentation of antigens by dendritic cells: implications for vaccines.* Trends Mol Med, 2001. **7**(9): p. 388-94.

Chapter IV: Adjuvants as Delivery Systems in Antigen-Specific Immunotherapies

1. Introduction

Adjuvants have a long history of use in immunizations, but only recently have adjuvants been explored in treatments attempting to tolerize the immune system to autoantigens. Antigen-specific immunotherapy (ASIT) for the treatment of autoimmune disease seeks to provide targeted immune suppression to an autoantigen. If achievable, ASIT would provide a marked improvement to most current autoimmune treatments, which include anti-inflammatory, immunosuppressant, and biologic drugs [1]. These drugs can moderate disease symptoms, but can have serious side effects, like global immune suppression [1, 2]. Moreover, targeted delivery of anti-inflammatories and immunosuppressants can be complicated by their poor water solubility. However, with an appropriate vehicle, these drugs may be co-delivered with an autoantigen to create a targeted ASIT. The properties of some adjuvants are amenable for solubilizing poorly water soluble drugs, and given the propensity of adjuvants to initiate antigen-specific immune responses via interactions with autoimmune-relevant cell populations, adjuvants provide a compelling delivery system for ASIT.

The combination of antigens and adjuvants to tolerize the immune system is not unfounded. Allergy shots were among the first to experiment with antigen-specific tolerization of the immune system. Current allergy shots 'hyposensitize' a patient to an allergen through subcutaneous injections of steadily increasing concentrations of allergen [3]. Similar approaches have been attempted with varying degrees of success in autoimmune diseases using adjuvanted-autoantigen. For instance, two separate studies that dosed Type 1 Diabetes (T1D) patients with either aluminum-adjuvanted GAD65 or insulin b-chain in Incomplete Freund's Adjuvant (IFA) showed characteristic markers of regulatory cell populations [4-6]. When tested in other models of autoimmune disease, such as multiple sclerosis (MS), similar desensitization methods actually increased the risk of destructive cell activation and cytokine release, especially with high doses of antigen [7, 8]. These disparate results motivate further investigation and optimization of adjuvant-based ASIT delivery systems.

The capacity of adjuvants to attract and interact with cells is attractive when attempting to induce immune tolerance. Although the mechanism of action of adjuvants like those shown in Table 1 can vary greatly based on their physiochemical properties, they are all hypothesized to interact with antigen presenting cells (APCs), particularly dendritic cells (DCs) [9-12]. DCs are specialized APCs, and are a key population in ushering T cells toward activation or tolerance [13]. While DCs have been suggested to maintain if not induce autoimmune diseases such as T1D, MS, rheumatoid arthritis, and systemic lupus erythematosus [14, 15], DCs which present self-antigens without proper co-stimulation have been shown to promote apoptosis, anergy, and tolerogenic phenotypes in T cells [13, 15, 16]. Thus, DCs have become a popular target for ASIT, and are potentially accessible via adjuvant delivery.

Both emulsions and aluminum adjuvants reported in Table 1 interact with DCs and are associated with promoting humoral responses, but the immune response can be skewed by delivering a second immunomodulatory molecule on these adjuvants. For instance, AS04 used in the HPV vaccine Cervarix (GSK) combines an aluminum adjuvant with monophosphoryl lipid A (MPL), a TLR4 agonist capable of initiating strong cellular immune responses. The combination of MPL and an aluminum salt creates an adjuvant system, which harnesses the strength of both components, creating strong humoral and cellular responses [10, 17, 18]. Potent cellular and humoral responses were also observed after enhanced uptake of CpG, an intracellular TLR9 agonist, in MF59 [19, 20]. Thus, an appropriate second molecule can expand the utility of traditional adjuvants and help shape downstream immune responses.

Following this same rationale, adjuvants which deliver an appropriate secondary signal should also be a valuable tool for promoting immune tolerance. Dexamethasone (DEX) has been categorized as a classic immunosuppressant currently used to treat autoimmunity and has also been found to promote immune tolerance. For instance, DEX has been used to create 'tolerogenic DCs' [21, 22], and DEX-treated DCs have been shown to enhance expression of tolerance-promoting factors in T cells [21, 23]. One method for generating 'tolerogenic DCs' requires treating the DCs with DEX and an activating stimulus, which may be achieved by the combination of adjuvant and DEX. Furthermore, DEX is a poorly soluble

glucocorticoid with intracellular receptors, therefore delivery with an adjuvant could help it to traverse the cell membrane and reach its site of action [24, 25].

In this study, we evaluated several common adjuvants (Table 1) as vehicles to co-deliver dexamethasone and a model antigen, ovalbumin (OVA). The release of DEX from adjuvants was investigated, and the effect of adjuvant, DEX, and OVA was tested *in vitro* using a DC line. An MF59 analog made in our lab was then advanced to co-culture studies using OVA-primed bone marrow-derived dendritic cells (BMDCs) and splenocytes from OT-II mice.

2. Materials and Methods

2.1. Materials

Ovalbumin, bovine serum albumin (BSA), Tween 80, Incomplete Freund's Adjuvant (IFA, DIFCO Laboratories), MEM alpha, RPMI, resazurin (Acros Organics)**,** phalloidin-AlexaFluor 568 (Molecular Probes), DAPI (Molecular Probes), Slowfade Gold (Life Technologies), 2-mercaptoethanol, and HPLC grade acetonitrile, trifluoroacetic acid, and dimethyl sulfoxide (DMSO) were purchased from Fisher Scientific. Dexamethasone, squalene, Span 85, lipopolysaccharide (LPS, *E. coli*), and red blood cell lysing buffer were purchased from Sigma.

2.2. Model antigen and secondary signal

Ovalbumin (OVA) served as the model antigen and was used at a final concentration of 50 μg/mL. A 10 mg/mL stock of OVA was prepared in ultrapure distilled water (18.2 MΩ/cm; Millipore, Billerica, MA). Dexamethasone (DEX) was used at a final concentration of 100 nM. A 100 μM stock of DEX was prepared in HPLC grade DMSO.

2.3. MF59 analog preparation

The MF59 analog (MF59a) used in these experiments was prepared based on methods published by Novartis (18390722). To prepare the emulsion the oil phase, composed of 39 mg/mL squalene and 4.7 mg/mL Span 85, was combined with the aqueous phase containing 4.7 mg/mL Tween 80 in 10 mM

citrate buffer (pH 5.5). The solution was then emulsified on ice for 2 minutes with pulsing (10 seconds on, 2 seconds off) at 50% amplitude using a probe sonicator (Sonics Vibracell, Newton, CT). The solution was then passed through a 0.22 μm PES filter (Millipore Cork, IRL) and stored in a glass vial at 4°C.

2.4. Antigen and dexamethasone formulations

All formulations were prepared at 2x concentration, and were diluted in cell culture medium or buffer, depending on the experiment. Alhydrogel (AH) and Adju-Phos (AP) (Brenntag, Denmark) based vaccines were used at a final concentration of 50 μg Al/mL. These adjuvants were combined with OVA (final concentration, 50 μg/mL) and/or DEX (100 nM for JAWS, 1 nM for BMDCs) in 10 mM MOPS buffer (pH 7.4) and were mixed end-over-end at 4°C for one hour.

The MF59a was prepared as described and was diluted to make formulations containing 5% MF59a by volume in experiments with JAWS II, and 1% by volume in experiments with BMDCs. MF59a+DEX formulations were made by mixing a DEX_{DMSO} into the oil phase prior to sonication, and in relevant formulations OVA was present in the diluting medium. IFA was emulsified in MOPS buffer by passing the solution through a 20G emulsification needle. OVA was mixed into the buffer and DEX_{DMSO} was mixed into the IFA prior to emulsification. Final IFA formulations contained 10% IFA by volume and were used immediately after emulsification. 0.1% DMSO by volume was present in all formulations.

2.5. OVA and DEX detection via HPLC-UV

OVA and DEX concentrations were measured by reversed-phase chromatographic analysis. A Waters HPLC system was used consisting of an e2695 separation module, a 2489 UV/Vis absorbance detector, and a 2414 refractive index indicator with a Waters C4 XBridge protein column (300 Å, 3.5 μm, 4.6 x 150 mm, 10-500 K). OVA and DEX were detected at 220 nm and 240 nm, respectively. Separation was achieved using a gradient method where mobile phase A contained water + 0.05% trifluoroacetic acid and mobile phase B contained acetonitrile + 0.05% trifluoroacetic acid. Gradient elution was performed at 1

mL/min beginning with 5% mobile phase B until 2.5 min, followed by 50% B at 10 min, 80% B from 18 – 20 min, and 5% B from 22 – 25 min. Chromatograms were acquired and analyzed with Empower version 3 software.

2.6. OVA and DEX association and particle sizing

The mean particle size was measured by dynamic light scattering using a ZetaPALS (Brookhaven, Holtsville, NY). The amount of OVA or DEX associated with the adjuvant particle was determined immediately after each sample was made, and was calculated based on the free OVA or DEX in solution. In the AH and AP solutions, 2 mL of each solution were centrifuged at 13,000 rpm for 5 minutes to pellet the adjuvant, and a sample was drawn from the supernatant. Samples of each emulsion vaccine were centrifuged in an AccuSpin 3R fixed upright at 2850xg for 20 minutes at 10°C to separate the oil and aqueous phases, and a sample was carefully drawn from the aqueous phase below. To concentrate the DEX samples they were frozen, lyophilized, and reconstituted in 50:50 acetonitrile:water. Free OVA and DEX were detected via HPLC, and the amount associated with the adjuvant was assumed to be the initial concentration added less the free concentration detected. Data is the average of at least 3 replicates.

2.7. Dexamethasone release

To determine how dexamethasone was released from the formulations with time, samples were placed in Slide-A-Lyzer MINI-Dialysis devices (10 MWCO, Thermo). Each device was suspended in a 15 mL beaker such that the bottom of the cup was approximately in the middle of the PBS dialysis buffer (pH 7.4). Each beaker was covered in parafilm to prevent evaporation and was placed in an incubated shaker (New Brunswick Scientific) set at 37°C and 80 rpm. At each time point, half the dialysis buffer was removed for analysis via HPLC and was replaced with an equal volume of fresh, warmed buffer.

To ensure DEX was detected in the dialysis buffer, samples were concentrated on the HPLC column via trace enrichment. Briefly, multiple injections of each sample were made using an isocratic method (95% Mobile Phase A: 5% Mobile Phase B) to load DEX on to the column, followed by a final injection using

the gradient method to elute the DEX. Samples collected before 24 hours were injected a total of four times, all others were injected twice.

2.8. In vitro testing of vaccines in JAWS II

All formulations were tested *in vitro* using JAWS II cells (ATCC Manassas, VA) to create a model dendritic cell (DC) population. DCs were cultured according to ATCC guidelines in culture medium containing MEM alpha, 20% FBS (Atlanta Biologicals), 1% penicillin-streptomycin (P/S, MP Biomedicals), and 5 ng/mL GM-CSF (PeproTech). DCs were seeded at 2.5 x 10^5 cells/well in 96 well plates in media, or media containing 1 mg/mL OVA for priming and were allowed to adhere to the plate overnight. The following morning, designated cells were activated with 100 ng/mL LPS for two hours. All cells were washed with warmed MEM alpha, and fresh media was added to the wells. An equivalent volume of each formulation at 2x concentration was added to the wells. Plates were incubated at 37°C and 5% CO_2. Each sample was run in duplicate, and data is the average of three independent experiments.

2.9. Bone marrow-derived dendritic cell isolation and differentiation

Five-week-old C57BL/6J mice were purchased from Jackson Laboratories and housed under specified, pathogen-free conditions at The University of Kansas. All protocols involving mice were approved by the Institutional Animal Care and Use Committee at The University of Kansas. Mice were sacrificed and their femurs were collected. The ends of the femur were clipped, and the bone marrow was flushed out using a 21-gauge needle attached to a 5 mL syringe containing RPMI supplemented with 1% P/S. Cells were collected and centrifuged for 7 minutes at 1,350 rpm at 4°C. The supernatant was removed, replaced with red cell lysis buffer, and incubated at room temperature for 10 minutes. Lysis was stopped with 6x volume of cold complete medium (RPMI, 10% FBS, 1% penicillin-streptomycin, 50 mM 2-mercaptoethanol). The cell solution was passed through a 70 μm nylon cell strainer and centrifuged for 5 minutes at 1,700 rpm and 4°C. The supernatant was removed and replaced with complete medium, and cells were plated at approximately 2x10^6 cells per T-75 culture flask in 12 mL complete medium spiked with 20 ng/mL GM-CSF. On day 3, the medium was removed to discard any floating cells, and 12 mL of

media with fresh GM-CSF was added to the cells. On day 8, the media with suspension cells were collected and the bottom of the flask was thoroughly rinsed to collect any loosely adherent cells. BMDCs were ready for treatment.

2.10. Treatment of BMDCs and co-culture with OT-II splenocytes

$3x10^6$ BMDCs for each treatment group were distributed to T-75 culture flasks. Medium was added to unstimulated BMDCs, and OVA-primed BMDCs were cultured with 1 mg/mL OVA prior to treatment as before. BMDCs were rinsed and then treated for two days. To maintain viability of the cells, primary BMDCs were treated with 1 v/v% MF59a and 1 nM DEX. After two days of treatment, BMDCs were collected and plated at $5x10^5$ cells/well of a 96 well plate.

OT-II transgenic mice (B6.Cg-Tg(TcraTcrb)425Cbn/J) were purchased from Jackson Laboratories, and were sacrificed at approximate 7-weeks of age. Spleens were harvested and passed through a 70 μm nylon mesh fitted over a 50 mL tube containing 5 mL of cold RPMI+1% P/S. Cells were centrifuged for 7 minutes at 1,350 rpm and 4°C. The supernatant was removed, replaced with red cell lysis buffer, and incubated at room temperature for 7 minutes. Lysis was stopped with 6x volume of cold complete media (RPMI supplemented with L-glutamine, 10% FBS, 1% P/S), and the solution was passed through another nylon strainer and centrifuged again as before. Cells were suspended in fresh medium, counted, and distributed to the 96 well plate containing the BMDCs at $5x10^5$ cells/well.

2.11. Metabolic Activity

Cell viability was inferred from metabolic activity measured by the resazurin assay. Wells were washed to remove as much of the formulations as possible and 100 μL of clear MEM alpha and 20 μL of 0.01% resazurin were added to the wells. Plates were incubated at 37°C for one hour, and the fluorescence was measured at ex/em 560/590 nm using a SpectraMax M5 plate reader (Molecular Devices, Sunnyvale, CA). Data within each stimulation group was normalized to the untreated media control at 24 hours.

2.12. Measurement of cytokines

Media from each sample was collected over several time points for cytokine analysis, and was stored at -80°C until the time of analysis. TNFα secretion by the JAWS II DCs was measured by ELISA (R&D systems, Minneapolis, MN) as per the manufacturer instructions. Data within each stimulation group was normalized to the untreated media control at 24 hours within an experiment. In the co-culture experiments, several cytokines were measured using a U-PLEX kit (Meso Scale Diagnostics, LLC, Rockville, MD) as per the manufacturer instructions. Data within each treatment was normalized to the unprimed, untreated media control at 24 hours, and was also normalized to the average metabolic activity of each treatment at each timepoint.

2.13. Dendritic cell imaging

6×10^5 cells/well were seeded on sterilized 12 mm glass coverslips (Fisher Scientific) in 24 well plates and were allowed to adhere overnight. Cells were stimulated and treated as described previously. After 120 hours the culture medium was removed, cells were washed in PBS, and fixed in 2% paraformaldehyde/PBS (Electron Miroscopy Sciences) for 10 minutes. Cells were then quenched in 25 mM Glycine/PBS for 5 minutes, permeabilized in 0.05% Triton X-100/PBS for 15 minutes, and were blocked with three washes of 1% BSA/PBS. Cells were simultaneously stained in 0.165 mM phalloidin-AlexaFluor 568 and 1 mM DAPI in 1% BSA/PBS for 20 minutes. After staining, cells were washed two times each in PBS and distilled water. Coverslips were removed from the wells and mounted on glass slides with Slowfade Gold. Cells were examined using an inverted fluorescence confocal microscope (Olympus IX-83 motorized microscope) with TRITC (tetramethyl rhodamine isothiocynate) and DAPI (4',6-diamidino-2-phenylindole) filters. Images were collected and processed with cellSens software**.**

2.14. Statistical analysis

Statistical analysis was performed using GraphPad Prism 6 (GraphPad Software, Inc., La Jolla, CA). Data were analyzed via two-way ANOVA in conjunction with Tukey's test. P-values less than 0.05 were considered significant.

3. Results

3.1. Vaccine particle characterization

The ability of each adjuvant to carry OVA and DEX was investigated via HPLC (**Table 2**). The 50 μg/mL of OVA in solution was completely adsorbed to AH, but associated much less with AP, and minimally with either emulsion. Conversely, both emulsions, particularly MF59a, could retain most of the 100 nM DEX added to the formulation, while neither aluminum adjuvant retained any. The particle size of the formulations containing an aluminum adjuvant was generally around a micron, whereas MF59a spanned approximately 230–300 nm, and IFA vaccine particles were about 130 nm.

3.2. Dexamethasone release from emulsions

Free DEX and DEX+adjuvant solutions were added to dialysis devices to determine the rate of release of DEX. The release of DEX was determined by measuring the concentration of free DEX in the PBS dialysis buffer. Within the first six hours of the experiment, the release of DEX was not statistically different between any of the groups (**Fig 1**b), but the trends indicated DEX release from MF59a was the slowest. After 24 hours, significantly less DEX was detected from the MF59a samples compared to the free DEX (Fig 1a). After 48 hours, the differences in DEX release were statistically significant between both emulsions and the free DEX. At no point in the study was the release profile of AH+DEX different than the free DEX.

3.3. In vitro testing of formulations

All combinations of adjuvant, OVA, and DEX were tested *in vitro* in a JAWS II-derived DC system. The DCs were either antigen-primed (-LPS/+OVA), LPS-activated (+LPS/-OVA), primed and activated (+LPS/+OVA), or left naïve (-LPS/-OVA). The concentration of TNFα from each sample was normalized against the 24 hour media control within each stimulation group. The baseline response of DCs across the groups, measured by the amount of pro-inflammatory cytokine TNFα, was first tested with the adjuvants alone (**Figure 2**).

In all DC groups, the aluminum adjuvants significantly increased levels of TNFα after 72 hours. In the non-LPS-activated conditions (Figure 2a,b), the cells incubated with AH or AP for 120 hours produced significantly more TNFα than the untreated cells, and at least 10 times more TNFα than the same cells at 24 hours. Conversely, the emulsions generally did not produce TNFα in significantly greater quantities than the untreated cells throughout the span of the experiment, and in several instances even maintained significantly lower concentrations than the untreated cells (Figure 2c,d). The viability of the adjuvant-treated cells was comparable to the untreated cells, except for the MF59a group, whose metabolic activity consistently waned after 72 hours. The viability of the +LPS/+OVA cells treated with IFA was lower than the control throughout the experiment (Figure 2d).

The DC response to the more traditional adjuvant-antigen particle was also tested. As expected, the aluminum adjuvants with OVA created a significant pro-inflammatory response in the cells, particularly the –LPS/-OVA and –LPS/+OVA cells (**Figure 3**a,b). In the OVA-primed cells, the aluminum-adjuvanted OVA prompted at least 10-times more TNFα than the untreated cells after 72 hours. In contrast, none of the DC groups cultured with either emulsion produced more TNFα than the OVA alone. TNFα levels where consistent among all adjuvants with OVA in the LPS-activated conditions (Figure 3c,d). The normalized concentration of TNFα in these samples was close to 1, and therefore similar to the concentration of their respective 24 hour media control over the span of the experiment. There were no significant differences between the OVA alone or any of the formulations. Trends in metabolic activity were similar to the cells treated with adjuvant alone, but with improved metabolic activity in the emulsions.

When free DEX was added to the DCs, the concentrations of TNFα remained approximately equal to the 24h media concentration within the respective stimulation groups (**Figure 4**). The addition of DEX also mitigated the inflammatory effect of AH and AP observed previously with and without OVA. Despite the greatly reduced effect of the aluminum adjuvants in the presence of DEX, AP still induced

significantly more TNFα than the DEX alone after 120 hours regardless of stimulation with LPS or OVA. Apart from the cells primed only with OVA (Figure 4b), the DC response to DEX delivered in the emulsions was statistically equivalent to free DEX. TNFα response again seemed homogenous in the LPS-activated groups.

Finally, formulations containing adjuvant, OVA, and DEX were tested with the DCs. In the DCs not activated with LPS, the presence of DEX in the formulation greatly inhibited TNFα production compared to the adjuvant with and without OVA, especially in the case of AH and AP. Even still, in the –LPS DCs, cells treated with AP+OVA+DEX generated significantly more TNFα than those treated with the unadjuvanted co-administered OVA+DEX (**Figure 5**a, b). MF59a with OVA+DEX never produced significantly more TNFα than the OVA+DEX at any of the sampled time points in any DC group, and IFA-based formulations only produced more after 120 hours in the OVA-primed DCs with and without LPS stimulation (Figure 5b,d). The DCs which were only primed with OVA produced more TNFα in response to the treatments compared to the naïve DC, but both the +LPS/-OVA and +LPS/+OVA DCs responded similarly to the formulations containing all components (Figure 5c,d). As previously observed, the stimulatory effect of the adjuvants appears to be absent in the LPS-activated DCs in that the formulations did not behave differently than the free components and there were no differences in response between the formulations, with the exception of the AP+OVA+DEX vaccine after 120 hours (**Supplementary Fig 1**).

In nearly every formulation and activation state, DEX overcame the increase in TNFα caused by the adjuvant with and without OVA. When the different treatment combinations of a single adjuvant were evaluated within a stimulation group, there was only one instance of a significant difference (+LPS/+OVA DC's with MF59a at 72 h) between the DEX and the OVA+DEX treatments over 120 hours of culture (**Supplementary Fig 2**). In nearly every adjuvant and activation state, the levels of

TNFα produced by the formulations containing adjuvant+OVA+DEX were significantly less compared to the adjuvant+OVA by 120 hours.

3.4. Fluorescent imaging of treated ±LPS/+OVA DCs

After 120 hours of culture, activated and non-activated OVA-primed DCs were fixed and actin-stained to observe how different treatments altered their morphology. Untreated –LPS/+OVA DCs were fairly round and gathered into colonies (**Figure 6**). Culture with free or adjuvanted OVA for 120 hours made the cells notably larger, and in the case of free OVA even more densely packed. AH+OVA and AP+OVA-treated cells had spread out on the glass slides and strands of actin-highlighted dendrites and veils were visible on the cells, morphology indicative of activation. In fact, evidence of this activated morphology could be observed in all adjuvanted-OVA samples. When the -LPS/+OVA cells were treated with free or adjuvanted-DEX, the cells somewhat recovered the size of the untreated cells without recolonizing; although there was evidence of activation in the free DEX-treated cells. Veils could be observed in both aluminum+DEX treated groups; however, the AH+DEX DCs had similar morphology and size as the free DEX DCs, while the AP+DEX-treated cells remained large. The emulsions behaved differently, particularly the MF59a+DEX treated cells which adopted a small but oblong morphology. Unlike the MF59a+DEX cells, the IFA+DEX cells had uneven pockets of high-intensity actin staining. When OVA and DEX were co-delivered, the cell did not show an activated morphology, like the OVA-treated cells, but were similar in size.

Unlike the –LPS/+OVA cells, the untreated +LPS/+OVA cells shown in **Figure 7** adopted a more activated morphology as they spread out and extended long dendrites. When these cells were cultured with free or adjuvanted-OVA, large colonies were again observed and the cells became much larger. Each group of +LPS/+OVA cells treated with adjuvanted-OVA displayed strong signs of activation, more so than the -LPS/+OVA cells. Addition of DEX again reduced the activated morphology of the cells, but did not eliminate evidence of activation in the free, AP-, or IFA- adjuvanted DEX groups. AH+DEX and MF59a+DEX treated cells regained the rounded shape of unactivated DCs. The

combination of free OVA+DEX in these cells appeared to activate more than subdue these cells, producing actin-polarized cell membranes and regions of uneven, high-intensity staining. The aluminum-adjuvanted OVA+DEX cells fared slightly better, showing less actin polarization and a more rounded shape compared to the free OVA+DEX. The low metabolic activity of IFA+OVA+DEX-treated cells reported by the resazurin assay in Figure 4d was observed in cells with damaged or absent cytoskeletons. The MF59a+OVA+DEX showed visible signs of having the least activated cell morphology in this group, although there was still evidence of membrane damage. The morphology of the cells treated with AH- and MF59a-adjuvanted DEX and OVA+DEX also suggests these treatments may have been more effective in reducing the activation of +LPS/+OVA DCs than indicated by the TNFα.

3.5. Coculture of MF59a-treated BMDCs with OT-II splenocytes

Based on its ability to slowly release DEX, maintain good viability, and decrease activation of DCs, MF59a was selected for further investigation in co-culture. Primary cells tend to be less robust, therefore to maintain the viability of these cells, they were treated with less MF59a (1% by volume) and DEX (1 nM). -LPS/+OVA BMDCs were treated for two days, washed, and then cocultured with splenocytes obtained from OT-II transgenic mice, which have an enhanced population of $CD4^+$ T cells that primarily recognize $OVA_{323-339}$. Metabolic activity of the cells cocultured with OVA-primed and MF59a-treated BMDCs was consistently lower than the activity of the unprimed, untreated BMDC coculture (**Fig 8**), but the viability of the coculture was improved in groups where DEX was delivered in MF59a compared to free DEX.

Cytokine data revealed DEX delivered in MF59a could also mitigate the production of pro-inflammatory cytokines as well as the free DEX. In fact, in all the tested cytokines there was no significant difference in cytokine concentration when DEX or OVA+DEX was free or delivered in MF59a. After 72 hours, TNFα concentrations were significantly reduced in both MF59a+DEX and MF59a+DEX+OVA cocultures compared to those left untreated or treated with OVA (**Fig 9**). IL-2 and GM-CSF, cytokines indicative of T cell and monocyte proliferation and activation, respectively, were

increased in MF59a+OVA+DEX samples compared to MF59+DEX alone and was not different from MF59a+OVA (**Fig 10** a,b). However, concentrations of the T_H1 polarizing cytokine IFNγ were not significantly different between the MF59a+DEX groups, and there was significantly less IFNγ in both samples compared to MF59a+OVA (Fig 10c). Furthermore, no significant differences in IL-4, a T_H2 polarizing cytokine, were found between any MF59a treatments (Fig 10d). Only free DEX significantly increased concentrations of the anti-inflammatory cytokine IL-10 (Fig 10e).

4. Discussion

Adjuvants have longstanding success helping to initiate antigen-specific immune responses, but little has been done to determine whether adjuvants could be part of a strategy to target and quell an autoimmune response. Immune cells like DCs play key roles in initiating immune responses and maintaining tolerance, and they are among the primary targets of most adjuvants [13, 26]. Therefore, adjuvants could be an excellent means to deliver small doses of antigen and a secondary signal, such as an immunosuppressant, to this key population of cells and downregulate their response to the antigen.

While each adjuvant was meant to co-deliver the model antigen OVA and DEX, each adjuvant was found to carry one component better than the other. Neither aluminum adjuvant carried DEX and neither emulsion adjuvant retained OVA; however, neither emulsion was expected to associate with OVA based on publications with other antigens. Moreover, antigen association is not required to create antigen-specific immune responses in emulsion adjuvants like MF59 [12, 27, 28]. Conversely, the hydrophobic components of each emulsion allowed them to solubilize DEX. Furthermore, IFA and MF59a extended the release of the drug, with MF59a prolonging its release most. Delivery of poorly soluble drugs in emulsions is not completely unprecedented, especially in oral formulations. The cancer drug paclitaxel and the immunosuppressants cyclosporine A and tacrolimus have all been formulated in emulsions to improve their solubility [29-31]. Delivery of these drugs in emulsions reduced their side effects, prolonged their release, and improved their uptake due to the enhanced cell permeability provided by the oil and surfactant [29-31].

The formulations capable of delivering DEX were better at suppressing TNFα production in JAWSII DCs. DEX effectively combated the TNFα stimulated by any adjuvant and OVA, but the concentrations were lowest in the emulsions. Moreover, the least activated morphology was observed in DCs treated with formulations containing MF59α+DEX [32]. DEX exerts some of its immunosuppressant activity as an antiproliferative agent, which is reflected in the metabolic activity of each of the treatments [24]. The metabolic activity plots of free DEX delivered with and without either aluminum adjuvant are similar, but differ from those of the emulsions, particularly MF59a, which may be an indication of the sustained release and enhanced membrane permeability provided by the squalene and surfactants [33, 34]. Although IFA also moderately extended the release of DEX, the short chain fatty acids in IFA have been observed to have detergent effects which can cause cell lysis [35, 36]. The lytic effects of IFA could have been responsible for the consistently low metabolic activity and cytoskeletal damage seen in IFA+DEX treated cells.

Although aluminum adjuvants have been used to tolerize the immune system to an auto-antigen [5], our results indicate they remain better suited for immune-activating applications. In addition to neither carrying nor sustaining the release of DEX, the particulate nature of AH and AP and their ability to stimulate DCs via lipid interactions likely caused them to consistently produce higher levels of TNFα compared to the other treatments at all levels of activation [37-39]. Although AH and AP significantly increased concentrations of TNFα in all activation groups, the treatments predominately affected DCs not exposed to LPS. LPS activation matures DCs and drastically reduces their endocytic ability, meaning they are less likely to take up the treatments [40]. Also, the normalization of the +LPS TNFα values may be somewhat misleading in that the TNFα concentration in these cells was often at least twice that of -LPS DCs. Thus, the normalized concentrations do not appear to vary greatly because of the sustained elevated TNFα levels. It is also possible the concentration of DEX used was insufficient to combat the robust activation. Although the morphology of +LPS/+OVA disease revealed DEX delivered in MF59a or with AH may have been moderately effective in reducing the activation of the

DCs. Since TNFα did not reflect this reduction in activation, monitoring additional cytokines such as IL-12, IL-10, and TGFβ would be helpful to better characterize the DC response to adjuvant-based ASITs in the future. Regardless, the studies with JAWS II DCs indicated MF59a, which was initially conceived as a delivery vehicle for lipophilic muramyl peptide MTP-PE [41, 42], was the best option for co-delivery of OVA and DEX.

The beneficial effects of co-delivering DEX and OVA in MF59a to OVA-loaded BMDCs were maintained in *ex vivo* experiments with primary cells. Although the cytokine concentrations did not differ significantly when DEX or OVA+DEX was delivered in MF59a, the viability of the co-culture was greater in the MF59a samples. Despite the enhanced proliferation indicated by the resazurin assay and the higher levels of IL-2 and GM-CSF, cytokine concentrations normalized to the metabolic activity revealed the addition MF59a did not augment the T_H1 or T_H2 polarizing cytokines IFNγ and IL-4, respectively. MF59 tends to promote T_H2 responses, ergo the lack of IFNγ was expected, but the lack of IL-4 upregulation would suggest the full activity associated with clinical MF59 was overcome in these experiments [42]. IL-10 concentrations were not significantly enhanced in any of the MF59a samples, but that does not preclude the potential presence of other cytokines which promote regulatory populations, such as TGFβ1 [43].

Further studies will be required to determine the presence of these and other tolerance-promoting factors, but BMDCs treated with either MF59a+DEX formulation showed promise for use in ASIT. *In vitro*, tolerogenic DCs could be created from BMDCs which were semi-matured by treatment with both a suppressing and activating agent [43, 44]. Tolerogenic DCs were maturation-resistant, enhanced anti-inflammatory cytokine synthesis, impaired synthesis of T_H1 cytokines, could migrate to the secondary lymph nodes, and could present antigen to antigen-specific T cells [43]. *In vivo* experiments will be required to evaluate whether adjuvant-based ASITs can enhance DC migration to the lymph nodes, but MF59 has been shown to greatly enhance the migration of antigen- and adjuvant-loaded immune cells to the lymph nodes [9, 45]. Additionally, emulsion formulations with other poorly soluble

drugs have been found to enhance their immunomodulatory activity by promoting their transport to the lymphatics and exposure to lymphocytes [46]. Therefore, emulsions like MF59 could hold promise for ASITs aiming to co-deliver auto-antigen and poorly-soluble immunomodulatory drugs.

5. Conclusions

Adjuvants have been exceedingly successful in creating pro-inflammatory, antigen-specific immune protection, but they also have the potential to serve as efficient vehicles in antigen-specific immunotherapies which promote immune tolerance. In these experiments, we sought to create an adjuvant-based ASIT to provide targeted delivery of an antigen, ovalbumin, and an immunomodulatory molecule, dexamethasone, to promote antigen-specific suppression in antigen-competent immune cell populations. We found both IFA and the MF59 analog produced in our lab solubilized the poorly-soluble immunosuppressant, but MF59a carried the most DEX and provided the most extended release of the drug. DEX delivered in MF59a also successfully mitigated the pro-inflammatory properties of both the adjuvant and OVA in dendritic cells. Furthermore, in co-culture with splenocytes from OT-II transgenic mice, BMDCs treated with formulations which included MF59a and DEX continued to reduce pro-inflammatory cytokines as well as free DEX formulations. MF59-based ASITs require further testing *in vivo*; however, their prospect for success is promising. MF59-based ASITs may not only enhance targeting of antigen and drug to immune populations of interest, but their ability to contain and slowly release poorly soluble drugs would also imply there is less risk for off-target interactions and side effects typically associated with these drugs. Therefore, the utility of emulsion adjuvants could be expanded outside their conventional realm of prophylactic vaccination, and should continue to be investigated as delivery vehicles in antigen-specific immunotherapy for autoimmune diseases.

Table 1. Properties and mechanisms of common adjuvants

Adjuvant	Class	Size (nm)	Ag association with adjuvant	Mechanisms of action	Ref
Alhydrogel	Particulate	~15000	Electrostatically adsorbed, Covalently bound	Enhanced phagocytosis, Causes membrane damage & inflammation, Immune cell recruitment	[47]
Adju-Phos	Particulate	~5000			
Incomplete Freund's Adjuvant	Emulsion	Variable	Free in aqueous phase, Adsorbed at interface	Forms depot, Drain to lymph	[48]
MF59	Emulsion	160		Create 'immunocompetent' environment, Enhanced uptake, Drain to lymph, Membrane permeabilization/damage	[9, 12, 33, 45]

Table 2. Vaccine particle characterization

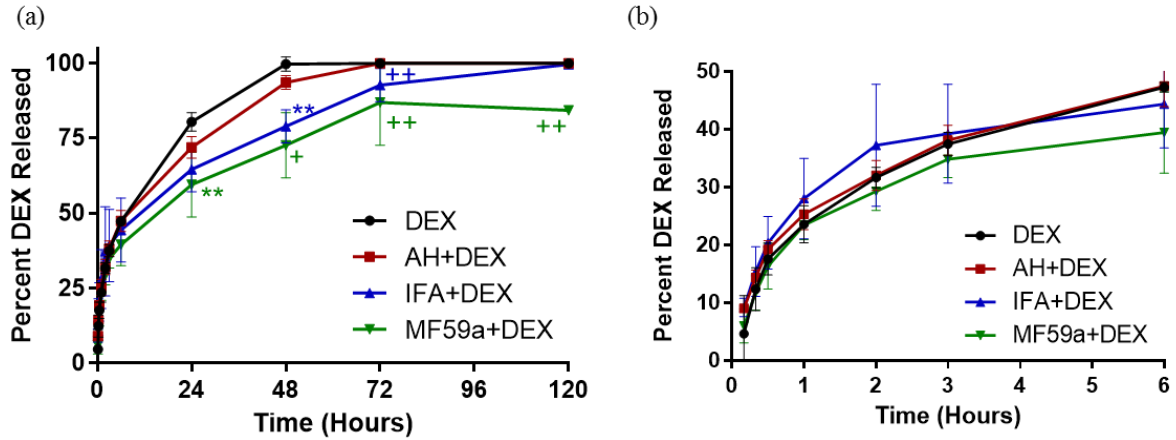| Adjuvant		Ovalbumin (µg/mL)	Dexamethasone (nM)	Size (nm)
Alhydrogel	OVA	50	--	1335.6 ± 39.5
	DEX	--	0	600.1 ± 1.5
	OVA+DEX	50	0	1056.5 ± 14.8
Adju-Phos	OVA	18.7	--	1051.4 ± 49.5
	DEX	--	0	985.4 ± 9.9
	OVA+DEX	11.8	0	979.6 ± 10.5
MF 59a	OVA	6.4	--	307.7 ± 22.7
	DEX	--	85	257 ± 12.3
	OVA+DEX	8.4	85	231.5 ± 12.2
IFA	OVA	9.3	--	135.5 ± 5.3
	DEX	--	47.5	131.8 ± 9.1
	OVA+DEX	1.5	35.5	129.5 ± 6.1

Figure 1. Dexamethasone release from each adjuvant. Free or adjuvanted DEX was added to a dialysis unit, and DEX release was measured based on DEX in the dialysis buffer. (a) The release of DEX was slowest in emulsions over 120 hours; however, (b) DEX release was not significantly different between the samples in the first 6 hours. Statistics are relative to free DEX ** $p<0.01$, ++ $p<0.0001$
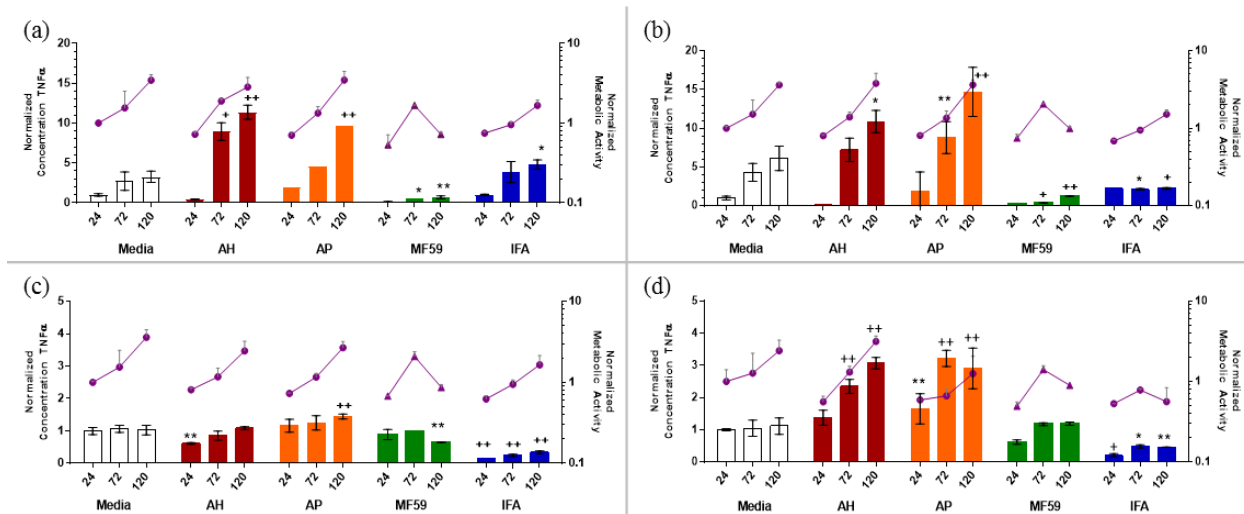
Figure 2. Adjuvant-only treated dendritic cells. (a) –LPS/-OVA, (b) –LPS/+OVA, (c) +LPS/-OVA, and (d) +LPS/+OVA dendritic cells were cultured with bare adjuvants. Aluminum adjuvants promote significantly more TNFα secretion after 72 hours, and emulsions maintain statistically similar or lower TNFα concentrations compared to the control. The normalized concentration of secreted TNFα is shown with bars corresponding to the left axis and the normalized metabolic activity is shown with purple lines corresponding to the right axis. Statistical significance is with respect to the media control at the corresponding time point: * p<0.05, ** p<0.01, + p<0.001, ++ p<0.0001

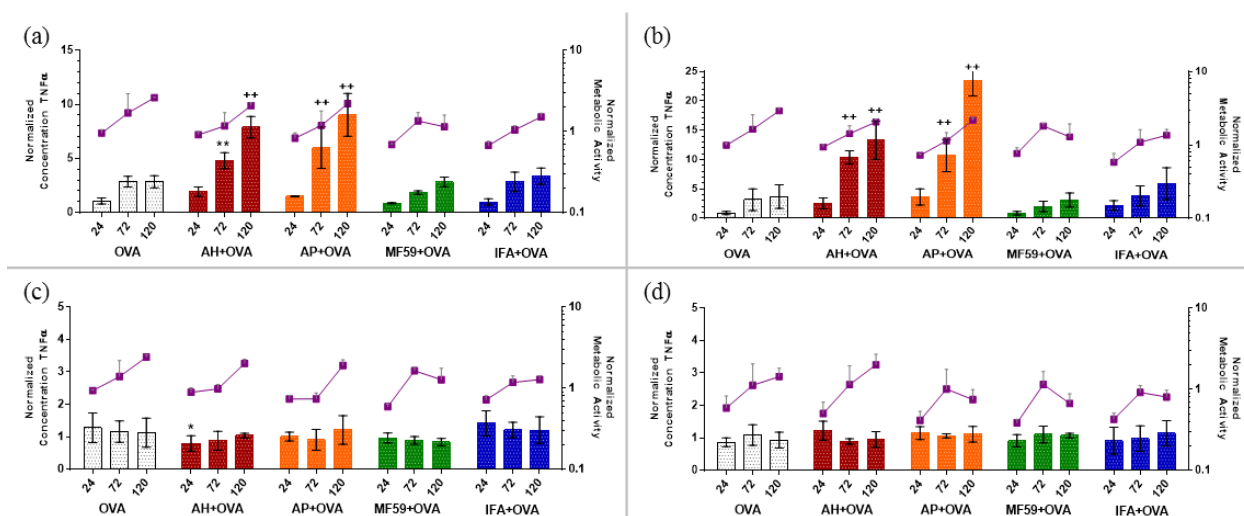**Figure 3.** Dendritic cells treated with adjuvant+ovalbumin. (a) –LPS/-OVA, (b) –LPS/+OVA, (c) +LPS/-OVA, and (d) +LPS/+OVA dendritic cells were cultured with adjuvants+OVA. While the aluminum adjuvants + OVA induced high levels of TNFα in non-activated conditions, the effect of the adjuvant was eliminated in +LPS conditions. Graphs formatted as described in Figure 2. Statistical significance is with respect to the ovalbumin control at the corresponding time point: * p<0.05, ** p<0.01, + p<0.001, ++ p<0.0001
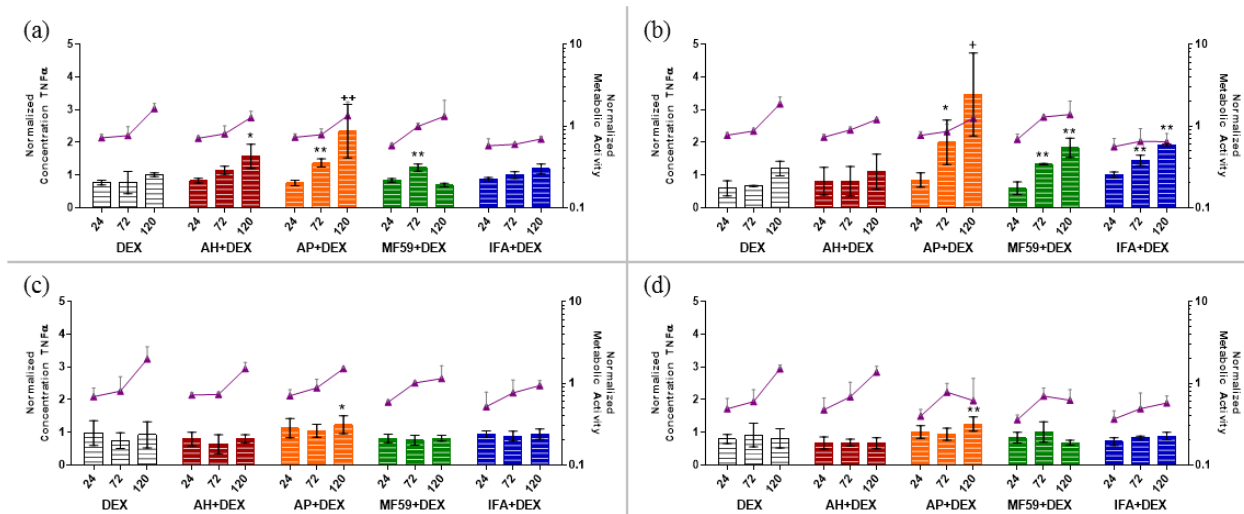
Figure 4. Dendritic cells treated with adjuvant+dexamethasone. (a) –LPS/-OVA, (b) –LPS/+OVA, (c) +LPS/-OVA, and (d) +LPS/+OVA dendritic cells were cultured with adjuvants+DEX. DEX delivered with adjuvants greatly mitigated resultant TNFα concentrations in –LPS DCs compared to the adjuvants or adjuvants+OVA.. Graphs formatted as described in Figure 2. Statistical significance is with respect to the dexamethasone control at the corresponding time point: * $p < 0.05$, ** $p < 0.01$, + $p < 0.001$, ++ $p < 0.0001$
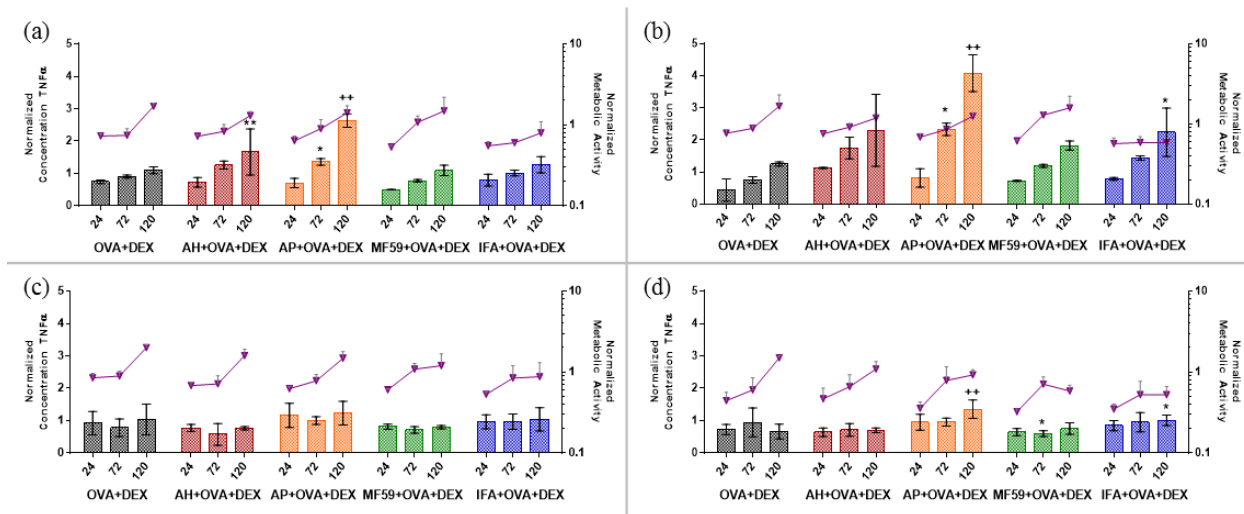

Figure 5. Dendritic cells treated with adjuvant+ovalbumin+dexamethasone. (a) –LPS/-OVA, (b) –LPS/+OVA, (c) +LPS/-OVA, and (d) +LPS/+OVA dendritic cells were cultured with adjuvants+OVA+DEX. Addition of OVA to the adjuvants and DEX did not negate the anti-inflammatory activity of DEX, and greatly reduced the TNFα levels. The normalized concentration of secreted TNFα is shown with bars corresponding to the left axis and the normalized metabolic activity is shown with purple lines corresponding to the right axis. Statistical significance is with respect to the OVA+DEX control at the corresponding time point: * $p < 0.05$, ** $p < 0.01$, + $p < 0.001$, ++ $p < 0.0001$
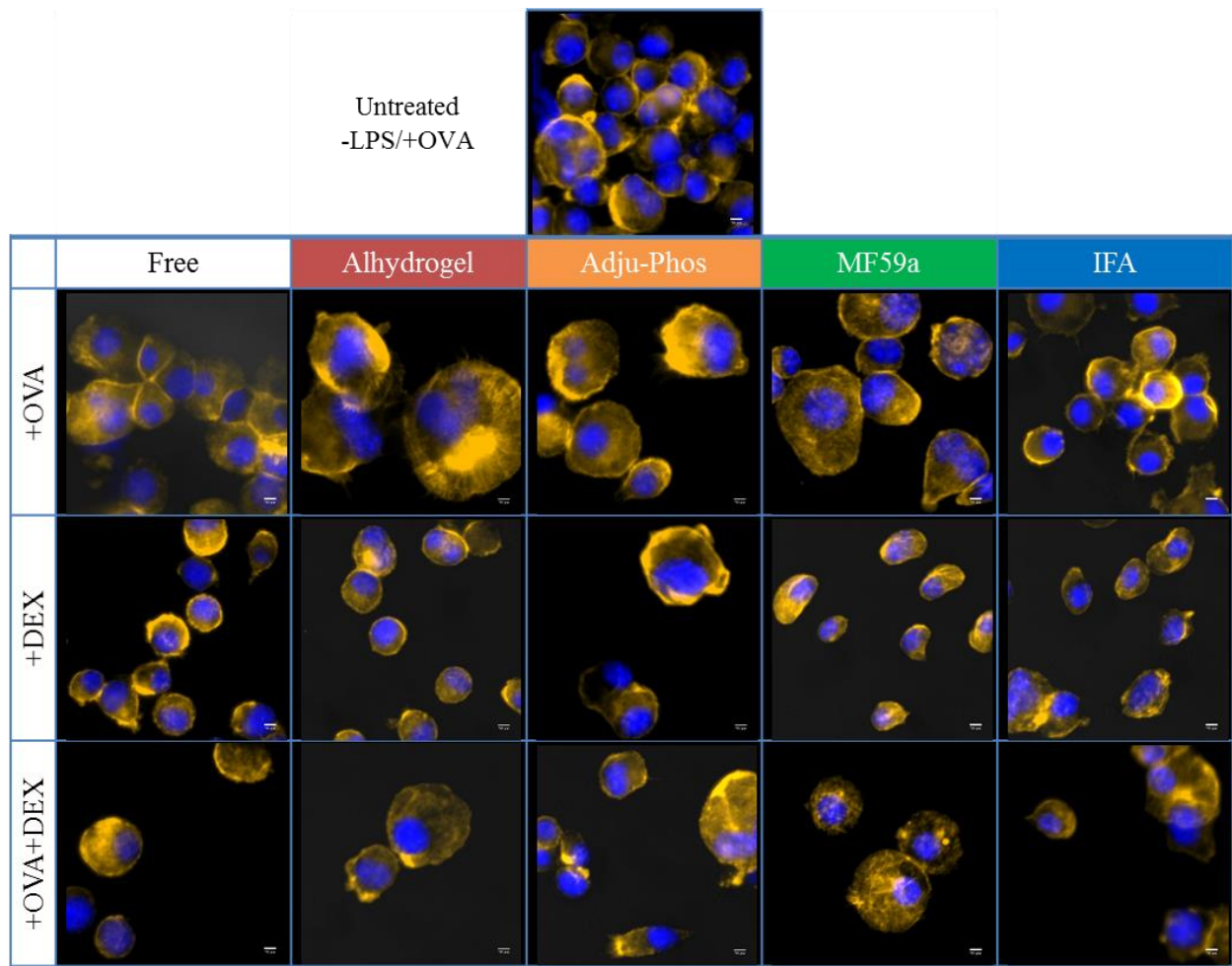
Figure 6. –LPS/+OVA dendritic cells cultured for 120 hours with free or adjuvanted ovalbumin and dexamethasone. Dexamethasone, even in the presence of ovalbumin and adjuvant, can reduce the size and activated morphology of primed DCs. Nuclei were stained using DAPI and are shown in blue, actin was stained with phalloidin-AlexaFluor 568 shown in yellow. Images shown are representative of at least two experiments. Scale bar is 10 μm.
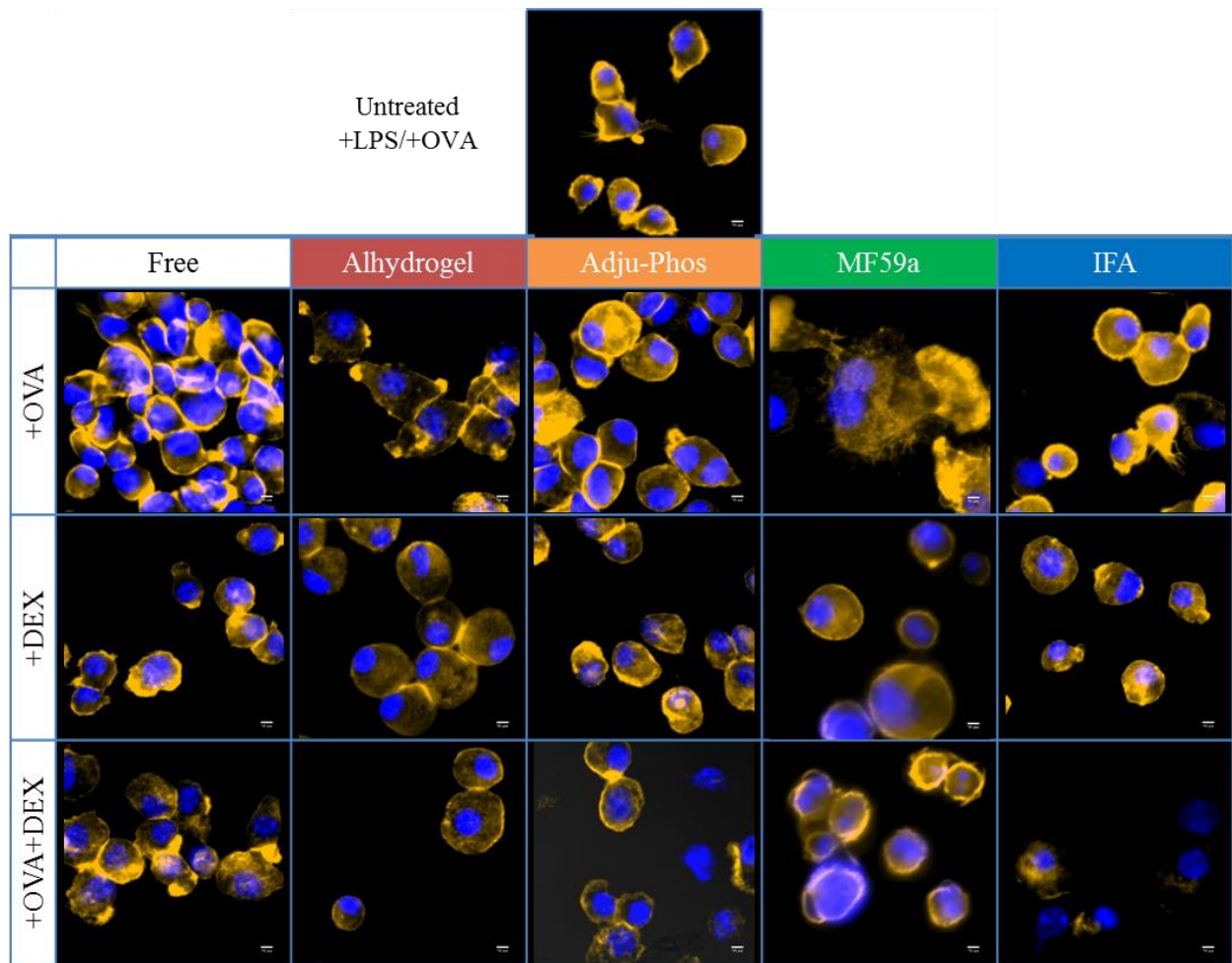
Figure 7. +LPS/+OVA dendritic cells cultured for 120 hours with free or adjuvanted ovalbumin and dexamethasone. Treatments including MF59a with DEX best maintained an inactivated DC morphology. Nuclei were stained using DAPI and are shown in blue, actin was stained with phalloidin-AlexaFluor 568 shown in yellow. Images shown are representative of at least two experiments.
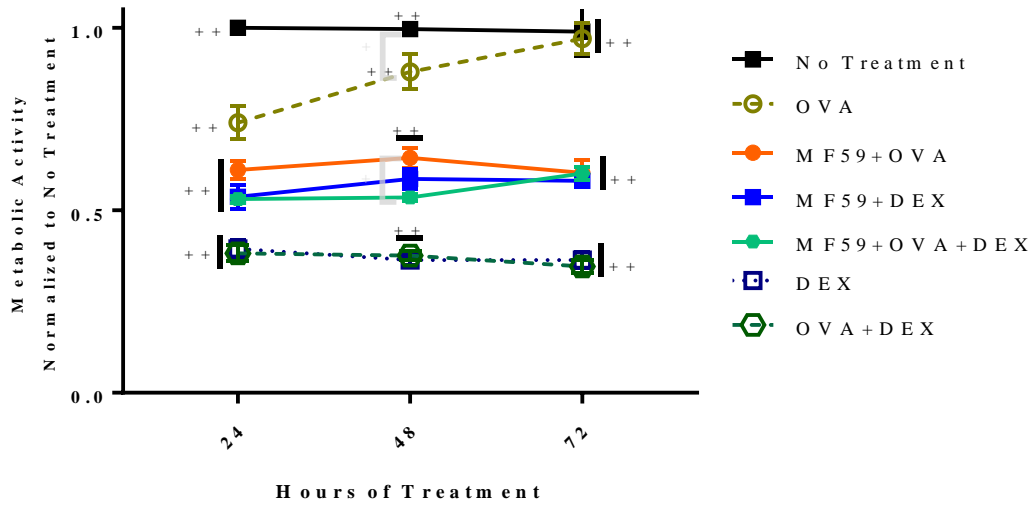
Figure 8. Normalized metabolic activity of BMDC-splenocyte coculture. Metabolic activity of all groups was normalized to the untreated cells at 24 hours. ++ p<0.0001
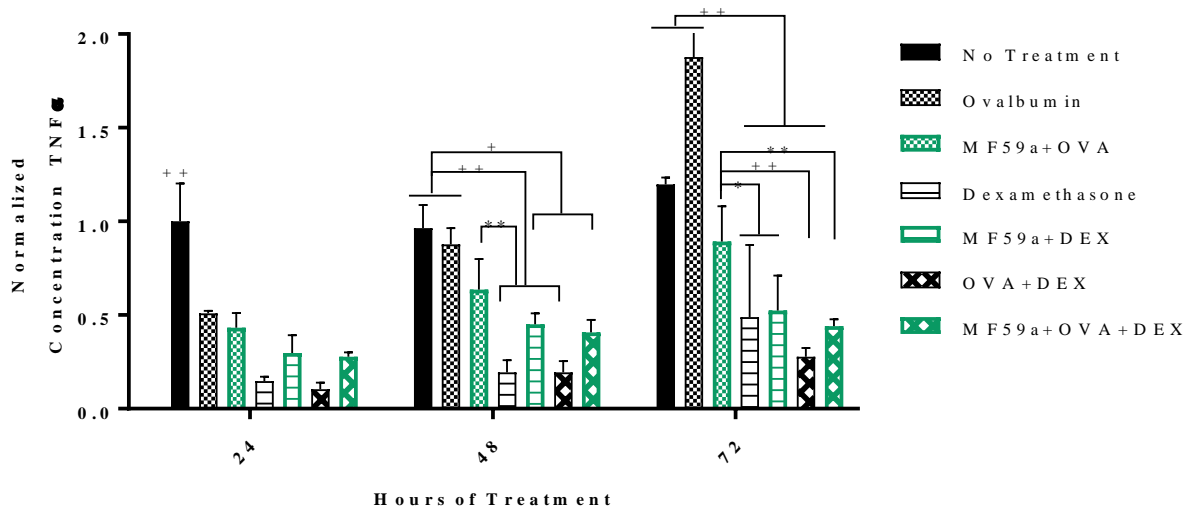

Figure 9. Normalized TNFa concentration in BMDC-splenocyte coculture. -LPS/+OVA BMDCs treated with either MF59a+DEX or MF59a+OVA+DEX maintained significantly lower concentrations of TNFa in co-culture with OT-II splenocytes compared to untreated and OVA-treated samples after 48 hours. Concentrations were normalized to the untreated cells at 24 hours. * p<0.05, ** p<0.01, + p<0.001, ++ p<0.0001
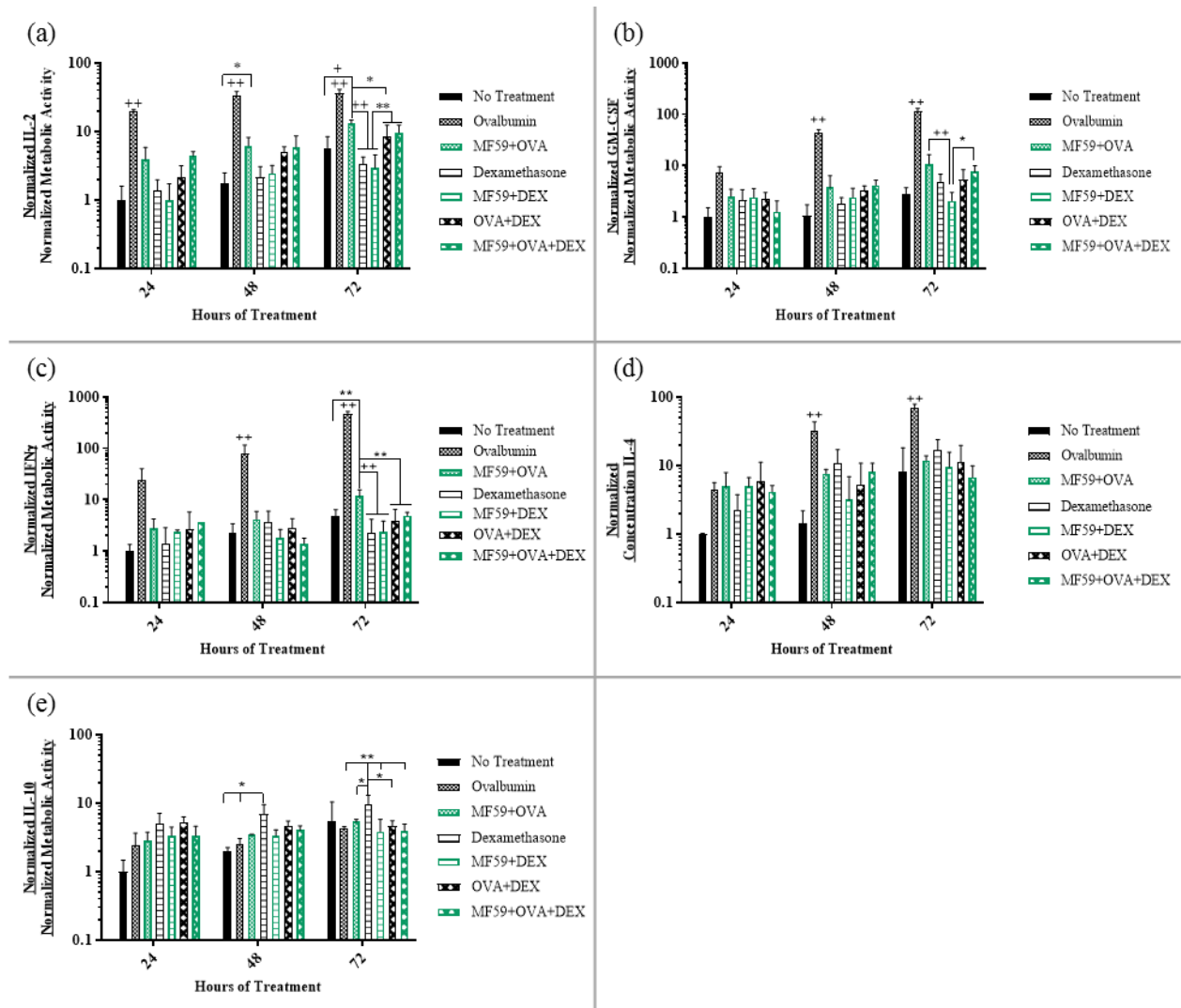
Figure 10. Normalized cytokines from treated BMDCs cultured with splenocytes. (a) IL-2, (b) GM-CSF, (c) IFNγ, (d) IL-4, (e) IL-10. Cytokines were normalized to the untreated cells at 24 hours and the average metabolic activity of each treatment group at the indicated time. * $p<0.05$, ** $p<0.01$, + $p<0.001$, ++ $p<0.0001$
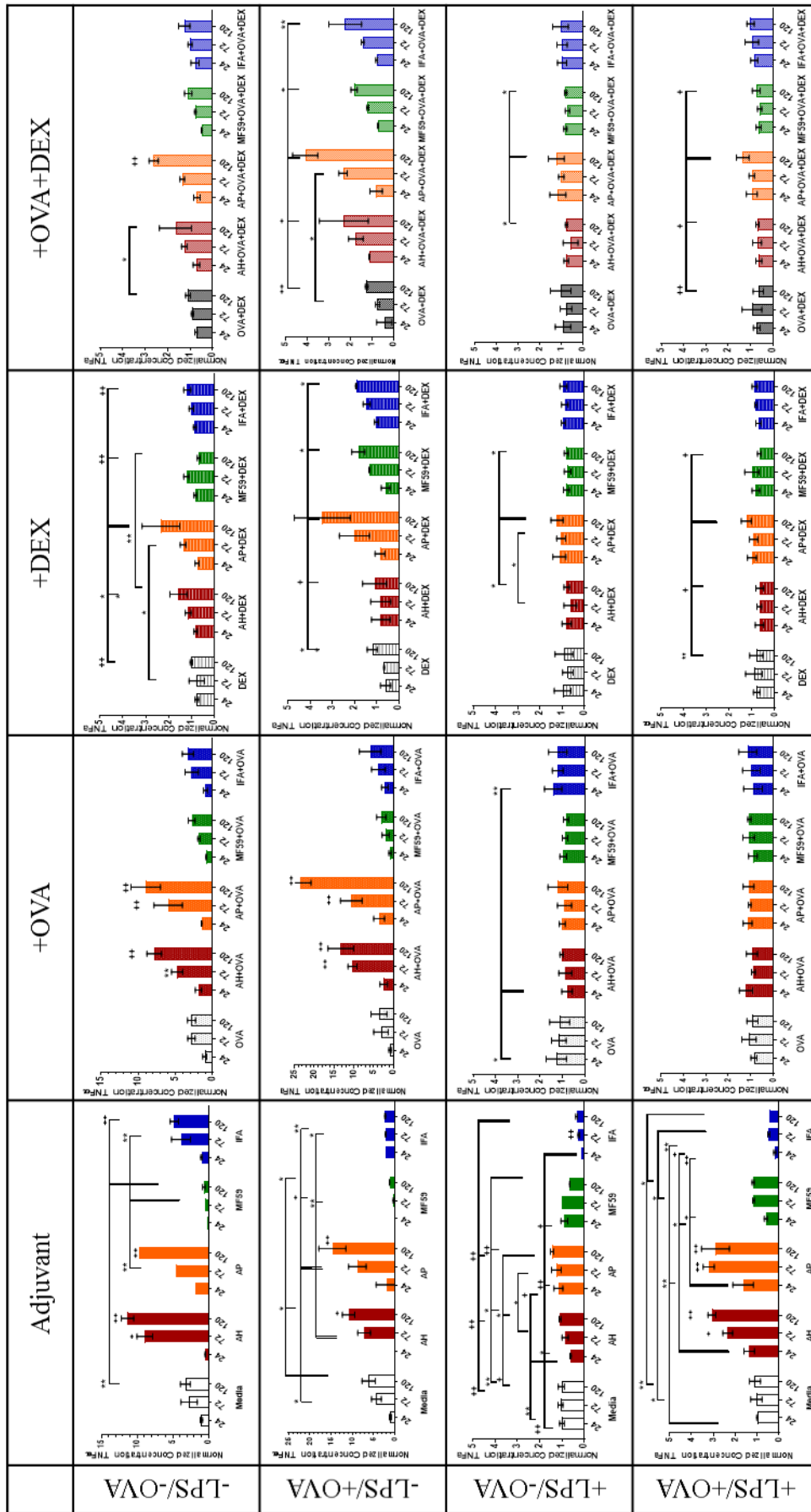
Supplementary Figure 1. Same normalized TNFα data as shown in Figures 2-5, but with all statistical significance reported.

* p<0.05, ** p<0.01, + p<0.001, ++ p<0.0001

97
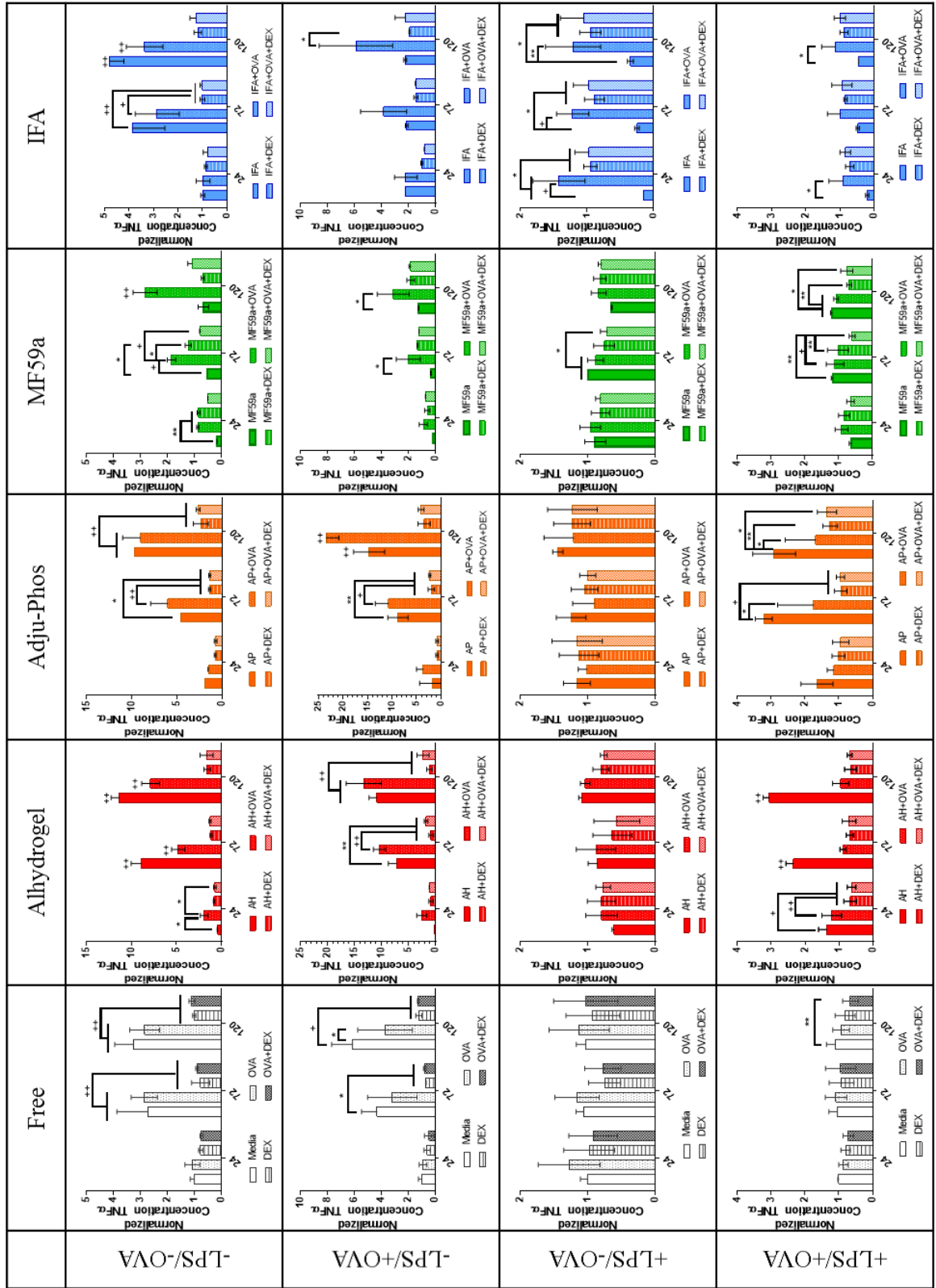
Supplementary Figure 2. Same normalized TNFα data as shown in Figures 2-5, but grouped to show statistical significance between different formulations of the same adjuvant. * p<0.05, ** p<0.01, + p<0.001, ++ p<0.0001

98

References

1. Northrup, L., et al., *Combining antigen and immunomodulators: Emerging trends in antigen-specific immunotherapy for autoimmunity.* Adv Drug Deliv Rev, 2016. **98**: p. 86-98.
2. Winkelmann, A., et al., *Multiple sclerosis treatment and infectious issues: update 2013.* Clin Exp Immunol, 2014. **175**(3): p. 425-38.
3. Valenta, R., *The future of antigen-specific immunotherapy of allergy.* Nat Rev Immunol, 2002. **2**(6): p. 446-53.
4. Agardh, C.D., et al., *Clinical evidence for the safety of GAD65 immunomodulation in adult-onset autoimmune diabetes.* J Diabetes Complications, 2005. **19**(4): p. 238-46.
5. Hjorth, M., et al., *GAD-alum treatment induces GAD65-specific CD4+CD25highFOXP3+ cells in type 1 diabetic patients.* Clin Immunol, 2011. **138**(1): p. 117-26.
6. Orban, T., et al., *Autoantigen-specific regulatory T cells induced in patients with type 1 diabetes mellitus by insulin B-chain immunotherapy.* J Autoimmun, 2010. **34**(4): p. 408-15.
7. Sabatos-Peyton, C.A., J. Verhagen, and D.C. Wraith, *Antigen-specific immunotherapy of autoimmune and allergic diseases.* Curr Opin Immunol, 2010. **22**(5): p. 609-15.
8. Miller, S.D., D.M. Turley, and J.R. Podojil, *Antigen-specific tolerance strategies for the prevention and treatment of autoimmune disease.* Nat Rev Immunol, 2007. **7**(9): p. 665-77.
9. Calabro, S., et al., *Vaccine adjuvants alum and MF59 induce rapid recruitment of neutrophils and monocytes that participate in antigen transport to draining lymph nodes.* Vaccine, 2011. **29**(9): p. 1812-23.
10. Reed, S.G., M.T. Orr, and C.B. Fox, *Key roles of adjuvants in modern vaccines.* Nat Med, 2013. **19**(12): p. 1597-608.
11. Leroux-Roels, G., *Unmet needs in modern vaccinology: adjuvants to improve the immune response.* Vaccine, 2010. **28 Suppl 3**: p. C25-36.
12. O'Hagan, D.T., et al., *The mechanism of action of MF59 - an innately attractive adjuvant formulation.* Vaccine, 2012. **30**(29): p. 4341-8.
13. Gallo, P.M. and S. Gallucci, *The dendritic cell response to classic, emerging, and homeostatic danger signals. Implications for autoimmunity.* Front Immunol, 2013. **4**: p. 138.
14. Blanco, P., et al., *Dendritic cells and cytokines in human inflammatory and autoimmune diseases.* Cytokine Growth Factor Rev, 2008. **19**(1): p. 41-52.
15. Schinnerling, K., et al., *Skewing dendritic cell differentiation towards a tolerogenic state for recovery of tolerance in rheumatoid arthritis.* Autoimmun Rev, 2015. **14**(6): p. 517-27.
16. Mackern-Oberti, J.P., et al., *Role of dendritic cells in the initiation, progress and modulation of systemic autoimmune diseases.* Autoimmun Rev, 2015. **14**(2): p. 127-39.
17. Giannini, S.L., et al., *Enhanced humoral and memory B cellular immunity using HPV16/18 L1 VLP vaccine formulated with the MPL/aluminium salt combination (AS04) compared to aluminium salt only.* Vaccine, 2006. **24**(33-34): p. 5937-49.
18. Hogenesch, H., *Mechanism of immunopotentiation and safety of aluminum adjuvants.* Front Immunol, 2012. **3**: p. 406.
19. Wack, A., et al., *Combination adjuvants for the induction of potent, long-lasting antibody and T-cell responses to influenza vaccine in mice.* Vaccine, 2008. **26**(4): p. 552-61.
20. Yang, M., et al., *MF59 formulated with CpG ODN as a potent adjuvant of recombinant HSP65-MUC1 for inducing anti-MUC1+ tumor immunity in mice.* Int Immunopharmacol, 2012. **13**(4): p. 408-16.
21. Gong, Y.B., et al., *Experimental study of the mechanism of tolerance induction in dexamethasone-treated dendritic cells.* Med Sci Monit, 2011. **17**(5): p. BR125-31.
22. Garcia-Gonzalez, P., et al., *A short protocol using dexamethasone and monophosphoryl lipid A generates tolerogenic dendritic cells that display a potent migratory capacity to lymphoid chemokines.* J Transl Med, 2013. **11**: p. 128.

23. Grohmann, U., et al., *Reverse signaling through GITR ligand enables dexamethasone to activate IDO in allergy.* Nat Med, 2007. **13**(5): p. 579-86.

24. Panyam, J. and V. Labhasetwar, *Sustained cytoplasmic delivery of drugs with intracellular receptors using biodegradable nanoparticles.* Mol Pharm, 2004. **1**(1): p. 77-84.

25. Panyam, J. and V. Labhasetwar, *Biodegradable nanoparticles for drug and gene delivery to cells and tissue.* Adv Drug Deliv Rev, 2003. **55**(3): p. 329-47.

26. O'Hagan, D.T. and E. De Gregorio, *The path to a successful vaccine adjuvant--'the long and winding road'.* Drug Discov Today, 2009. **14**(11-12): p. 541-51.

27. Fox, C.B. and J. Haensler, *An update on safety and immunogenicity of vaccines containing emulsion-based adjuvants.* Expert Rev Vaccines, 2013. **12**(7): p. 747-58.

28. Morel, S., et al., *Adjuvant System AS03 containing alpha-tocopherol modulates innate immune response and leads to improved adaptive immunity.* Vaccine, 2011. **29**(13): p. 2461-73.

29. Mu, L. and S.S. Feng, *A novel controlled release formulation for the anticancer drug paclitaxel (Taxol): PLGA nanoparticles containing vitamin E TPGS.* J Control Release, 2003. **86**(1): p. 33-48.

30. Constantinides, P.P., A. Tustian, and D.R. Kessler, *Tocol emulsions for drug solubilization and parenteral delivery.* Adv Drug Deliv Rev, 2004. **56**(9): p. 1243-55.

31. Borhade, V., H. Nair, and D. Hegde, *Design and evaluation of self-microemulsifying drug delivery system (SMEDDS) of tacrolimus.* AAPS PharmSciTech, 2008. **9**(1): p. 13-21.

32. Shutt, D.C., et al., *Changes in the motility, morphology, and F-actin architecture of human dendritic cells in an in vitro model of dendritic cell development.* Cell Motil Cytoskeleton, 2000. **46**(3): p. 200-21.

33. Reddy, L.H. and P. Couvreur, *Squalene: A natural triterpene for use in disease management and therapy.* Adv Drug Deliv Rev, 2009. **61**(15): p. 1412-26.

34. Yang, Y.W., C.A. Wu, and W.J. Morrow, *Cell death induced by vaccine adjuvants containing surfactants.* Vaccine, 2004. **22**(11-12): p. 1524-36.

35. Gupta, R.K., et al., *Adjuvants--a balance between toxicity and adjuvanticity.* Vaccine, 1993. **11**(3): p. 293-306.

36. Batista-Duharte, A., E.B. Lindblad, and E. Oviedo-Orta, *Progress in understanding adjuvant immunotoxicity mechanisms.* Toxicol Lett, 2011. **203**(2): p. 97-105.

37. Bachmann, M.F. and G.T. Jennings, *Vaccine delivery: a matter of size, geometry, kinetics and molecular patterns.* Nat Rev Immunol, 2010. **10**(11): p. 787-96.

38. Flach, T.L., et al., *Alum interaction with dendritic cell membrane lipids is essential for its adjuvanticity.* Nat Med, 2011. **17**(4): p. 479-87.

39. Antunez, L.R., et al., *Physiochemical Properties of Aluminum Adjuvants Elicit Differing Reorganization of Phospholipid Domains in Model Membranes.* Mol Pharm, 2016. **13**(5): p. 1731-7.

40. Bhardwaj, N., *Processing and presentation of antigens by dendritic cells: implications for vaccines.* Trends Mol Med, 2001. **7**(9): p. 388-94.

41. Ott, G., G.L. Barchfeld, and G. Van Nest, *Enhancement of humoral response against human influenza vaccine with the simple submicron oil/water emulsion adjuvant MF59.* Vaccine, 1995. **13**(16): p. 1557-62.

42. Knudsen, N.P., et al., *Different human vaccine adjuvants promote distinct antigen-independent immunological signatures tailored to different pathogens.* Sci Rep, 2016. **6**: p. 19570.

43. Morelli, A.E. and A.W. Thomson, *Tolerogenic dendritic cells and the quest for transplant tolerance.* Nat Rev Immunol, 2007. **7**(8): p. 610-21.

44. Wu, H.J., et al., *Alternatively activated dendritic cells derived from systemic lupus erythematosus patients have tolerogenic phenotype and function.* Clin Immunol, 2015. **156**(1): p. 43-57.

45. Seubert, A., et al., *The adjuvants aluminum hydroxide and MF59 induce monocyte and granulocyte chemoattractants and enhance monocyte differentiation toward dendritic cells.* J Immunol, 2008. **180**(8): p. 5402-12.

46.	Trevaskis, N.L., W.N. Charman, and C.J. Porter, *Correction to "targeted drug delivery to lymphocytes: a route to site-specific immunomodulation?".* Mol Pharm, 2011. **8**(6): p. 2484.
47.	Lindblad, E.B., *13 - Mineral adjuvants A2 - Schijns, Virgil E.J.C*, in *Immunopotentiators in Modern Vaccines*, D.T. O'Hagan, Editor. 2006, Academic Press: London. p. 217-233.
48.	Maatta, J.A., et al., *Physical state of the neuroantigen in adjuvant emulsions determines encephalitogenic status in the BALB/c mouse.* J Immunol Methods, 1996. **190**(1): p. 133-41.

Chapter V: Conclusions and Future Work

1. Conclusions

Adjuvants have been a vital component of many successful vaccines in that they create stronger antigen-specific immune responses with smaller doses of purified antigen. Despite the prolific use of aluminum-based adjuvants and growing experience with other adjuvants, their mechanisms of action remain poorly understood. While aspects of their immune-stimulating effects may be attributed to receptor-mediated signaling, few have considered how the interaction between an adjuvant and the cell membrane can contribute to its mechanisms of action, or even explain discrepancies in the many proposed mechanisms. As reviewed in chapter 1 the physiochemical properties of many adjuvants make them capable of interacting with cell membranes; and in chapters 2, 3, and 4 we confirmed the organizing potential of adjuvant-lipid interactions and observed their potential to stimulate or diminish immune responses. Given the strong evidence of adjuvant-mediated lipid organization and its potential involvement in shaping immune responses shown here, it is evident that lipid interactions may be a valuable consideration while selecting or developing the physiochemical properties of an adjuvant.

Aluminum adjuvants have been observed to cause cell damage, but they have also been implicated in signal activation by promoting lipid clustering via interactions with sphingomyelin and cholesterol. In chapter 2, the aluminum adjuvants Alhydrogel (AH) and Adju-Phos (AP) were observed to enhance lipid domain clustering even in a simple, monolayer model of the bulk plasma membrane composed of saturated dipalmitoyl-phosphatidylcholine (DPPC) and unsaturated dioleoyl-phosphatidylcholine (DOPC). Surface pressure measurements and fluorescence microscopy images verified aluminum adjuvant-induced increase in lipid domain size. Additionally, adjuvant-induced lipid clustering differed based on the physicochemical properties of the adjuvants, especially charge and morphology. AH appeared to reduce monolayer compressibility and insert into the monolayer, while AP induced more significant changes in domain size, without compromising the integrity of the monolayer. The AH- and AP-mediated reorganization of domains in simple phospholipid membranes supported the

new mechanistic paradigm proposed by Shi and co-workers [1], and motivated further investigation in more complex membrane systems.

In chapter 3, we investigated the interaction of AH and AP with membranes which included the major lipid components of lipid rafts, sphingomyelin (SM) and cholesterol (Ch). To model the dendritic cell membrane, SM and Ch were added to palmitoyl-oleoyl-phosphocholine (POPC) and palmitoyl-oleoyl-phosphoethanolamine (POPE). Consistent with the findings of chapter 2, disparities in particle charge and shape continued to differentiate adjuvant-monolayer interactions. Both adjuvants stabilized larger condensed domains and delayed the miscibility transition of the monolayer. In fact, a miscibility transition was not observed in the presence of AH through the surface pressures tested. Our results suggested AH is present in the monolayer and promotes domain clustering by reducing line tension, while AP promotes domain clustering at the air-water interface. The lipid-sorting capacity of each adjuvant was still apparent even in the presence of highly surface active ovalbumin (OVA). *In vitro*, AH and AP were observed to enhance lipid raft clustering in dendritic cells, especially in activated dendritic cells which are reported to have higher levels of SM [2, 3]. Cytokine analysis of these activated cells also revealed greater levels of the pro-inflammatory cytokine TNFα in response to bare adjuvant, but not any condition containing OVA. Along with increased SM content, mature dendritic cells lose their endocytic capacity [3-5]; therefore, the enhanced TNFα concentrations induced by bare adjuvants would further support the hypothesis that aluminum-based adjuvants may promote pro-inflammatory signaling via enhanced clustering of lipid rafts.

In chapter 4, knowledge of adjuvant-membrane interactions was used to rationally design immune quelling, adjuvant-based antigen-specific immunotherapies (ASIT). Given the ability of adjuvants to interact with antigen presenting cells, they provided a compelling vehicle to co-deliver antigen and immunosuppressing drug to a more limited, key population of cells which initiate and propagate many autoimmune diseases. Compared to the other adjuvants tested, a lab-produced analog of MF59 was found to carry dexamethasone (DEX) at the greatest concentration, and could more slowly

release DEX into medium, thus suggesting utility for co-delivering this immunosuppressant and antigens. In general, the addition of DEX subdued the pro-inflammatory activity of adjuvant with or without OVA in dendritic cells. However, the MF59 analog, whose hydrophobic properties promote non-specific uptake, maintained consistently low concentrations of TNFα in dendritic cells at different levels of activation. When treated dendritic cells were cultured with splenocytes from OT-II transgenic mice, formulations which included the MF59 analog and DEX improved the viability of the co-culture, and also maintained low concentrations of several pro-inflammatory cytokines. Therefore, adjuvants like MF59 may be an ideal co-delivery vehicle for ASITs by reducing global concentrations of poorly soluble immunosuppressant drugs in the body, but promoting enhanced drug uptake to relevant immune cell populations.

2. Future Work

Although this work highlights the importance of considering adjuvant-lipid interactions in both immune-activating and immune-suppressing formulations, there are many aspects of this interaction that remain to be explored. The results presented here suggest the adjuvant-lipid behavior observed in our biophysical model systems may be relevant to adjuvant interactions with the plasma membrane; however, these models fall short of representing the true heterogeneity and complexity of the living cell membrane. Future studies will require more complex systems and sophisticated experimental methods to fully grasp and utilize the immune-regulating mechanisms provided by membrane interactions.

The adjuvant-membrane interactions in chapters 2 and 3 were almost entirely based on zwitterionic lipid monolayers. Monolayers are valuable in proof-of-concept studies, but bilayers would provide a more accurate representation of the plasma membrane. Lipid bilayers would also offer a better model to investigate how adjuvant particles interact with, or traverse the plasma membrane, and therefore the extent of their binding, organization, and incorporation. The nature of the adjuvant-bilayer interaction could more qualitatively be observed in giant unilamellar vesicles which would more closely resemble the curvature of a cell. Giant plasma membrane vesicles (GPMVs) are harvested from the blebs of cell

membranes and have been shown to preserve the lipid and protein composition of a cell's plasma membrane [16]. GPMVs could therefore be used to investigate adjuvant interaction with a far more accurate model of the surface of a cell of interest. More quantitative analysis would be possible using supported lipid bilayers, where lipid-adjuvant interaction could be measured and the location of the adjuvant visualized via atomic force microscopy (AFM), or quartz crystal microbalance with dissipation (QCM-D) monitoring with the inclusion of a fluorescent probe.

With a more rounded set of experimental methods, adjuvant interactions could also be investigated in different environments. Although aluminum adjuvant-induced membrane sorting was proposed to inhibit phagocytosis in dendritic cells [1], many have visually confirmed uptake of multiple adjuvants in phagocytic cells. Moreover, aluminum adjuvants in particular have been suggested to destabilize lysosomes, resulting in the activation of the NLRP3 inflammasome [6-10]. Therefore, it would be worthwhile to investigate lipid-adjuvant interactions under lysosomal conditions. The pH of the lysosome ranges from about 4.5 to 5.4 [11], which could not only alter the ionization state of the lipids, but, in the case of aluminum adjuvants, could also alter the charge of AP (point of zero charge is approximately at pH 5 [10]), or allow the formation of aluminum ions. The deleterious effects of free Al^{3+} on cell membranes in plants and animals have been well-documented at low pH [12], therefore studying aluminum adjuvants' interaction with cell membranes at lysosomal pH could not only add another layer of dimension to their interaction, but could also explain how these adjuvants rupture lysosomes to activate the inflammasome.

The membrane models used in these experiments were modeled after dendritic cell membranes, but future studies could study lipids, or lipid mixtures representative of other cells of interest in different levels of activation. As the field of lipidomics grows, the lipid content of different cells is more accurately defined and may highlight differences between cells, and potentially different modes of interaction with adjuvants. Additionally, the lipid environment of an immune cell can change due to lipid metabolism linked to its activation. Different means of cell activation have been shown to upregulate lipids like

cholesterol and sphingomyelin or ceramide in the cell membrane, and in some cells activation has been shown to alter phosphatidylserine (PS) asymmetry, such that some PS is distributed to the outer leaflet of the plasma membrane [2, 3, 13]. Anionic phospholipids such as PS and phosphatidylinositol, especially phosphatidylinositol (4,5) bisphosphate (PIP2), are known to play major roles in signaling related to immune silencing or activation from the cytosolic leaflet of the membrane. PS and PIP2 also cluster to regulate signaling, and the domains can be linked to lipid rafts on the outer leaflet [13-15]. Ergo, adjuvants which sort raft lipids may also have a reciprocal organizational effect on PS or PIP2 on the cytoplasmic face of the plasma membrane, and could also participate in lipid-mediated signaling.

Likewise, further *in vitro* or *in vivo* studies could be conducted to evaluate the metabolic products of different adjuvants. As reviewed in chapter 1, metabolism of emulsion surfactants results in excess accumulation of neutral lipids, which can cause inflammation and apoptotic signaling [17]. Although emulsions could be formulated to produce metabolites to tune inflammatory signaling, emulsions could also incorporate components which promote anti-inflammatory pathways. For instance, polyunsaturated fatty acids (PUFAs) have been found to either enhance or disrupt immune activation depending on the chain length of the fatty acid. Several PUFAs, including omega-3 PUFAs, have been observed to suppress the activity of T cells, neutrophils, monocytes, and macrophages *in vitro* and *in vivo* by incorporating into the sn-2 position of phospholipids and altering lipid packing, making the membrane more fluid and disrupting immune signaling [13, 18, 19]. Abnormal expression or packing of lipid raft lipids has been implicated in several autoimmune and inflammatory diseases such as systemic lupus erythematosus, multiple sclerosis, and inflammatory bowel diseases [13, 20, 21], thus, compounds which alter effective packing of these lipids could be an effective therapy.

Alternatively, emulsions composed of different immunomodulating compounds could also be investigated to expand on the MF59 analog-based ASIT formulation investigated in chapter 4. For instance, tocopherols, like vitamin E, are oils with inherent antioxidant and anti-inflammatory properties which have been successfully emulsified using other tocopherol derivatives [22]. These emulsions would

retain the enhanced non-specific, hydrophobic uptake by cells, would likely still be able to solubilize and slowly release hydrophobic immunosuppressive drugs, and would have the added benefit of providing additional anti-inflammatory capacity. *In vivo* experiments of any emulsion-based ASIT will be necessary to confirm if (1) the reduction in anti-inflammatory signaling observed *in vitro* is maintained, (2) the immune suppression is antigen-specific, and (3) the suppression is maintained following challenge with the antigen. It will also be valuable to identify the key populations with which these formulations interact to more specifically study how they manipulate the immune response and affect indicators of immune activation, such as expression of cytokines, co-stimulatory surface proteins, and T cell proliferation. Development of tocopherol-based emulsions is ongoing in our lab with promising preliminary results in an animal model of multiple sclerosis. Other iterations of emulsion-based ASITs could include different poorly-soluble immunosuppressant drugs, such as rapamycin, and other antigens associated with autoimmunity. Especially as the field grows closer to being able to finely observe nanoscale lipid motility and metabolism in individual cells in real time, adjuvant-lipid interactions will continue to be a valuable consideration in creating novel and creative vehicles to tune pro- and anti-inflammatory ASITs.

References

1. Flach, T.L., et al., *Alum interaction with dendritic cell membrane lipids is essential for its adjuvanticity.* Nat Med, 2011. **17**(4): p. 479-87.
2. Santinha, D.R., et al., *Profiling changes triggered during maturation of dendritic cells: a lipidomic approach.* Anal Bioanal Chem, 2012. **403**(2): p. 457-71.
3. Koberlin, M.S., et al., *A Conserved Circular Network of Coregulated Lipids Modulates Innate Immune Responses.* Cell, 2015. **162**(1): p. 170-83.
4. Bhardwaj, N., *Processing and presentation of antigens by dendritic cells: implications for vaccines.* Trends Mol Med, 2001. **7**(9): p. 388-94.
5. Anderson, H.A. and P.A. Roche, *MHC class II association with lipid rafts on the antigen presenting cell surface.* Biochim Biophys Acta, 2015. **1853**(4): p. 775-80.
6. Eisenbarth, S.C., et al., *Crucial role for the Nalp3 inflammasome in the immunostimulatory properties of aluminium adjuvants.* Nature, 2008. **453**(7198): p. 1122-6.
7. Hornung, V., et al., *Silica crystals and aluminum salts activate the NALP3 inflammasome through phagosomal destabilization.* Nat Immunol, 2008. **9**(8): p. 847-56.
8. Marrack, P., A.S. McKee, and M.W. Munks, *Towards an understanding of the adjuvant action of aluminium.* Nat Rev Immunol, 2009. **9**(4): p. 287-93.
9. Oleszycka, E. and E.C. Lavelle, *Immunomodulatory properties of the vaccine adjuvant alum.* Curr Opin Immunol, 2014. **28**: p. 1-5.
10. Hogenesch, H., *Mechanism of immunopotentiation and safety of aluminum adjuvants.* Front Immunol, 2012. **3**: p. 406.
11. Trombetta, E.S., et al., *Activation of lysosomal function during dendritic cell maturation.* Science, 2003. **299**(5611): p. 1400-3.
12. Suwalsky, M., et al., *Interactions of Al(acac)3 with cell membranes and model phospholipid bilayers.* J Inorg Biochem, 1999. **75**(4): p. 263-8.
13. Wu, W., X. Shi, and C. Xu, *Regulation of T cell signalling by membrane lipids.* Nat Rev Immunol, 2016. **16**(11): p. 690-701.
14. Levental, I., et al., *Calcium-dependent lateral organization in phosphatidylinositol 4,5-bisphosphate (PIP2)- and cholesterol-containing monolayers.* Biochemistry, 2009. **48**(34): p. 8241-8.
15. Wang, Y.H., et al., *Divalent cation-induced cluster formation by polyphosphoinositides in model membranes.* J Am Chem Soc, 2012. **134**(7): p. 3387-95.
16. Johnson, S.A., et al., *Temperature-dependent phase behavior and protein partitioning in giant plasma membrane vesicles.* Biochim Biophys Acta, 2010. **1798**(7): p. 1427-35.
17. Kalvodova, L., *Squalene-based oil-in-water emulsion adjuvants perturb metabolism of neutral lipids and enhance lipid droplet formation.* Biochem Biophys Res Commun, 2010. **393**(3): p. 350-5.
18. Wanten, G.J. and P.C. Calder, *Immune modulation by parenteral lipid emulsions.* Am J Clin Nutr, 2007. **85**(5): p. 1171-84.
19. Granato, D., et al., *Effects of parenteral lipid emulsions with different fatty acid composition on immune cell functions in vitro.* JPEN J Parenter Enteral Nutr, 2000. **24**(2): p. 113-8.
20. Kabouridis, P.S. and E.C. Jury, *Lipid rafts and T-lymphocyte function: implications for autoimmunity.* FEBS Lett, 2008. **582**(27): p. 3711-8.
21. Varshney, P., V. Yadav, and N. Saini, *Lipid rafts in immune signalling: current progress and future perspective.* Immunology, 2016. **149**(1): p. 13-24.
22. Constantinides, P.P., J. Han, and S.S. Davis, *Advances in the use of tocols as drug delivery vehicles.* Pharm Res, 2006. **23**(2): p. 243-55.